Separation Performance of MOF Adsorbents and Membranes: Effect of Charge Equilibration Methods

by

Özge KADIOĞLU

A Thesis Submitted to the

Graduate School of Engineering

in Partial Fulfillment of the Requirements

for the Degree of

Master of Science

in

Chemical and Biological Engineering

Koç University

August 2018

Koç University

Graduate School of Sciences and Engineering

This is to certify that I have examined this copy of a master's thesis by

Özge KADIOĞLU

and have found that it is complete and satisfactory in all respects,

and that any and all revisions required by the final

examining committee have been made.

Committee Members:

_____

Assoc. Prof. Seda KESKİN AVCI (Advisor, Koç University)

_____

Assoc. Prof. Alper UZUN (Advisor, Koç University)

_____

Asst. Prof. İlknur ERUÇAR FINDIKÇI (Özyeğin University)

_____

Date: _____

ABSTRACT

Metal organic frameworks (MOFs) have emerged as strong alternatives to traditional membrane and adsorbent materials due to their wide range of pore sizes, permanent porosities, and high surface areas. Considering the potential deficit of He, it is very important to develop efficient technologies for He recovery from the natural resources. In this thesis study, the first large-scale computational study to predict He/CH_4 separation performances of various MOF membranes was conducted. Predictions of the molecular simulations were compared with the experimental data for He permeability of several MOF membranes. Motivated from the good agreement between experiments and simulations, 139 different MOF membranes were examined for He/CH_4 separation. These 139 MOF membranes were compared with the traditional polymer and zeolite membranes. A significant number of MOF membranes was identified to exceed the Robeson's upper bound due to their high gas selectivities and permeabilities. Ideal and mixture selectivities of MOF membranes were also compared by performing molecular simulations both for single-component gases and binary gas mixtures. Results showed that selectivities and permeabilities calculated using the single-component gas data can significantly overestimate the ones calculated using the mixture data. Results of this study will be useful to guide the experiments for selecting the most promising MOF membranes for efficient He/CH_4 separations. In the second part of this thesis, effects of using different charge equilibration methods, IQEq and QEq, on the ranking of MOF adsorbents for CO_2/N_2 and CO_2/CH_4 separations were investigated using 2244 MOF structures. Results show that, CO_2 uptake is more sensitive to the charge assignment methods due to its quadrupolar nature. IQEq method was found to overestimate the adsorption selectivities and adsorption performance scores (APSs) of MOFs compared to the QEq method. The Spearman's rank correlation coefficients (SRCC), quantifying the similarity on the adsorption evaluation metrics predicted from two different sets of simulations using the IQEq and QEq methods, were found to be in the range of 0.73-0.84, indicating that there is a good similarity between the MOF rankings performed by using two different charge equilibration methods. Thus, it might be a good strategy to start a high-throughput computational screening study with the IQEq and narrow down the list of MOFs before implementing the DDEC method. Results of this work will be a guide for future computational studies to screen larger numbers of MOFs as adsorbents for the separation of quadrupolar molecules.

ÖZET

Metal organik-yapılar (MOF) geniş ve çok sayıdaki gözenekleri ve geniş yüzey alanları sayesinde geleneksel membran ve adsorban malzemelere güçlü bir alternatiftir. Potansiyel helyum (He) kıtlığı, bu gazın doğal kaynaklardan elde edilebilmesini ve dolayısıyla da bu ayrımı başarabilecek yüksek verimli teknolojilerin geliştirilmesini önemli kılmıştır. Bu tezin ilk bölümünde, literatürde bir ilk olarak, çeşitli MOF membranlarının He/CH_4 ayrımındaki performansları hesaplamalı olarak çalışılmıştır. Moleküler simülasyonlardan elde edilen He geçirgenliği, deneylerle ölçülmüş olan geçirgenlikler ile karşılaştırılmıştır. Deneyler ve simülasyonlar arasındaki uyuma dayanarak 139 tane MOF membranı He/CH_4 gaz ayrımı için incelenmiş ve en çok tercih edilen polimer ve zeolit yapıdaki membranlar ile karşılaştırılmıştır. Yüksek gaz seçicilikleri ve geçirgenlikleri sayesinde önemli sayıda MOF membranının Robeson üst sınırını geçtiği görülmüştür. Bunların yanısıra, tek tip gaz ve ikili gaz karışımları için moleküler simülasyonlar yaparak MOF membranlarının ideal ve karışım gaz seçicilikleri de karşılaştırılmıştır. Sonuçlar, tek tip gaz kullanılarak hesaplanan seçiciliklerin ve geçirgenliklerin, karışım kullanılarak hesaplananları önemli ölçüde yüksek tahmin edebildiklerini göstermiştir. Bu çalışmadan elde edilen sonuçlar, He/CH_4 gaz ayrımını en verimli şekilde gerçekleştirebilecek olan MOF membranlarını belirlemede, deneyleri yönlendirici niteliktedir. Bu tezin ikinci kısmında, MOF adsorbanlarının CO_2/N_2 ve CO_2/CH_4 ayrımlarındaki başarı sıralamalarının farklı yük dengeleme metotlarından (IQEq ve QEq metotları) nasıl etkilendiği 2244 tane deneysel MOF kullanılarak incelenmiştir. Sonuçlar, CO_2 gazının, yüksek kuadrupol momentinden dolayı yük atama metotlarına daha hassas olduğunu göstermiştir. IQEq metodunun, QEq metoduyla hesaplanmış olan seçicilik ve APS değerlerini daha yüksek tahmin etme eğiliminde olduğu gözlemlenmiştir. IQEq ve QEq metotları baz alınarak her adsorbsiyon değerlendirme metriği için MOFlar sıralanmış ve ikişer liste oluşturulmuştur. İkili sıralamalar arasındaki benzerliği gösteren korelasyon katsayıları IQEq ve QEq için 0.73-0.84 aralığında hesaplanmıştır ve bu aralık iyi bir benzerliğe işaret etmektedir. Yüksek korelasyon katsayıları, yüksek çıktılı MOF taramalarında, DDEC metodunu uygulamadan önce MOF listesini IQEq kullanarak daraltmanın iyi bir strateji olabileceğini işaret etmiştir. Bu çalışmanın sonuçları, MOFların, kuadrupol moleküllerin ayrımında adsorban olarak yüksek çıktılı ve hesaplamalı olarak taranmasına rehberdir.

ACKNOWLEDGEMENTS

I have always been so excited about writing this part. It always felt like this is the most relieving part. There is a lot to say when I consider how differently my professional career evolved since the beginning, which I am very glad about the result. The last four years of my life have not been easy. I put a lot of effort to reach this point in my life and I am so grateful for all the people with whom I crossed paths.

Here I am acknowledging all the people who made these two years unforgettable and valuable on every aspect. First, I want to thank my advisor Assoc. Prof. Seda Keskin Avcı for her dedication and excitement in research, constant guidance during my master's, and for being an inspiring academician who started her academic career in early ages. Asst. Prof. İlknur Eruçar Fındıkçı has always been a supportive, indulgent, and caring person. I remember the day when I came to Koç University as a prospective student to get to know NEMO. She was the person I sat next to and who gave a lot of information about the research here. Now, she is one of the committee members for my thesis defense and I am so proud. I want to thank her and Assoc. Prof. Alper Uzun for accepting my invitation to be committee members for my defense and their valuable comments and suggestions regarding my work.

I feel so privileged to meet Prof. Burak Erman and to have taken lectures from him. I am truly amazed by his achievements and constant interest in learning. I want to thank him for inviting me to the round table in his office, giving me advices, sharing anecdotes, and making good conversations with me. He is the most motivated, humble, and supportive professor who I will never forget in my life. I also want to thank my professors in Boğaziçi University, Prof. Ahmet Kerim Avcı and Assoc. Prof. Burak Alakent who have supported me for my master's degree application. Prof. Berend Smit has been another professor who left a mark on my life. He has been very supportive and indulgent whenever I feel lost during my internship at his lab. I want to express my gratitude to him for encouraging me in my academic career and boosting my motivation by believing in my skills.

The greatest joy was spending these two years in such a friendly work environment. First, I want to express my special thanks to Çiğdem Altıntaş for being the uniting and the teaching soul in our office. Without her, my last semester would not be any better and more lovable. Thanks for the nights that you spent with me and carrying my monitor to the library when we had to leave our building because of the fleas. I am so glad that Dr.

Sadiye Velioğlu has joined our research group. All the support and knowledge she passed me are truly appreciated. I want to thank all NEMO members for sharing meals, laughter, knowledge, memories, days, and nights: Hilal, Ayda, Harun, Gökay, Zeeshan, Mert, Safiye, Derya, Pelin, Zeynep, Vahid, Burak (randomly ordered). There are also some lovely people who I met in my master's journey and I want to thank for their sincere support and company: Salim, Zeynep (İnönü), Tuğçe, Riley, and Simge.

I should thank Berfin for her endless love and keeping me in her thoughts during my last semester. I deeply appreciate the emotional support that she provided me through all the hard times. I want to thank, my friends from Boğaziçi, Melis, Ege, Neslihan, and Canberk for their support, love, hugs, and sincere friendship. It is such a privilege to have friends to call whenever you need. I am sure they will always be with me whenever I come back home and we will keep this togetherness for life.

My beloved family deserves the greatest gratitude for always supporting and trusting in me, thanks for trying to keep up with my educational life full of action. I appreciate my mom Nurcan for always doing her best for my dreams to come true and being such a strong and realistic woman. My sister Sinem is my precious, I know how much she wishes the best for me and how excited she is for my future life. Thanks for always being by my side. I also want to thank my brother-in-law Vural for his support, love, and caring. Lastly, my angel dad Erdal deserves a very big gratitude for teaching me how to be dedicated on whatever we do and honest in every occasion, putting lots of effort for my education, and always believing in me.

Besides, the financial support provided by ERC-2017-Starting Grant, grant agreement no. 756489-COSMOS, is acknowledged.

I came to the end of my journey in Koç University. These years became more meaningful thanks to the people I acknowledged above. Next years might be a lot harder, I hope to fight every battle successfully and to be proficient and happy in whatever I do. Just a small note to myself: it is all about perspective.

Özge Kadıoğlu

06.08.2018

TABLE OF CONTENTS

LIST OF TABLES

LIST OF FIGURES

NOMENCLATURE

acc	Acceptance criteria
APS	Adsorption selection parameter
CO_2	Carbon dioxide
CH_4	Methane
EA	Electron affinity
EMD	Equilibrium molecular dynamics
EQEq	Extended charge equilibration method
GCMC	Grand canonical Monte Carlo
He	Helium
IP	Ionization energy
IQEq	Ionizing charge equilibration method
IRMOF	Isoreticular MOF
LCD	Largest cavity diameter
LJ 12-6	Lennard Jones 12-6
MOF	Metal organic framework
N_2	Nitrogen
PCN	Porous coordination network
PLD	Pore limiting diameter
PQEq	Periodic charge equilibration method
QEq	Charge equilibration method
R	Percent regenerability
UFF	Universal force field
ZIF	Zeolite imidazolate framework
$\vec{a}, \vec{b}, \vec{c}$	Translational symmetry vectors of the real-space lattice

$\overrightarrow{a^{-1}}, \overrightarrow{b^{-1}}, \overrightarrow{c^{-1}}$	Translational symmetry vectors of the frequency-space lattice
c	Adsorbed gas amount
D_{self}	Self-diffusivity
D_t	Transport diffusivity
$E(Q)$	Energy of the atom with charge Q
E_0	Energy at the neutral state
f	Bulk phase fugacity
F	Force
h	Planck constant
h	Radial distance in frequency-space
I	Ionization energy
J	Gas flux
k_B	Boltzmann constant
m	Mass
N, M	Number of moles
P	Gas permeability
Q, q	Atomic charge
R	Interatomic distance
r	Radial distance in real-space
s^N	Reduced coordinates
S	Selectivity
T	Temperature
U	Potential energy
$v(t)$	Velocity at time t
V	Volume
V_{LJ}	Interatomic potential

J^0	Idempotential, atomic hardness
χ	Electronegativity
μ	Chemical potential
ϕ^{slat}	Slater orbital
ϵ_r	Dielectric strength
ϵ_0	Permittivity constant
Ω	Volume of unit cell in real-space
η	Splitting-parameter
∇	Gradient vector
λ	Scaling parameter
ξ	Size of an atom
Λ	Thermal de Broglie wavelength
ρ	Particle density
σ	Kinetic size
ε	Energy parameter
δ	Time step
ϕ	Porosity
ΔN	Working capacity

Chapter 1
Introduction

Helium (He) is the lightest noble gas and widely used in industry, medicine, and many other scientific research areas. Of the numerous properties, its low boiling temperature (4.2 K) and non-flammable inert nature make this gas favorable in industry.[1-2] Its major application area with 21% use is as a liquid coolant in superconductors of magnetic resonance imaging (MRIs) equipment. Helium is also used in the pressurization and purging including rockets, leak detection, semiconductors, optic fibers, and weather balloons and utilized as a blanket gas in welding, in helium/oxygen gas mixtures for deep-sea divers, and as a carrier gas in the analysis including chromatographs.[1, 3] Although He is a preferred gas in many applications, the sources to produce it and the storage are limited. Radioactive decay of uranium and thorium contained in mineral/rocks is the natural and the ultimate source of He in Earth, which is known to be a highly slow process.[4] Approximately 3,000 metric tons of He is produced annually in the Earth's crust and most of it runs away to the atmosphere. Although He is ranked after hydrogen in terms of the abundance in the universe, it is barely present in the atmosphere due to its escape to the space.[5] Air contains He with a considerable volume but 5 ppm is a notably low concentration for extraction of He from the atmosphere.[1] Thus, the only practical source of He is from natural gas fields. In general, He composition in reserves is less than 1%, however, several high-quality fields have helium reserves with a composition greater than 4%.[6]

The notable increase in the global usage of He brought the problem of a potential shortage. From 2000 to 2015, global usage of He has increased by 990 million cubic feet.[6] Every year this number goes up and brings the supply problem with it. This increase in

global demand can only be met by a broadened production capacity of He, otherwise, the demand dominates the supply.

Recovery of He from natural gas fields is generally performed using conventional cryogenic distillation process also known as nitrogen rejection unit (NRU), followed by pressure swing adsorption (PSA) as the final step.[1, 7] Although this process provides purity of 99% or higher, it is very energy intensive and economically disadvantageous.[6] Therefore, more efficient and cost-friendly separation technologies are needed to extract He from natural gas fields in order to prevent the potential deficit of He. Research on alternative separation methods such as adsorption-based and membrane-based separation for purification of He has recently gained importance.

Recovery and purification of He with adsorption-based separation might be challenging because He is generally the component having the least affinity to the adsorbent in a gas mixture, which results in the adsorption of other gases present in the mixture.[1] Thus, the efficiency of the adsorption-based He separation process strongly depends on the type of materials used as adsorbents in addition to the composition of the feed gas. Similarly, the success of a membrane-based separation process for He recovery is highly dependent on the type of the material used as a membrane. A membrane should have a high He selectivity for an efficient separation. Besides selectivity, permeability is another key factor that determines the efficiency of a membrane-based gas separation. A highly selective membrane would be useless if the gas permeability is low since a membrane with low throughput requires a large surface area and high capital cost. A membrane with high gas permeability but low selectivity is also undesirable since it would not achieve the separation with high purity. Both high gas selectivity and high gas permeability are required for an efficient and economic membrane-based gas separation in addition to the mechanical stability and chemical resistance of the membrane material.[8] Current membrane materials are not highly selective or permeable for He to recover it from natural gas, which is mainly consisted of methane (CH_4). Therefore, design and

development of new materials that can efficiently recover He from CH_4 with high selectivity and high permeability are crucial.

Metal organic frameworks (MOFs) are crystalline nanoporous materials formed by the coordination bonds between the metal complexes and the organic linkers. Such a nature provides the opportunity of having high porosity, and MOFs have become a potential alternative to conventional adsorbent and membrane materials. Exceptional physical and chemical properties such as large surface areas (500-6000 m^2/g), high pore volumes (1-4 cm^3/g), a wide range of pore sizes from micro to mesoscale (1-98 Å), and reasonable thermal and mechanical stabilities make MOFs inherently promising candidates for gas adsorption and separation processes. MOFs are tremendously advantageous over other porous materials as their physical, chemical and structural properties can be tuned during the synthesis, which results in a large diversity of materials with different geometry, pore size, and chemical functionality.[9] Thousands of MOFs have been synthesized and reported to date.[10] These MOFs have been tested for a wide range of chemical and biological applications including gas adsorption,[11] gas separation,[12] catalysis,[13] optical and luminescent applications.[14] Gas storage and separation can be considered the most developed application area of MOFs.

On the other hand, tens of thousands of MOFs are quite challenging to handle while finding the optimal MOF for a particular application. However, having such a large number of options is a great advantage to find the material which gives the best performance for a specific purpose. Since experimental synthesis of a material and testing its performance can take several weeks, computational techniques are very critical for evaluating the capabilities of large numbers of candidate MOFs in a time-efficient manner.[15] Gas separation simulations in MOF materials requires the use of Grand Canonical Monte Carlo (GCMC) techniques[16] which is detailly explained in Chapter 3.

Adsorption and diffusion processes are modeled with intermolecular interactions of adsorbate-adsorbate and adsorbate-adsorbent, and those interactions are non-bonded. Thus, the energy of a system is composed only of van der Waals and Columbic

interactions.[17] For the applications such as methane storage,[18] hydrogen storage,[11] and CH_4/H_2 separation,[19] adsorption of the gas molecules is not notably affected by the electrostatic interaction between the adsorbate and the adsorbent since it is mainly driven by the dispersion interactions. However, for applications with polar or quadrupolar molecules, such as CO_2 storage,[20] CO_2/N_2 separation,[21] CO_2/CH_4 separation,[22] and CO_2/H_2O separation,[23] adsorption becomes highly sensitive to the electrostatic interactions. For the applications where Coulomb interactions are dominant on adsorption, it is essential to model those interactions properly. Therefore, the accuracy of a charge assignment method depends on its ability to describe the electrostatic potential (ESP) of a MOF. There are several methods in literature to compute atomic partial charges. Some of these methods are based on the density functional theory (DFT) calculations such as REPEAT[24] (based on the fitting of the ESP around the molecule), DDEC[25] (based on partition of the electron density), and Mulliken[26] (based on population analysis of the wavefunction) charges. Those methods are known to be time-inefficient regarding their computational demand for high-throughput screening.

On the other hand, there is a class of methods known as charge equilibration methods. These methods depend on the electronegativity equalization and charges are assigned by considering atomic ionization potentials. Most of them are inspired by the charge equilibration (QEq) method proposed by Rappe and Goddard.[27] Later, the QEq method was tailored by Ramachandran et al.[28] to include periodic structures. Wilmer and colleagues modified Rappe and Goddard's QEq to calculate partial atomic charges in MOF materials and renamed it as extended charge equilibration method (EQEq).[29] Another charge equilibration method is the Ionizing Charge Equilibration Method (IQEq)[30] where the molecule is considered as a collection of ions rather than atoms. These methods computing charges based on the electronegativity equalization are favorable for rapid-charge assignments but have their own limitations, which should be a concern while implementing. For instance, in EQEq method, the user should define oxidation states of the elements included in a MOF as input. Assigning an oxidation state to the elements

with many possible states may be improper. MEPO-QEq[31] which was parametrized to reproduce the ab-initio derived ESP has a major limitation regarding the structural building units. This method was trained for only a small group of SBUs, which causes a transferability problem. The restrictions are usually related with the diversity of the training set used for the parametrization of a method, the inputs that should be defined by the user, or the structures with specific features such as having buried atoms or open metal sites.

The first part of this thesis focused on the atomically-detailed simulations to examine the membrane-based separation performances of various MOFs for He/CH_4 mixture. In the second part, the comparison of different charge assignment methods in the sense of MOF rankings constructed by using different adsorbent selection metrics for CO_2/N_2 and CO_2/CH_4 mixtures was examined. Chapter 2 represents the literature review on these subjects with related experimental and computational studies conducted. Experimental studies on He recovery through nanoporous MOF membranes and/or adsorbents are given in Chapter 2 together with the computational studies on charge equilibration methods. Besides, the studies that are on CO_2/N_2 and CO_2/CH_4 mixture separations are discussed as the MOFs were ranked for these gas separations. Computational techniques used to model adsorption and diffusion systems are given in Chapter 3 together with the calculations of adsorbent/membrane properties of MOFs. Investigation of He/CH_4 separation performances of MOF membranes is given in Chapter 4. This is the first large-scale computational study conducted on He/CH_4 separation. Simulations were performed not only for single-component gases but also for the binary mixture to mimic the industrial process. In Chapter 5, charge equilibration methods were discussed referring to CO_2/CH_4 and CO_2/N_2 separation performances of MOF adsorbents. Finally, the findings of these two studies were discussed in Chapter 6.

Chapter 2
Literature Review

2.1. Gas Separation by MOFs

MOFs have gained a tremendous attention for the gas separations due to their large surface area and good thermal and chemical stability. The possibility of designing theoretically numerous MOFs by changing the organic linkers and the metal types, this material group provides the opportunity of finding the most optimal adsorbent or membrane for a given application. One of the separation types handled with MOFs is equilibrium-based separation which is superior to other techniques due to its easy and simple operation, low-cost and ability to achieve high purities. Depending on the type of interaction between the adsorbate and the adsorbent, this process can be named as either physisorption or chemisorption. Adsorption of gas molecules inside MOFs is categorized under the physical adsorption which occurs due to the intermolecular forces (Van der Waals forces) and does not cause perturbation in the chemical structure of the species involved in the process. When an adsorbent is subjected to a gas mixture in a closed space, the weight of the adsorbent will increase due to the gas molecules adsorbed on its surface. Once the dynamic equilibration is established between the gas and solid phase, gas molecules will be no longer adsorbed. Unlike chemisorption, in physisorption, the adsorbent can be regenerated with physical treatments such as decreasing the pressure.[32]

The key metric in choosing the optimal adsorbent is perhaps the type of the material. High porosity, as well as high surface area which provides more binding sites for the gas molecules, is desired for an adsorbent. However, as long as the adsorption selectivity of a material is low, high surface area to achieve the desired separation can only be

succeeded by increasing the amount of adsorbent, which will increase the operation cost. Working capacity is another widely used metric and it is defined as the difference between the loadings in adsorption and desorption pressures. The ratio of working capacity to the amount of adsorbed gas at adsorption pressure gives the regenerability which is highly critical for the industrial operations as it determines the performance of the adsorbate in long-term use.

A thin layer of materials that substances can pass through is called membrane. Membrane-based separation is highly preferred due to its less energy consumption and easy operation. Polymeric membranes have the biggest share in the market because they are mechanically flexible, lower-priced, and provide high fluxes.[33] However, low thermal and chemical stabilities in addition to short lifetimes make them disadvantageous to be employed as membranes for a gas separation. MOFs are good membrane candidates considering their high thermal and chemical stabilities as well as pore sizes that can be tailored during the synthesis.[33-34]

Computational studies on MOF membranes and adsorbents mostly focus on the separations of CO_2/CH_4,[35-37] CO_2/N_2,[38-41] CH_4/N_2,[21, 42-43] and CH_4/H_2[37, 42, 44-48] and CO_2[20, 49-50] and H_2 storage.[51-54] Of all gas separation and storage applications, the focus of this thesis is the He recovery from CH_4 therefore, the literature review on membrane-based separation in MOFs will be held only for He/CH_4 separation. He recovery from CH_4 is a recent research interest, however, there are several experimental studies conducted on He/CH_4 separation. Ranjan et al.[55] synthesized continuous MMOF (microporous metal organic framework) membranes on porous α-alumina supports. They measured permeance of He through this membrane as 1.1×10^{-8}mol/m^2·s·Pa but did not report the He/CH_4 selectivity since CH_4 permeance was not measured. Takamizawa et al.[56] synthesized a MOF membrane, $[Cu(II)_2(O_2CPh)_4(pyz)]_n$, and measured the single-component permeability of 8 different gases including He and CH_4. Ideal selectivity of this MOF membrane was calculated as 7.3 for He/CH_4 separation. Yoo et al.[57] reported single-component gas permeation data through IRMOF-3 (isoreticular metal organic

framework) membrane for different gas molecules including He and CH_4. Ideal membrane selectivity of IRMOF-3 was reported as 1.6 for He/CH_4 separation. This study was followed by Zhao et al.[58] who synthesized one of the most widely studied IRMOFs, IRMOF-1 (MOF-5), as membranes. They reported He permeance through this membrane as 3.02×10^{-7}mol/m^2·s·Pa. Cao et al.[59] fabricated CuBTC membrane and measured single-component gas permeation data both for He and CH_4. Ideal selectivity of the membrane for He/CH_4 separation was reported as 2.07. They discussed that compared to the previously reported MOF membranes, CuBTC exhibited higher ideal selectivity for He under the condition of similar He permeance, while it exhibited higher He permeance with similar ideal selectivity. Hara et al.[60] measured single-component gas permeation data for 8 different gas molecules including He and CH_4 for ZIF-8 (zeolitic imidazolate frame-work) membrane and reported the ideal selectivity of this membrane as 2.4 for He/CH_4 separation. Kasik et al.[61] recently synthesized highly-crystalline ZIF-68 membrane and reported its He permeance as 2.6×10^{-7} mol/m^2·s·Pa. Even though there are plenty of experimental data available, the literature lacks a large-scale computational study on separation of He from CH_4. Chapter 3 of this thesis covers the first large-scale computational study that was conducted on 139 different MOF membranes to investigate their separation performances.

2.2. Adsorption of Quadrupolar and Polar Molecules in MOFs

To calculate adsorption of quadrupolar and polar molecules inside the materials, electrostatic interactions between adsorbate molecules and adsorbent in addition to the repulsion and dispersion potentials must be described. Electrostatic interactions are due to the partial atomic charges of adsorbent atoms and the polar nature of the adsorbates. Thus, the accuracy of a charge assignment method depends on its ability to describe the electrostatic potential of the adsorbent through chemically reasonable partial atomic charges. In classical atomistic simulations, the energy of a system consists of bonding ($E_{bonding}$) and non-bonding energies ($E_{non\text{-}bonding}$). $E_{bonding}$ is directly related to the bonded atoms and represented by bond, angle, and torsion force parameters that describe the

material's flexibility. The energy between non-bonded atoms includes van der Waals and the Coulomb interactions. While repulsion/dispersion interactions are described by typical 12-6 Lennard-Jones, electrostatic interactions are represented by Coulomb potential. 12-6 Lennard-Jones parameters are commonly taken from empirical force fields such as DREIDING,[62] UFF,[63] and TraPPE[64] (Transferable potentials for phase equilibria). Those parameters employed to describe the interactions between different types of atoms are computed by using Lorentz-Barthelot[65] or the Jorgensen mixing rules.[66] The generic force fields are usually transferable between atom types and are reasonable enough to describe the systems for applications where the adsorption is mainly driven by dispersion interactions such as methane storage,[18] hydrogen storage,[11] and CH_4/H_2 separation.[19] However, there are many applications where adsorption is highly sensitive to the electrostatic interactions such as CO_2 storage,[20] CO_2/N_2 separation,[21] CO_2/CH_4 separation,[22] and CO_2/H_2O separation.[23] In this case, atomic partial charges must be computed for each material. As electron density of solids is the major factor on the atomic charges, obtaining different values for the MOFs with small structural (or chemical) differences from each other is inevitable.[17]

Adsorption and diffusion processes are modeled with intermolecular interactions of adsorbate-adsorbate and adsorbate-adsorbent, and those interactions are non-bonded. Thus, the energy of a system is composed only of van der Waals and Columbic interactions.[17] Using very different charges than those employed for the force field parametrization inherently results in the variation between the calculated and experimental data since the force field will not be able to model intermolecular interactions.

CO_2/N_2 separation has gained attention as CO_2 can be captured from the flue gas that is emitted by power plants. Similarly, CO_2 can be removed from natural gas in order to obtain enriched and clean fuel. There are many studies that model CO_2 capture through MOF adsorbents.[49-50] Watanabe and Sholl[67] screened 1163 MOFs for CO_2/N_2 mixture and analyzed pore geometry of these materials to examine the possible molecular sieving

effects. Watanabe and Sholl used ChelpG method to compute framework point charges. Qiao et al.[68] performed atomically-detailed simulations under realistic operation conditions to investigate 4764 MOFs from CoRE-MOF (Computation-Ready Experimental MOF)[69] database for CO_2 capture from flue gas and natural gas. Atomic charges were assigned with the MEPO-QEq (MOF electrostatic potential optimized)[31] method. Qiao and colleagues analyzed the MOFs depending on the adsorbent evaluation criteria, metal type, and the structural characteristics and concluded that Ln-MOFs are favorable for CO_2 capture from flue gas and natural gas.[68] Wu et al.[70] employed a different charge assignment method, CBAC (Connectivity-based atom contribution method),[71] to investigate the separation performance of 105 MOFs for CO_2 capture from flue gas. The most important finding of this study was the first QSPR (Quantitative structure-activity relationship) model representing the effect of porosity and isosteric heat of adsorption on the adsorbent selectivity, which is highly essential regarding the provided insight into the design of new MOFs for a given application by tuning the porosity. In addition to the studies on the adsorbent-based separation of CO_2 from the flue gas and natural gas, membrane-based separation of these gases has also gained attention. Qiao et al.[72] screened 137953 MOF membranes for the ternary mixture of CO_2, N_2, and CH_4 gases. Qiao and colleagues used MEPO-QEq to assign partial atomic charges to the MOF atoms. They found out that while both diffusion and adsorption positively affect the CO_2/CH_4 separation, diffusion is the dominant factor on the N_2/CH_4 separation. Keskin and coworkers[73] investigated both adsorption-based and membrane-based separation performances of 20 different porous coordination networks (PCNs) for which the electrostatic potential was described with the EQEq method for CO_2/H_2 and CO_2/CH_4 mixtures. They also reported simple models as functions of the structural properties such as pore volume, surface area, and pore diameter in order to predict adsorption, diffusion, and permeation selectivities of PCNs for CO_2/H_2 mixture. Besides, Keskin and coworkers showed that a variety of PCN membranes can exceed the Robeson's upper bound for CO_2/CH_4 and CO_2/N_2 mixtures. Keskin and Sholl studied these mixtures specifically for MOF-5 (IRMOF-1) by performing binary adsorption and diffusion calculations.[39]

Canepa et al.[74] used a different charge assignment method, Bader,[75] for the screening of MOF-74 materials containing 25 different metal type for the adsorption of CO_2 and H_2O. They identified metal types that favor the adsorption of CO_2, which lead to the conclusion that a material containing those metals can be promising for CO_2 capture. Canepa and his colleagues' work showed that H_2O lowers the adsorption and transport properties of desired adsorbate molecule.[74]

In this section, only the studies that investigated the separation performances of MOFs for the gas mixtures where the adsorption and diffusion of the adsorbates are mainly driven by the electrostatic interactions were reviewed so far. Several different charge assignment methods were employed by these screening studies, however, none of them discussed the accuracy of these methods. There are several metrics to judge the performance of a charge equilibration method: the agreement with the experimental isotherms and the heats of adsorption, reproducibility of the electrostatic potential of the material, or the computational time efficiency. Therefore, sticking to only one of these metrics might not be really accurate to identify a method as the best. Each method has its own advantages and limitations for different evaluation criteria. Charge equilibration methods are the most efficient ones regarding the computational demand. Their ability to describe the electrostatic potential of a framework is mostly compared with the methods known to be the most accurate, namely density functional theory (DFT)-based methods. In literature, there are recent studies that investigate the performance of charge equilibration methods. Li et al.[76] compared the results from EQEq and DDEC methods by computing the Henry's law constants of gas species in CO_2/CH_4 and CO_2/N_2 mixtures for computation-ready, experimental (CoRE) MOFs.[69] They showed that 8 out of the top 15 materials from the screening of MOFs by using DDEC and EQEq charges were identical. By following the same strategy, Li et al.[77] also compared the Henry's law constants of CO_2, N_2, and H_2O by using charges calculated from EQEq and a more accurate method, namely REPEAT from plane-wave DFT calculations instead of DDEC. The authors who used only 15 MOFs in their study reported that the Henry's law constant

of H_2O is underestimated compared to the results obtained using REPEAT charges. Kadantsev et al.[31] tested their method named as MEPO-QEq on the validation set consisting of 693 MOFs by evaluating the CO_2 uptake and heat of adsorption of CO_2 in MOFs. They reported correlation coefficients of 0.98 for CO_2 uptakes and the heats of adsorption computed with MEPO-QEq charges when compared to those computed with the DFT-derived charges. However, to the best of our knowledge, a study that critically examines IQEq method and compares its performance with the other charge assignment methods is missing in the literature.

With these motivations, in Chapter 4 of this thesis, two different charge equilibration methods were compared, namely QEq and IQEq, in the sense of MOF rankings considering different adsorbent selection metrics. Moreover, the effect of different gas mixtures was also investigated, since CO_2/CH_4 mixture represents a quadrupolar/non-polar whereas CO_2/N_2 mixture represents two polar molecules-system. Adsorption data of 2244 MOFs for CO_2/CH_4 and CO_2/N_2 mixtures were obtained from the GCMC simulations where electrostatic potentials are described by these two methods. For each material, charges were assigned using QEq and IQEq during the molecular simulations and then results of the simulations were used to calculate four adsorbent selection metrics, adsorption selectivity, working capacity, adsorbent performance score (APS), and regenerability. The similarity between the MOF rankings created through two different charge assignment methods was examined by calculating correlation coefficients. It is essential to underline that the aim of this study was not to determine the most accurate method but to understand how the ranking of MOFs changes based on the simulations using QEq and IQEq, which were also compared to a method known to give more accurate charges, namely DDEC method.

Chapter 3
Computational Methods

3.1. MOF Datasets

In Chapter 4, we studied 139 MOFs. These MOFs were taken from the solvent-free MOF database constructed by Chung and coworkers[78] and some widely studied MOFs taken from our previous work[79] were also included to cover subfamilies of MOFs such as IRMOFs (isoreticular metal-organic frameworks) and ZIFs (zeolitic imidazolate frameworks). We specifically focused on MOFs which have limiting pore diameters (LPD) larger than the kinetic diameters of gases (3.73 Å for CH_4 and 2.56 Å for He) so that both CH_4 and He can pass through the membrane's pores. The complete list of the studied MOFs can be found in Table A.1 in Appendix A together with the Cambridge Crystallographic Data Centre (CCDC) names and common literature names of each material. Pore volumes, densities, surface areas, limiting pore diameters (LPDs) and the largest cavity diameters (LCDs) of MOFs were calculated using Zeo++ algorithm[80] and more details of these calculations can be found in the literature.[81] All these structural properties of MOFs were also listed in Table A.1.

In Chapter 5, we used the most recent collection of MOFs which is integrated within the CSD.[82] This database has 69666 MOFs than span a broad range of chemical and structural properties. The bound and unbound solvents in MOFs were removed by using the Python script available in the literature.[82] Physical properties of the materials were calculated using Zeo++ software package.[80] We then refined the collection in a way that all materials have nonzero gravimetric surface areas. Two different datasets were created for the mixtures that we used in our study. We set the PLD of materials to 3.75 Å for both

CO_2/CH_4 and CO_2/N_2 so that all molecules in the mixtures can be adsorbed into the pores. Although N_2 is a smaller molecule then CH_4, we preferred using the same database since the correlation coefficients will be compared for the two mixtures. Another factor that narrows down the dataset is the metal atom(s) of the material of interest because the electron affinities and ionization potentials that are included in the source code to apply the IQEq method are restricted to a group of metal, up to krypton, and palladium. Thus, the materials containing a metal that is not considered in the code were excluded from the dataset in Chapter 5.[30] However, it is perhaps possible to extend IQEq methodology to heavier atoms in periodic table by inserting experimental ionization potentials for the new atom types to the code. Wilmer and colleagues[29] reported ionization energies and atom energies for all elements up to atomic number of 8. For the atoms whose oxidation states are not given on the graphs, two-point interpolations might be performed to calculate their ionization potentials. Eventually, all these refinements led us to have 2244 different MOFs to be investigated for the separation of for CO_2/CH_4 and CO_2/N_2 mixtures.

In the second part of the thesis, QEq and IQEq methods were compared to DDEC as a DFT-based method expected to compute more reliable charges. For the comparison, the optimized structures were directly taken from CoRE MOF database[69] consisting of 3852 optimized MOF materials with already computed DDEC charges. 355 MOFs were common in the CoRE MOF database and the dataset consisting of 2244 materials with PLDs greater than 3.75 Å, which were later used with the IQEq method in order to obtain the optimized structures with IQEq charges.

3.2. Charge Assignment Methods

3.2.1. Charge Equilibration (QEq) Method

QEq method is the first charge equilibration method that is reported by Rappe and Goddard[27] back in 1991 and modified by many researchers to propose new charge assignment methods. This method assigns charges to atoms in the molecule based on the experimentally available ionization potential and electron affinity, and atomic radius.

Ionization potential is the energy needed to remove the valence electron while electron affinity means the energy needed to add an electron to a neutral atom. The energy of an atom that changes upon its charges can be written as a second-order Taylor expansion centered on neutral state:

$$E_A(Q) = E_{A0} + Q_A\left(\frac{\partial E}{\partial Q}\right)_{A0} + \frac{1}{2}{Q_A}^2\left(\frac{\partial^2 E}{\partial Q^2}\right)_{A0} \quad (1)$$

where, $E_A(Q)$ is the energy of atom A with charge Q. According to the equation (1), we can write the energy of an atom which loses $E_A(+1)$ or gains an electron $E_A(-1)$ from/to its neutral state. Thus, the Taylor expansion becomes:

$$E_A(+1) = E_{A0} + \left(\frac{\partial E}{\partial Q}\right)_{A0} + \frac{1}{2}\left(\frac{\partial^2 E}{\partial Q^2}\right)_{A0} \quad (2)$$

$$E_A(-1) = E_{A0} - \left(\frac{\partial E}{\partial Q}\right)_{A0} + \frac{1}{2}\left(\frac{\partial^2 E}{\partial Q^2}\right)_{A0} \quad (3)$$

where "0" denotes the neutral state. If equation (2) is subtracted from (3), electronegativity (χ_A) can be obtained as function of ionization potential (IP) and electron affinity (EA). Please note that:

$$IP = E_A(+1) - E_A(0) \quad (4)$$

$$EA = E_A(0) - E_A(-1) \quad (5)$$

so that

$$\left(\frac{\partial E}{\partial Q}\right)_{A0} = \frac{1}{2}(IP + EA) = \chi_A^0 \quad (6)$$

$$\left(\frac{\partial^2 E}{\partial Q^2}\right)_{A0} = IP - EA = J_{AA}^0 \quad (7)$$

Zero (0) the superscript is to indicate that the reference is the neutral state (Q=0). J_{AA}^0 corresponds to the Coulomb repulsion between two electrons in the outer atomic orbital,

which is also referred as idempotential or self-Coulomb integral. Atomic hardness is another term that refers to J_{AA}^0 in some sources.[29] Equation (1) can be rewritten by including χ_A and J_{AA}^0.

$$E_A(Q) = E_{A0} + \chi_A^0 Q_A + \frac{1}{2} J_{AA}^0 {Q_A}^2 \tag{8}$$

Equation (8) is valid only for the range between the electron needed to fill and empty the valence shell of an atom. For instance, for carbon atom, the equation is restricted between the charges from -4 to +4 and outside the range, $E_A(Q) = \infty$.[27]

χ_A and J_{AA}^0 are directly computed from the atomic data. Molecules for which χ_A and J_{AA}^0 are used, may contain all spins paired, however, atomic states have unpaired spins. Thus, for the exchange interactions that are not present in molecules but in atoms, atomic IP and EA must be corrected. There are generalized Mulliken-Pauling electronegativities and idempotentials for several elements.[27]

To derive the charge distribution, interatomic electrostatic interactions, $\sum_{A,B} Q_A Q_B J_{AB}$, must be considered. For a system of N atoms, total electrostatic energy consists of the energy of each atom and the pairwise interactions between these atoms.

$$E_A(Q_1 .. Q_N) = \sum_A (E_{A0} + \chi_A^0 Q_A) + \sum_{A,B} Q_A Q_B J_{AB} \tag{9}$$

where J_{AB} represents the Coulomb interaction between the unit charges located in the centers of atom A and B. J_{AB} depends on the distance between A and B. The derivative of total energy with respect to Q_A results in the atomic-scale chemical potential, μ_A:

$$\mu_A(Q_1 .. Q_N) = \frac{\partial E}{\partial Q_A} = \chi_A^0 + \sum_B J_{AB} Q_B \tag{10}$$

or

$$\mu_A(Q_1..Q_N) = \frac{\partial E}{\partial Q_A} = \chi_A^0 + J_{AA}^0 Q_A + \sum_{B \neq A} J_{AB} Q_B \quad (11)$$

$$\mu_1 = \mu_2 = \cdots = \mu_N \quad (12)$$

where μ_A is a function of the charges on all atoms. In equilibrium, the atomic chemical potentials, first derivative of Equation (9), are expected to be equal for all atoms. Thus, there will be N-1 equations after setting the χ_A equal for a system of N atoms.

Total charge of the system is simply the summation of the charges on all the atoms.

$$Q_{tot} = \sum_{i=1}^{N} Q_i \quad (13)$$

Thus, a total of N simultaneous equations and N unknowns can be solved to obtain partial charges for a given structure.[41]

For large distances between A and B, $J_{AB}(R)$ should be derived as:

$$J_{AB}(R) = \frac{14.4}{R} \quad (14)$$

where, 14.4 is for the unit conversion to enable R and J to be in the units of Å and electronvolts, respectively. If the charge distributions on center A and B overlap, Equation (14) does not hold, which results in $J_{AB}(R) \to \infty$ as $R \to 0$. For bonded atoms, this overlap and shielding corrections are quite large and the latter is computed as the Coulomb integral between the atomic densities. In the implementation of QEq, Rappe and Goddard described the atomic density in terms of a normalized ns Slater orbital for an atom whose outer valence orbital is ns, np, or nd.

$$\phi_{n\xi}^{slat} = N_n r^{n-1} e^{-\xi r} \quad (15)$$

where N_n is the normalization constant. The interatomic term, J_{AB}, then can be rewritten and calculated as a two-center electron repulsion integral that is constructed using the atomic densities .[41] Details of the calculation of this integral was reported by Kitao et al.[83]

3.2.2. Periodic Charge Equilibration (PQEq) Method

Unlike QEq, PQEq can be applied to periodic structures. The lattice effects on charge distribution are included in the expressions for chemical potential. The significance of electronegativities χ_A^0, idempotentials J_{AA}^0, and Coulomb integrals J_{AB} have been explained in the previous method. PQEq differs from the QEq with the extra term added to Equation (9). The summation over L corresponds to the effect of the lattice for a system of N atoms in a periodic lattice.[28, 41] Thus, the total electrostatic energy as a function of charge for a crystalline unit cell becomes as such in Equation (16).

$$E_A(Q_1..Q_N) = \sum_A (E_{A0} + \chi_A^0 Q_A + \frac{1}{2} J_{AA}^0 Q_A^2 + \frac{1}{2}\sum_{B\neq A} J_{AB} Q_A Q_B) + \frac{1}{2}\sum_{L\neq 0}\sum_A\sum_B J_{ABL} Q_A Q_B \quad (16)$$

Derivative of Equation (16) with respect to charge gives the molecular chemical potential:

$$\mu_{A,periodic}(Q_1..Q_N) = \frac{\partial E}{\partial Q_A} = \chi_A^0 + \chi_{c,A}^0 + J_{AA}^0 Q_A + \sum_{B\neq A} J_{AB} Q_B \quad (17)$$

where $\chi_{c,A}^0$ denotes the lattice electronegativity which is represented by Equation (18).

$$\chi_{c,A}^0 = \sum_{L\neq 0}\sum_B J'_{ABL} Q_B + \sum_{L\neq 0}\sum_B \frac{Q_B}{R_{ABL}} \quad (18)$$

J'_{ABL} is to express the cloud penetration which converges into zero with the interatomic distance R_{ABL}. The summation term in Equation (17) is a direct Coulomb interaction term and it can be calculated with the Ewald summation. Ewald summation method enables the electrostatic energy to get a finite value since the summations are performed over neutral cells. Ewald sum brings an iterative approach to finding the lattice charges. A set

of equations can be obtained with the chemical potential equalization given in Equation (18). Solving the equations starts with assigning initial values to the lattice charges. Those fixed values are changed and the lattice electronegativity $\chi^0_{c,A}$ is calculated using Equation (18) for each iteration step. The total charge of the system must be zero wherein lattice charges are given chemically realistic values.[28]

$$\sum_{i=1}^{N} Q_i = 0 \tag{19}$$

Thus, the lattice charges are checked if they stay in the region identified by the possible occupation of the valence shell of an atom. Iteration is terminated when the charge distribution is converged.[28]

3.2.3. Extended Charge Equilibration (EQEq) Method

EQEq method was developed by Wilmer et al.[29] in 2012. As an extended version of QEq, The EQEq uses higher ionization energies than the first level and only two global parameters: a dielectric strength and a modified parameter for hydrogen atoms. The most appealing feature of this method is its non-iterative approach, however, the QEq makes the energy minimization iteratively. In the EQEq, partial atomic charges are computed simultaneously by solving a set of equations. Such a nature lowers the computational demand and makes the method favorable for the screening of thousands of materials.

Computation of EQEq charges starts with the energy calculation. While in Equation (1), Taylor series was expanded around neutral state ($Q^* = 0$), in Equation (20), $E_A(Q)$ centers around a particular partial charge (Q^*), the oxidation state of an isolated atom. Thus, we obtain the following equation for the total energy of atom A:

$$E_A(Q) = E_A(Q^*) + \left(\frac{\partial E}{\partial Q}\right)_{Q=Q^*}(Q - Q^*) + \frac{1}{2}\left(\frac{\partial^2 E}{\partial Q^2}\right)_{Q=Q^*}(Q_A - Q^*)^2 \tag{20}$$

where, higher than quadratic terms were neglected so that the final set of equations become linear and can be solved simultaneously without an iteration. Considering

Equation (20), we can obtain the energy of atom A with one electron added $E_A(Q^* - 1)$ and removed $E_A(Q^* + 1)$ which is analogous with Equations (2) and (3). These relations led us to the following equations:

$$\frac{I_{Q^*+1} + I_{Q^*}}{2} = \left(\frac{\partial E}{\partial Q}\right)_{Q=Q^*} = \chi_{Q^*} \tag{21}$$

$$I_{Q^*+1} - I_{Q^*} = \left(\frac{\partial^2 E}{\partial Q^2}\right)_{Q=Q^*} = J_{Q^*} \tag{22}$$

where χ_{Q^*} and J_{Q^*} denote the nth electronegativity and nth hardness, respectively. I_n represents the nth ionization energy. Ionization energy (I_n) is the quantity of energy required to remove an electron from an isolated neutral atom, going from the charge of n-1 to n. On the other hand, electron affinity defines the energy needed to become a negative ion for a neutral atom (gaseous phase). Thus, I_0 means going from charge -1 to 0 and quantitatively equals electron affinity, with the opposite sign. Incorporating Equations (21) and (22) into Equation (20), we obtain de the following quadratic energy:

$$E_A(Q) = E_A(Q^*) + \chi_{Q^*}(Q - Q^*) + \frac{1}{2}J_{Q^*}(Q_A - Q^*)^2 \tag{23}$$

which can be used for every element in the periodic table and is based on measured quantities. In the original QEq method, atomic energies are much less likely to be calculated precisely because of the neutral state that the Taylor series is expanded around, especially for the transition metals with large positive charges. In the EQEq paper, measured ionization energies of all atoms with their associated atomic energies which are the summation of ionization energies are given. With an appropriate center for the Taylor expansion, the polynomial of the atomic energy curve can pass through more than two measured points so that the extrapolation can give more precise atomic energy values.

The total energy of the system of N atoms can be computed as the summation of individual atomic energies and the Coulomb interactions between the pair of atoms.

$$E_{sys}(Q_1,\ Q_2,..,\ Q_N) = \sum_{k=1}^{N}\left(E_{Ak}(Q_k^*) + \chi_{Q_k^*}(Q_k - Q_k^*) + \frac{1}{2}J_{Q_k^*}(Q_k - Q_k^*)^2 + E_{Ck} + E_{Ok}\right) \quad (24)$$

where, Q_k is the charge of k[th] atom. E_{Ok} is the damping term to prevent the infinite charge on the k[th] atom in case that it interact with an arbitrarily close atom. E_{Ck} denotes the pairwise interactions of atoms, the energy of the charge on the k[th] atom interacting with the charges of all other atoms in the system.[29] This Coulombic interaction terms are implemented to be computed in three forms: non-periodic, direct sum, and Ewald sum. Only the latest form is given in Equation (25) as it is the one used for our calculations in RASPA simulation package.[84]

$$E_{Ck} = \sum_{m\neq k^*}^{N} KQ_kQ_m\left(\sum_{u=-L}^{L}\sum_{v=-L}^{L}\sum_{w=-L}^{L}E_{Wr}(r_{km}) + E_{Wh}(h_{km})\right) - \frac{K}{\eta\sqrt{\pi}}Q_m^2 \quad (25)$$

where, K is constant which equals $1/4\pi\epsilon_r\epsilon_0$. ϵ_r and ϵ_0 are the dielectric strength and permittivity constant, respectively, and L is defined as the number of "shells" of repeating unit cells. r_{km} and h_{km} are the radial distances between k[th] and m[th] atom in real and frequency-space, respectively, which are calculated in terms of lattice parameters:

$$r_{km} = \left|\overrightarrow{r_{km}} + u\vec{a} + v\vec{b} + w\vec{c}\right| \quad (26)$$

$$h_{km} = \left|\overrightarrow{h_{km}} + u\overrightarrow{a^{-1}} + v\overrightarrow{b^{-1}} + w\overrightarrow{c^{-1}}\right| \quad (27)$$

$\vec{a}$, $\vec{b}$, and $\vec{c}$ are the translational symmetry vectors of the real-space lattice and $\overrightarrow{a^{-1}}$, $\overrightarrow{b^{-1}}$, and $\overrightarrow{c^{-1}}$ are those of frequency-space lattice. E_{Wr} and E_{Wh} are the components of Ewald sum. The real-space and frequency-space components of Ewald sum are computed as following:

$$E_{Wr}(r_{km}) = \frac{erfc\left(\frac{r_{km}}{\eta}\right)}{r_{km}} \tag{28}$$

$$E_{Wh}(h_{km}) = \left(\frac{4\pi}{\Omega}\right)\frac{e^{\left(\frac{h_{km}\eta}{2}\right)^2}\cos(\overrightarrow{h_{km}}\cdot\overrightarrow{r_{km}})}{h_{km}^2} \tag{29}$$

where, Ω is the volume of unit cell in real-space. η was defined as the splitting-parameter that decides how much of the energy will be summed in frequency versus real-space.

Finally, charges are computed after the energy minimization which is done through Equation (24) and that procedure is independent of the periodicity of structure. As similar to the other charge equilibration methods, total net charge of a system consisting of N atoms is calculated:

$$\sum_{k=1}^{N} Q_k = Q_T \tag{30}$$

where Q_T represent total charge of the system which is expected to be "zero" in periodic case. The minimization is ensured via Lagrange multiplies:

$$\nabla E_{sys} - \lambda\nabla\left(\sum_{k=1}^{N} Q_k - Q_T\right) = 0 \tag{31}$$

∇ is the gradient vector that spans the N dimensional space described by the partial charges. Next and the last step is to get the N-1 equations to solve simultaneously without any iteration. When the vector components of Equation (31) are paired:

$$\frac{\partial E_{sys}}{\partial Q_1} = \frac{\partial E_{sys}}{\partial Q_2} = \cdots = \frac{\partial E_{sys}}{\partial Q_N} = 0 \tag{32}$$

N-1 equations coming from Equation (32) and (30) giving the total net charge of the system makes N different equations with N unknowns so that the equation is solvable.

More detail about the mathematics of this method can be found in the Supporting Information of the EQEq paper.

3.2.4. Ionizing Charge Equilibration (IQEq) Method

IQEq is another electronegativity equalization method like QEq and IQEq. It has a new approach to calculating the particle atomic charges due to the way Taylor series is expanded and the hydrogen charges are computed.[30] To remember, QEq uses charge dependent parameters for hydrogen atoms while EQEq uses the global dielectric constant strength, ϵ, and another ad hoc parameter. The reference state that the Taylor series is expanded around was defined as the neutral state for QEq method. EQEq modified the reference state as the ionic charge for the metal cations while keeping the neutral state for the non-metals due to the inaccurate calculation of the ionization potential for the ionic bonded materials as MOFs. Keeping the center of Taylor expansion as neutral for the non-metals such as oxygen and nitrogen requires giving a background positive charge to the framework. To overcome the effect of this background charges, a minimization is done through the dielectric constant determined empirically. The only way to avoid the use of a background charge is to consider both positive and negative ionization states of atom in the calculations. Since determining the ionization state to supply as an input to the calculation can be challenging for some metals, an approach that enables the calculation of those as a part of the whole calculation rather than definition as an input, which was the case for EQEq, must be held. IQEq attains this calculation by assuming that the expansion charges equal to the atomic charges in an ideal solution. Then, those atomic charges and the Taylor expansion charges can be found iteratively in a self-consistent manner. Such an approach avoids the need of ionization states or formal charges. It is also reported by Wells et al.[30] that the IQEq is robust for the structures with ill-defined bonding and for which the standard empirical rules do not work to calculate the formal charges. It must be noted here that iterative nature of the IQEq costs a higher computational time.

In the EQEq, ionization energies are taken from the experimental data. Even if this approach is useful and proper for the atoms taking on positive charges, it fails for the atoms taking on negative charges. IQEq needs electron affinities after the first ionization potentials for the atoms taking on negative charges, but, they are not experimentally available. IQEq uses the data obtained from the high-level quantum mechanics calculations for electron affinities and ionization potentials. The energy data for several ionization state is available for each atom in periodic table up to krypton and also palladium.

First and second derivative of the energy can be calculated by using simple three-point derivative formulas with the ionization data that was obtained from the high-level quantum calculations. Definition of the overall energy of the molecule requires an expression for the Coulomb interaction. IQEq assumes that the charge on atom is spread over an atomic orbital such as a Slater as given in the QEq. Equation (33) and (34) give the energy interaction between two charges and the Slater function, respectively.

$$J_{ij}(r_{ij}) = \int \frac{\phi_i(r_i)\phi_j(r_j)}{|r_i - r_j|} dr_i dr_j \tag{33}$$

$$\phi_i(r_i) = N|r_i|^{n-1} e^{-\xi|r_i|} \tag{34}$$

However, evaluation of the integral in Equation (33) is quite complex so that an approximation is needed to have a practical solution. Slater integral was approximated by using the DasGupta-Huzinaga equation.[30, 85] Then, $J_{ij}(r_{ij})$ becomes:

$$J_{ij}(r_{ij}) = \frac{1}{|r_i| + \frac{1}{2}(J_{ii}e^{k|r_{ij}|} + J_{jj}e^{k|r_{ij}|})^{-1}} \tag{35}$$

where k is Klondike parameter which was taken as 0.1 as Oda and Hirono used.[86] In Equation (34), ξ_i, represents the size of the ith atom and it is fitted by using a relationship between average atomic radius, r_i, estimated from the crystal structure data and the scaling parameter, λ, and Slater function, as given in Equation (36):

$$\langle r_i \rangle = \lambda \frac{(2n-1)}{2\xi_i} \quad (36)$$

Default λ value defined in the source code shared by the authors is 0.8. Atomic radius varies with the calculated charge on the atom. Increasing the scaling parameter, radius can be more closely match that of the isolated ion.[30]

IQEq can be applied to both molecules and periodic structures. In the case of the periodic materials such as MOFs, lattice potential must be considered. In literature, the calculation of the lattice interaction in addition to the rewritten form of the energy between two charges can be found.[30]

3.3. Grand Canonical Monte Carlo (GCMC) Simulations

The Monte Carlo (MC) techniques help us to compute the equilibrium properties of classical man-body systems. "Classical" is a word that represents the core motion of constituent particles obeying the law of classical mechanics. In MC simulations, a system is assumed to be present in a large number of configurations (ensemble). Each configuration may have different properties, but, the ensemble average is supposed to show the general behavior of the macroscopic system.

We can simulate MC for any ensemble of interest. The general approach of the technique is similar for each ensemble. First the microstate probability distribution is determined for the ensemble, which defines the probability of finding a particular configuration (microstate). Then, a set of moves is identified, e.g. deletion, insertion, rotation, which will create fluctuations in energy, volume, or number of particles depending on the ensemble type. The terminal step is defining an acceptance criterion.

In adsorption simulation, we can obtain the average number of particles in a system as a function of external conditions like pressure or temperature of the reservoir that the adsorbent is in contact with.[87]Such information can be attained by using Grand Canonical (μVT) Monte Carlo (GCMC). In grand canonical ensemble, the chemical potential (μ), volume (V), and the temperature (T) are fixed. This ensemble can be confused with μPT

which would not be thermodynamically appropriate because there should be at least one extensive conserved quantity. In GCMC simulation, the temperature and chemical potential are imposed whereas the number of particles and the energy fluctuates.

As a real-life system, for adsorption, we can think of a system kept in a heat bath that particles can exchange between these two. Eventually, system comes to the equilibrium where the chemical potential and the temperature of the adsorbed gas and the gas outside the adsorbent must be equal. Thus, it is necessary to know chemical potential and the temperature of this reservoir to be able to compute the equilibrium concentration inside the adsorbent. Pressure is indirectly involved in these calculations as the pressure inside the adsorbent cannot be defined. It is related to the chemical potential with an equation of state so that the pressure of a gas corresponding to the given chemical potential can be calculated.

Figure 3.1 shows that a system (gas adsorption) in contact with a reservoir that imposes chemical potential and temperature on the system. The gas molecules in V can interact while those in $V - V_0$ act like an ideal gas and do not interact. Thus, when a particle is moved from the reservoir to the simulation box, the energy changes as much as the interaction potential of the atom moved with the all atoms in the box.

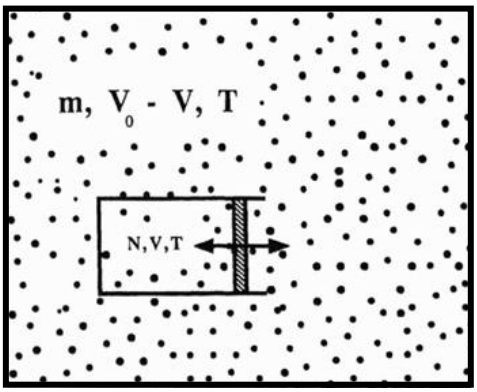

Figure 3.1. Schematic representation of an adsorbent in contact with a reservoir.

To understand the basis of GCMC, we should think of statistical mechanics. The partition function of a system of N interacting particles in volume V is expressed as follows:

$$Q(N,V,T) = \frac{V^N}{\Lambda^{3N} N!} \int ds^N \exp[-\beta U(s^N)] \tag{37}$$

where s^N represents the reduced coordinates (fractional coordinates). Λ is the thermal de Broglie wavelength which equals $\sqrt{h^2/(2\pi m k_B T)}$. k_B, h, and m denote the Bolzmann constant, Planck constant, and the mass of a gas atom, respectively.

Using Equation (37), we can write the partition function of a combined system of N interaction particles in volume V and M-N particles in volume $V - V_0$ as a multiplication of the partition functions of these two.

$$Q(N,M,V,V_0,T) = \frac{(V-V_0)^N\, V^N}{\Lambda^{3M}(M-N)!\, N!} \int ds^{(M-N)} \int ds^N \exp[-\beta U(s^N)] \tag{38}$$

The total partition function of this system is obtained by including all possible distributions of the M particles over the two subvolumes as shown in Equation (39).

$$Q(M,V,V_0,T) = \sum_{N=0}^{M} \frac{(V-V_0)^{(M-N)}\, V^N}{\Lambda^{3M}(M-N)!\, N!} \int ds^{(M-N)} \int ds^N \exp[-\beta U(s^N)] \tag{39}$$

Then, probability density for finding a system with N interaction particles in volume V and M-N particles in volume $V - V_0$.

$$\mathcal{N}(s^M; N) = \frac{V'^{(M-N)}\, V^N}{Q(M, V, V', T)\Lambda^{3M}(M-N)!\, N!} \exp[-\beta U(s^N)] \tag{40}$$

Considering that the reservoir is much larger than the system where the particles interact, we can say that M (total particle in the whole system) goes to infinity, so does V'. M/V' can be expressed with ρ, which denoted particle density. For an ideal gas the chemical potential is related to ρ: $\mu = k_B T\, ln\Lambda^3\rho$. The limit M/N goes to infinity so that Equation (39) becomes:

$$Q(\mu, V, T) = \sum_{N=0}^{\infty} \frac{\exp(\beta\mu N)\, V^N}{\Lambda^{3N} N!} \int ds^N \exp[-\beta U(s^N)] \tag{41}$$

The probability density corresponding to Equation (41) is:

$$\mathcal{N}_{\mu VT}(s^N; N) \propto \frac{\exp(\beta\mu N)\, V^N}{\Lambda^{3N} N!} \int ds^N \exp[-\beta U(s^N)] \tag{42}$$

Equations (41) and (42) are the general equations for GCMC simulations. In these expressions, all explicit terms related to the ideal gas system are avoided.

The set of moves used in a GCMC simulation consists of displacement, insertion, and deletion of the particles. A randomly selected particle is displaced randomly and this move is accepted with a probability:

$$acc(s \to s') = min(1, exp\{-\beta[U(s'^N) - U(s^N)]\}) \tag{43}$$

which can be derived by taking the ratio of the probability densities written for both s and s', as given in Equation (42). It must be noted that if a particle i is moved from s_i in the volume $V - V_0$ to the same reduced coordinate in the volume V, the potential energy U changes to $U(s^{N+1})$. Similarly, the potential energy of a particle moved from s to s' becomes $U(s'^N)$ being no longer $U(s^N)$.

If a particle is inserted at a random position in the interacting system, this move is accepted with a probability:

$$acc(N \to N+1) = \min\left[1, \frac{V}{\Lambda^3(N+1)} \exp\{\beta[\mu - U(N+1) + U(N)]\}\right] \qquad (44)$$

which can be derived in a similar way with the Equation (43) as the ratio between the probability densities calculated separately for N and N+1 particles in the interacting system. Chemical potential of the reservoir can be related to the reservoir's pressure due to equation of state. Similarly, a random particle in the system can be deleted, for which the acceptance probability:

$$\mathrm{acc(N+1 \to N)} = \min\left[1, \frac{\Lambda^3 \mathrm{N}}{\mathrm{V}} \exp\{-\beta[\mu + \mathrm{U(N-1)} - \mathrm{U(N)}]\}\right] \qquad (45)$$

The most time-consuming part of the simulation is calculating all interactions between the particles in the system. However, considering the intermolecular forces are present in short distances, we can get rid of the particles located outside of a fictitious circle that we will define. This restriction to limit the number of particles for which the interaction will be evaluated is called cut-off. Two times of the cut-off should be smaller than the length (each direction) of a unit cell. However, if the unit cell is non-cubic and does not have 90-90-90 angles, we should look at the orthogonal lengths. In this case, perpendicular width of the unit cell should be calculated, and the smallest perpendicular must be considered in the test: half of the smallest perpendicular width should be greater than the cut-off.[88] In Appendix B, the python script that helps to compute the cut-off distance by reading the cell properties from crystal structure file itself.

Non-bonding interactions can be calculated by considering Lennard-Jones (LJ) 12-6 potential as given in Equation (46).

$$V_{LJ} = 4\varepsilon_{ij}\left[\left(\frac{\sigma_{ij}}{r_{ij}}\right)^{12} - \left(\frac{\sigma_{ij}}{r_{ij}}\right)^{6}\right] \qquad (46)$$

where σ and ε represent the kinetic size (Å) and the energy parameter (K), respectively. V_{LJ} is the interatomic potential between the ith and jth atom which stay in distance r_{ij} to each other (from center to center). While the first term in parenthesis represents the short-range repulsion arises from the overlapping electron clouds, the second is the Van der Waals attraction. The parameters σ and ε are taken from the generic (transferable) force-fields such as DREIDING,[62] UFF,[63] and TraPPE[64]. Figure 3.2 shows the change in interatomic potential as function of the distance between the atoms. When atoms are very far from each other (r/σ), they cannot interact with each other so that (V/ε) becomes closer to zero which means interatomic potential is converged to zero. If atoms get close to each other as much as they become bound, the atoms will attract to each other and the interatomic potential between them will decrease until the point (r_{min}) of equilibrium where the minimum potential is reached. If the atoms keep getting close to each other after r_{min}, the interatomic potential starts increasing due to the repelsion forces occuring between the atoms. Once the $r = \sigma$ is reached, potential energy is minimized becoming zero. At that point, the pair of atoms are in a position where they are the most stable.

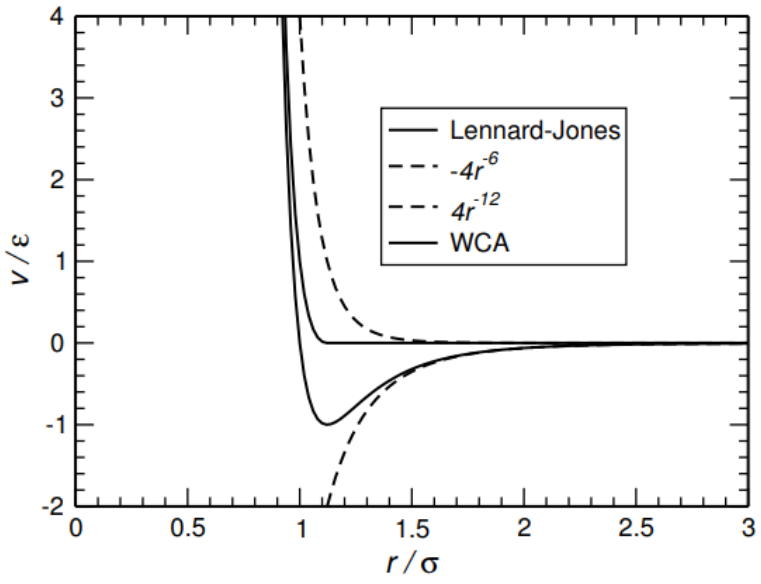

Figure 3.2. Lennard Jones 12-6 potential.[89]

In addition to repulsive and attractive interactions, Coulombic interaction must also be considered in the molecular modelling while calculating the total energy of the system by using Equation 3.47.

$$U_{LJ} = \frac{1}{4\pi\varepsilon_0}\frac{q_i q_j}{r_{ij}} \quad (47)$$

where q_i and q_j represent the partial atomic charges of ith and jth atoms, respectively, and ε_0 is the electric constant which also known as the absolute permittivity of free space. Partial atomic charges are computed by several methods of some were given in Section 3.2.

Another significant point in the GCMC simulations is the use of buoundary conditions. Especially, boundary effect is much more pronounced in small systems. Let us imagine a cubic lattice with 1000 atoms. 488 of these atoms are positioned on the surface and inevetiably they will be exposed to different forces than the other atoms in the bulk.[90] Periodic boundary conditions eliminates this surface effect while creating an infinite number of indentical unit cell around the computational system in the simulaiton. Thus each atom interacts with the atoms in the computational cell within the cut-off range in addition to their images in the adjacent boxes. If the potential is long ranged, there will be an interaction between an atom and its images in the adjacent boxes. This long-range potential can be handled with the Ewald summation.[90]As shown in Figure 3.3, while an atom leaves the box, its identical atom will enter. With an other word, if an atom moves, all identical images of this atom in each unit cell moves in the exact same direction.[90]

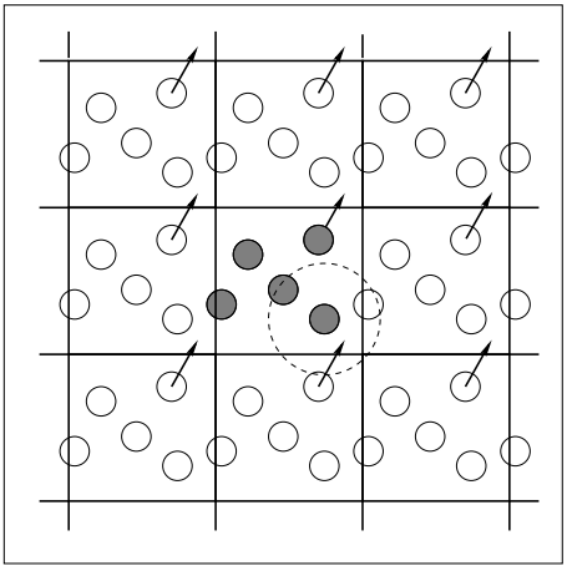

Figure 3.3. A 2D periodic system to represent the periodic boundary conditions.[89]

3.4. Equilibrium Molecular Dynamics (EMD) Simulations

Molecular dynamics (MD) simulations are used to study many-body systems and gives information about the dynamics of the system, e.g. diffusivity, viscosity, time-dependent responses to perturbations.[89] There are two types of MD simulations depending on the calculation basis: classical and ab-initio MD. While the former technique solves the classical equations of motion for a system of N interacting molecules, the latter solves the problem using quantum equations, from the first principles, which requires a high computational time.[90] Time-scale of MD simulations range from picoseconds to several nanoseconds which cannot be surpassed regardless of the computational power.

A classical MD simulation starts with initialization step to locate the particles in the framework. The number of particles to load in the framework is computed by using GCMC simulation. Using Monte Carlo technique, lowest-energy configuration is identified to find the initial positions of the guest molecules. Initial velocity of the particles is assigned randomly, and the next step starts. During the equilibration steps,

MD calculations are performed. Newton's equation of motions is solved to compute the velocities.

$$F_i = m_i \ddot{r}_i \tag{48}$$

where m_i, r_i, and F_i are the mass, cartesian coordinate vector of the ith atom, and the force on the ith atom, respectively. The force on the particles is caused by the interatomic interactions and is the derivative of the potential with respect to the position. Being the most computationally demanded part of the simulation, potentials are computed by considering LJ 12-6 and Coulombic interactions as introduced in Section 3.3. Of the several ensembles, the one used in our membrane calculations is the NVT ensemble (NVT = constant number of molecules, volume, and temperature).

The ordinary differential equations like Newton's equation of motion given in Equation 3.48 are solved with the finite difference approach. The idea behind this approach is to predict the position and velocities of the atoms at a later time, t+δt, by using the position and velocity of the atoms are initialized at time t through a time-dependent equation. The time step, δt, is much smaller than the standard time spent by a molecule to travel its own length [90]. Also, the time step should be as small as the energy of the system is conserved. The Verlet's predictor algorithm is perhaps the most used method for integrating the Newton's equation of motion. This method is based on the positions ($r(t)$ and $r(t-\delta t)$) and accelerations ($\ddot{r}(t)$) as shown in Equation 3.49.

$$r(t+\delta t) = 2r(t) - r(t-\delta t) + \delta t^2 \ddot{r}(t) \tag{49}$$

There is no any velocity term in the Equation 3.49 advanced by the Verlet's algorithm because the velocity terms disappear when the two Taylor expansions around $r(t)$ below are summed.

$$r(t+\delta t) = r(t) + \delta t \dot{r}(t) + \left(\frac{1}{2}\right)\delta t^2 \ddot{r}(t) + \cdots \tag{50}$$

$$r(t-\delta t) = r(t) - \delta t\dot{r}(t) + \left(\frac{1}{2}\right)\delta t^2\ddot{r}(t) + \cdots \quad (51)$$

Thus, position of the atoms in later times can be calculated without the velocity of the atoms. However, they might be useful to estimate the total energy of the system through the kinetic energy of the particles.

$$v(t) = \frac{r(t+\delta t) - r(t-\delta t)}{2\delta t} \quad (52)$$

The terms in the numerator of the Equation 3.52 shows that the Verlet's algorithm is time-reversible due to the r terms being symmetrical.

Once the new velocities, positions, and the accelerations are predicted for the time $t + \delta t$, the force on the atoms is recalculated by using those predicted at time $t + \delta t$. Then, the predicted velocities, positions, and the accelerations are corrected with the new ones calculated from the new force using Equation 3.48. This procedure is repeated until the total simulation step defined is reached.

In MD simulation, three steps are defined; initialization, equilibration, and production. In initialization, the initial position of the atoms is determined using Monte Carlo technique in NVT ensemble while the initial velocity of the atoms is assigned randomly. Equilibration and production steps are the same regarding the procedure and the algorithm they follow. However, in equilibration step, steeper fluctuations are observed on the pressure, energy, or temperature. In order to get rid of these sudden and steep fluctuation, we perform equilibration step and then start the production. In both steps, velocity of the particles is rearranged by controlling the temperature and pressure of the system via Nosé-Hoover[91-92] or the Berendsen[93] methods.

MD simulations in NVT ensemble in Chapter 4, were performed to calculate the corrected diffusivity ($D_{o,i}$) of single-component gases. The corrected diffusivity represents the collective motion of the adsorbed molecules and it was calculated based on the number

of molecules (N), time (t), dimensionality number for diffusion (d), the three-dimensional position vector of molecule l of species i at time t, $r_{il}(t)$:

$$D_{o,i} = \lim_{t\to\infty} \frac{q}{2dNt} \left\langle \left(\sum_{l=1}^{N_i} [r_{il}(t) - r_{il}(0)] \right)^2 \right\rangle \quad (53)$$

Corrected diffusivities were computed at average loadings calculated from the GCMC simulations performed at the feed and permeate pressures of the membrane. Single-component transport diffusivity (D_t) was then obtained by multiplying the corrected diffusivity with the thermodynamic correction factor $\left(\frac{\partial lnf}{\partial lnc}\right)$, the partial derivative relating the adsorbed gas amount, c, and bulk phase fugacity, f,:[94]

$$D_{t,i}(c) = D_{o,i}(c)\ \frac{\partial lnf_i}{\partial lnc_i} \quad (54)$$

In order to compute permeability of gas species in the mixtures, self-diffusivities of each gas component were computed using the EMD simulations. The self-diffusivity of each species was described as the motion of individual tagged particles. In an isotropic three-dimensional material, self-diffusivity is related to the mean-squared-displacement (MSD) of tagged particles by the Einstein's relation:[95]

$$D_{self,i} = \lim_{t\to\infty} \frac{q}{2dt} \left\langle \frac{1}{N} \sum_{j=1}^{N} \left[\vec{r}_j(t) - \vec{r}_j(0)\right]^2 \right\rangle \quad (55)$$

Here, $\vec{r} \rightarrow$ (t) is the position of the tagged particle at time t, N is the number of particles, d is the dimensionality number for diffusion, and the angular brackets represent the ensemble average. Self-diffusivities of gas species were computed at the direct adsorbed loadings of the gases calculated from the GCMC simulations performed at the feed pressure of the membrane.

The Nosé-Hoover thermostat[96] was used in NVT-EMD simulations. At least 20 independent EMD simulations with a length of 16 ns were performed to compute

corrected-diffusivities of gases since using a large number of independent trajectories is vital to accurately compute these diffusivities. Initial states of EMD simulations were created with the appropriate loadings determined from the GCMC simulations. Each system was first equilibrated with EMD for about 20 ps prior to taking data. He loadings were generally very low compared to the CH_4 loadings since He is weakly adsorbed into the pores of MOFs. Therefore, the size of the simulation volume was increased up to 12 × 11 × 11 unit cells to contain enough He atoms in order to increase the statistical accuracy of the EMD simulations. More details of using GCMC and EMD simulations to obtain adsorption equilibria and diffusion coefficients in various MOFs were described in our previous studies.[97-98]

3.5. Adsorption Calculations

GCMC simulations were performed to model the gas adsorptions in each framework at 0.1 and 1 bar. We performed mixture GCMC simulations as implemented in the RASPA molecular simulation software[84] at room temperature. Four different type of moves including rotation, translation, regrowth, swap of a molecule, and identity exchange of molecules were considered. Simulation cells were constructed to be at least 26 Å in each direction. Periodic boundary conditions were applied in all simulations. For each MOF, total 10,000 cycles were used, which from the first 5,000 cycles were for initialization followed by 5,000 cycles to calculate ensemble averages.

Dispersion/repulsion and electrostatic interactions were described by Lennard-Jones 12-6 and Coulombic potentials, respectively. The potential parameters of materials were taken from Universal Force Field[63] while estimating the dispersion and repulsion interactions between the gas and the MOF material. Gas molecules were modelled by using potentials from the TraPPE force field for N_2,[99] CH_4[64], and CO_2[100] gas molecules. Lorentz-Barthelot combining rules were employed for each pairwise interaction. MOFs were assumed to be rigid in all simulations so that a considerable amount of computational time was saved. Since the size of gas molecules (3.4-3.75 Å) used in this

study are relatively smaller compared to the pore sizes of MOFs, flexibility is expected to have a negligible effect on the gas adsorption.[101]

To show that the IQEq method was accurately used for the charge assignments in this thesis, we performed sample calculations to reproduce the CO_2 adsorption data reported in the original paper.[30] For those calculations, we increased number of cycles to 2×10^6 cycles to be in line with the original and computed adsorption data for only 0.1 and 1 bar.

3.6. Calculating Adsorbent and Membrane Properties of MOFs

The shell model was applied to calculate the single-component, steady state fluxes of gases through a MOF membrane based on Fick's Law:[94]

$$J_i = -D_{t,i}(c) \cdot \nabla c_i \tag{56}$$

Here, ∇c is the concentration gradient of the adsorbed species based on the difference between the feed and permeate pressures of the membrane, which was set to 2 bar and 1 bar, respectively, in Chapter 4. D_t is the transport diffusivity for adsorbed species.

Gas flux (J) in MOFs was then converted to gas permeability (P) using the following formula:

$$P_i = \frac{J_i}{\Delta P / L} \tag{57}$$

where ΔP is the pressure drop and L is the membrane thickness. Ideal selectivity (S^{ideal}) of the MOF membranes was calculated as the ratio of gas permeabilities of two components:

$$S_{i/j}^{ideal} = \frac{P_i}{P_j} \tag{58}$$

In binary mixture case, permeability of each gas species in the mixture was calculated as suggested in the literature:[102]

$$P_i^{mix} = \frac{\phi \cdot D_{i,self} \cdot c_i}{f_i} \tag{59}$$

where P_i^{mix} is the permeability of species i (mol/m·s·Pa), ϕ is the porosity of the materials which are given in Table A.1, $D_{i,self}$ is the self-diffusivity of species i in the mixture (m^2/s) c_i is the concentration of i at the feed side of the membrane (mol/m^3), and f_i is the bulk phase fugacity of i (Pa). This approach assumes that the self-diffusivities are estimated at the feed side of the membrane and the permeate side is kept under vacuum. Therefore, membrane selectivities of MOFs were reported for a feed pressure of 2 bar and permeate pressure of vacuum. Gas permeabilities are generally reported in Barrer (10^{-10} cm^3(STP)·cm/s·cm^3·cm Hg) in the literature to make comparisons between different membrane materials, therefore we converted our gas permeabilities to this unit. Mixture selectivity of the membranes (S^{mix}) was then calculated as the ratio of gas permeabilities of the components in their mixtures:

$$S_{i/j}^{mix} = \frac{P_i^{mix}}{P_j^{mix}} \tag{60}$$

In order to understand the effects of adsorption and diffusion of gases on the separation performances of the MOF membranes, we also calculated adsorption and diffusion selectivities of MOFs. Ideal adsorption selectivity was calculated as the ratio of adsorbed amounts of single-component gases (c_i) whereas mixture adsorption selectivity was calculated as the ratio of the molar fractions of the adsorbed gas molecules (x_i) in the mixture normalized by the ratio of molar fractions of the bulk gas (y_i):

$$S_{ads,i/j}^{ideal} = \frac{c_i}{c_j} \tag{61}$$

$$S_{ads,i/j}^{mix} = \frac{(x_i/x_j)}{(y_i/y_j)} \tag{62}$$

Similarly, ideal and mixture diffusion selectivities were estimated as follows performing the EMD simulations at the adsorbed loadings (c_i, c_j) of the gases.[97, 102-103]

$$S_{diff,i/j}^{ideal} = \frac{D_{t,i}(c_i)}{D_{t,j}(c_j)} \tag{63}$$

$$S_{diff,i/j}^{mix} = \frac{D_{i,self}(c_i, c_j)}{D_{j,self}(c_i, c_j)} \tag{64}$$

3.7. Adsorbent Evaluation Metrics

To predict the separation performance of materials, we considered four common evaluation metrics such as adsorption selectivity (S_{ads}), working capacity (ΔN), adsorbent performance score (APS), and regenerability (R). Mathematical definitions of these metrics are represented in Table 3.1.

Table 3.1. Adsorbent selection metrics used in the ranking of MOFs.

metric	formula
adsorption selectivity	$S_{ads(1/2)} = \frac{x_1/x_2}{y_1/y_2}$
working capacity	$\Delta N = N_{ads} - N_{des}$
adsorbent performance score	$APS = S_{ads(1/2)} \times \Delta N_1$
percent regenerability	$R = \frac{\Delta N_1}{N_{1,ads}} \times 100$

Adsorbent selectivity is defined as the ratio of compositions of the adsorbed gases (x) in the adsorbent normalized by the ratio of bulk phase compositions (y) of the components. In Table 3.1, subscript 1 represents the strongly adsorbed species (mixture 1,2: CO_2) and while subscript 2 represents the weakly adsorbed species (mixture 1: CH_4, mixture 2: N_2). Working capacity defined as the difference between the gas uptakes at the adsorption and desorption pressures in the unit of mol gas per kg framework.[104] In this work, ΔN is calculated only for strongly adsorbed species in the mixtures. APS is a recently developed

metric defined by Chung et al.[105] and is the product of working capacity and the adsorption selectivity. Regenerability (R%) is another metric used in this work. Being an important metric in the design of PSA units, *R*% is defined as the percent regeneration of the adsorption sites under desorption pressure.[104, 106] All those metrics were calculated for both CO_2/CH_4 (50/50) and CO_2/N_2 (15/85) mixtures at room temperature and at adsorption pressure of 1 bar and desorption pressure of 0.1 bar. To make an efficient and industrially reasonable ranking, the materials having *R*% smaller than 85% were eliminated. Then, the remaining materials were ranked based on their APSs which consider both working capacity and the adsorption selectivity.

Chapter 4

MOF Adsorbents and Membranes for He/CH_4 Separation*

We validated the accuracy of our computational approach used to predict the membrane permeabilities and selectivities of MOFs by comparing the results of simulations with the experiments in several previous studies.[107-108] For example, we showed the good agreement between our simulations and experiments for single-component CH_4 permeability through different MOF membranes.[19] Since this is the first study in the literature that predicts He permeability through MOF membranes using molecular simulations, we validated the accuracy of our approach by comparing simulation results of single-component He permeability with the available experimental data for 7 different MOF membranes, CuBTC,[59] MOF-5,[58] IRMOF-3,[57] ZIF-8,[60] ZIF-68,[61] MMOF,[55] and $[Cu(II)_2(O_2CPh)_4(pyz)]_n$.[56] All of our atomically-detailed simulations were performed at the same conditions, membrane operating pressure and temperature, with the experiments and these conditions were listed in Table A.2. He permeability was reported at three different temperatures for CuBTC membrane and we did the simulations at all these temperatures. Figure 4.1 shows that there is a very good agreement between experiments and simulations leading to a high regression coefficient. Our simulations slightly overestimated experimental gas permeability of MOF membranes, which can be attributed to the perfect, defect-free membrane assumption of the molecular simulations. During the synthesis of membranes from crystalline materials, defects may be formed

* The results given in this chapter were published in Separation and Purification Technology with following reference: Kadioglu, O., & Keskin, S. (2018). Efficient separation of helium from methane using MOF membranes. *Separation and Purification Technology, 191*, 192-199.This chapter is the reformatted version of the mentioned research paper.

and these defects may reduce the gas permeability of the membranes. However, molecular simulations do not consider these defects and assume perfect membranes made of single-crystals. Overall, the good agreement between experiments and simulations supports the validity of our computational approach to accurately estimate He permeability and hence He/CH_4 selectivity of the MOF membranes.

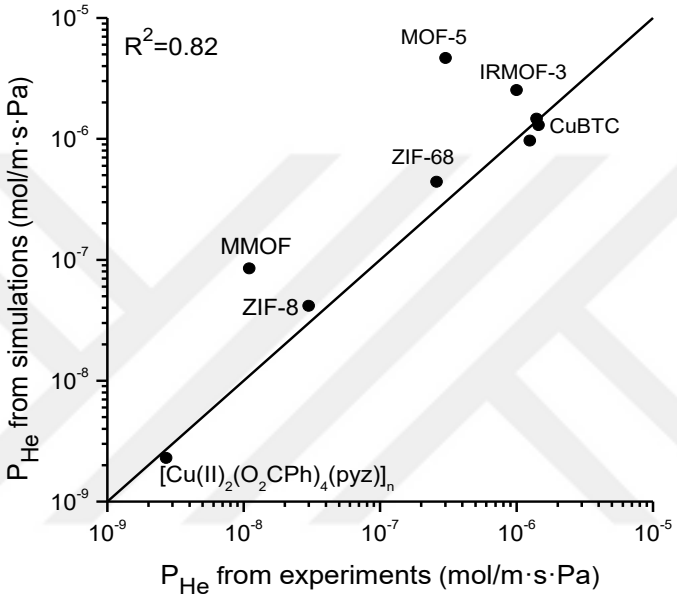

Figure 4.1. Comparison of the simulations with the experimental measurements for He permeability of several MOF membranes.

Motivated from this agreement, we predicted both single-component and mixture permeabilities of He and CH_4 for 139 different MOFs, which have not been fabricated as membranes yet. Figure 4.2 represents selectivity of MOF membranes for He/CH_4 separation as a function of He permeability. Separation performances of MOF membranes were computed at a feed pressure of 2 bar at room temperature. Data on this figure was produced using the adsorption and diffusion data obtained from the single-component He and CH_4 simulations. Therefore, we will discuss ideal He/CH_4 selectivity and single-component He permeability of the MOF membranes for this figure. The red

line divides the plot into two regions to show the gas preference of the membranes. While a significant number of MOF membranes, 131 out of 139, were identified to be CH_4 selective, 4 MOFs were found to be He selective. Selectivities of 4 membranes were computed to be unity which means these MOFs have no preference either for He or for CH_4 and they cannot find place in practical applications. In order to compare He/CH_4 separation performance of MOF membranes with traditional polymeric membranes, we included the Robeson's upper bound, the solid black line in Figure 4.2. [109] This bound was created empirically from the experimental studies on polymeric membranes for He/CH_4 separation.[109-110] Discovery of the new membranes that can exceed this bound is very important because new membrane materials that can exhibit higher selectivity and/or higher gas permeability than the widely used commercial polymeric membranes have the potential to start up a new and efficient He separation technology. According to the upper bound, He/CH_4 selectivities of polymeric membranes range from 10^{-1} to 10^3 whereas their He permeabilities are between 10-10^5 Barrer. Our molecular simulations showed that MOF membranes' He/CH_4 selectivities are in the range of 0.015-34.4 whereas their He permeabilities are between 1×10^4-6.7×10^5 Barrer. Figure 4.2 shows that MOF membranes are located on the bottom-right corner of the Robeson's upper bound since MOFs generally have lower He selectivities but higher He permeabilities compared to the polymeric membranes. 66 of the MOF membranes we examined in this work could exceed the upper bound. Most MOF membranes exceed the upper bound due to their high He permeabilities and some exceed as a result of combination of high He selectivities and high He permeabilities. It must be also noted that we extended the upper bound with the dashed line to better represent the high He permeabilities of MOFs. These high gas permeabilities of MOFs can be attributed to the higher porosities of the MOFs compared to the polymers.

We also compared the He separation performances of MOF membranes with the zeolite membranes. For example, DDR-type zeolite membrane was reported to exhibit a very high ideal selectivity, 24.4, for He/CH_4 separation but it suffers from low He permeance,

4.2×10^{-8} mol/m^2·s·Pa, corresponding to 3.7×10^{2} Barrer for a membrane thickness of 3 μm.[111] Similarly, several other zeolite membranes were reported to have low He permeance. For example, single-component He permeances of MFI,[112] DD3R,[113] NaA,[114] and ZSM-5[115] type zeolite membranes were reported to be in the range of 4×10^{-8}-8×10^{-7} mol/m^2·s·Pa which corresponds to 4.2-478 Barrer based on the membranes' thicknesses. This comparison shows that MOFs we considered in this work have significantly larger He permeabilities than the zeolite membranes.

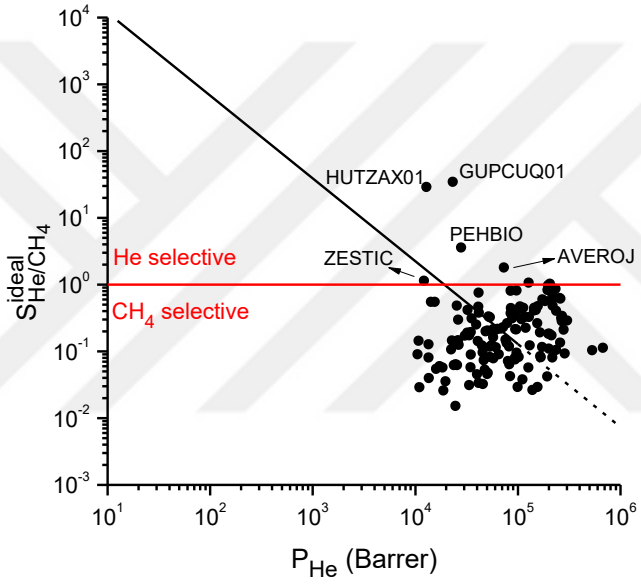

Figure 4.2. Ideal He/CH_4 selectivity and single-component He permeability of 139 MOF membranes. Black line represents Robeson's upper bound[109] and red line shows the selectivity preference of MOF membranes.

We showed the promising MOF membranes that are He selective over CH_4 in Figure 4.2. These are GUPCUQ01, HUTZAX01, PEHBIO, and BIYTEJ. We also listed permeabilities and selectivities of the top 3 MOFs in Table 4.1, omitting BIYTEJ since its selectivity is less than 3. Ideal He/CH_4 selectivities of the MOF membranes listed in Table 4.1 are significantly higher (3.6, 29, and 34.4) than the ones reported for the experimentally fabricated MOF membranes (1-3) we discussed at the beginning. These

high He selectivities of the MOF membranes can be explained by the individual effects of the adsorption and diffusion of gases in the pores. Ideal selectivities were calculated by the ratio of single-component gas fluxes, multiplication of the ratio of transport diffusivities of gases with the ratio of the concentration gradient of the adsorbed species as shown in Equation (57). Adsorption always favors CH_4 over He in all MOFs since He has weaker interactions with the framework atoms compared to CH_4. Therefore, the ratio of concentration gradient of He to CH_4 is always less than unity, ranges from 0.006 to 0.15. In other words, CH_4 adsorption is stronger, at least 6 times, than the He adsorption in the MOFs' pores. In contrast to adsorption, diffusion favors He over CH_4 in all MOF membranes. Transport diffusivity of He (2.68×10^{-4}-8.01×10^{-3} cm^2/s) was computed to be at least one order of magnitude higher than that of CH_4 (3.92×10^{-7}-4.25×10^{-3} cm^2/s) in most MOFs since He is a lighter and smaller gas compared to CH_4. The ratio of transport diffusivity of He to CH_4 is in the range of 0.92-1140. When diffusion preference for He overcompensates the adsorption preference for CH_4, the MOF membrane becomes He selective. For example, GUPCUQ01 is the MOF with the highest ideal selectivity of 34.4 in Table 4.1. The ratio of concentration gradient of He to CH_4 is very low, 0.052 in this MOF but this low value is overcompensated by the high diffusion selectivity towards He, 657.51, and the MOF becomes strongly He selective membrane.

Table 4.1. Predicted separation performances of the top performing He selective MOF membranes. Ideal and mixture selectivities for adsorption and diffusion were also reported. The first component in the subscript represents the selected one over the second.

	P_{He}^{ideal} (Barrer)	$P_{CH_4}^{ideal}$ (Barrer)	S_{He/CH_4}^{ideal}	P_{He}^{mix} (Barrer)	$P_{CH_4}^{mix}$ (Barrer)	S_{He/CH_4}^{mix}	$S_{ads,CH_4/He}^{ideal}$ ($S_{ads,He/CH_4}^{ideal}$)	$S_{ads,CH_4/He}^{mix}$ ($S_{ads,He/CH_4}^{mix}$)	$S_{diff,He/CH_4}^{ideal}$	$S_{diff,He/CH_4}^{mix}$
GUPCUQ01	2.32×10^4	6.74×10^2	34.43	1.14×10^4	3.85×10^2	29.62	19.10 (0.052)	21.74 (0.046)	657.51	644.13
HUTZAX01	1.28×10^4	4.42×10^2	28.97	1.03×10^3	2.43×10^2	4.26	39.37 (0.025)	182.34 (0.005)	1140.68	776.19
PEHBIO	2.79×10^4	7.81×10^3	3.57	1.76×10^4	5.71×10^3	3.08	22.54 (0.044)	26.08 (0.038)	80.59	80.26

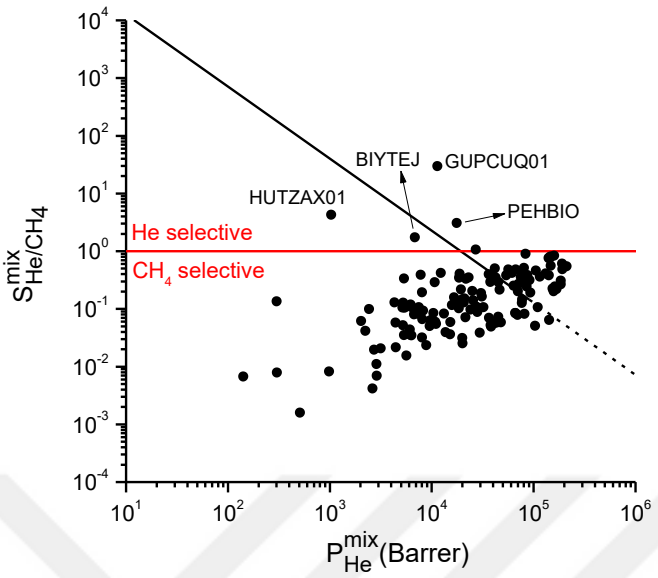

Figure 4.3. Mixture He/CH_4 selectivity and He permeability of 139 MOF membranes. Black line represents Robeson's upper bound[109] and red line shows the selectivity preference of MOF membranes.

Figure 4.3 also represents the He/CH_4 selectivity of MOF membranes as a function of He permeability but this time the data was produced using the results of molecular simulations performed for an equimolar binary gas mixture. Therefore, we will refer this selectivity as the mixture selectivity. Most of the membranes, 133 out of 139, were CH_4 selective whereas 4 MOFs were identified as He selective and 2 MOFs were not selective. Same three MOFs, GUPCUQ01, HUTZAX01 and PEHBIO were found to be promising with the highest He/CH_4 selectivities. Mixture selectivities of MOFs were found to be in the range of 0.0016-29.62, lower than the ideal selectivities shown in Figure 4.2. He permeabilities were estimated in the range of 1.4×10^{2}-2.1×10^{5} Barrer, an order smaller than the single-component He permeation shown in Figure 4.2. Smaller number of MOF membranes, 40, could exceed the upper bound compared to Figure 4.2. Table 4.1 also shows that mixture He/CH_4 selectivities of MOF membranes are less than their ideal selectivities. For example, GUPCUQ01 was identified to have the highest mixture selectivity, 29.62, among all MOFs but this value is lower than its predicted ideal

selectivity, 34.4. There is a significant decrease in the selectivity of HUTZAX01 when a binary mixture was considered instead of the single-component gases. The ideal He/CH_4 selectivity of this membrane was predicted to be 29 whereas the mixture selectivity was computed to be significantly lower, 4.3. For PEHBIO, the mixture selectivity, 3.1, is slightly lower than its ideal selectivity, 3.6. This comparison shows that ideal selectivities predicted using the single-component adsorption and diffusion data may overestimate the mixture selectivities. Therefore, it is important to use mixture simulation data rather than the single-component data to make reliable predictions about the potential of MOF membranes.

In order to understand the physical reasons behind the differences in ideal and mixture selectivities and permeabilities of MOF membranes shown in Figure 4.2 and Figure 4.3, we examined the changes in adsorption and diffusion selectivities of MOFs when a binary gas mixture was considered instead of single-component gases. We first focused on the adsorption selectivities of MOFs. In most experimental studies of MOFs, single-component adsorption isotherms of gases have been measured and the adsorption selectivity of MOF is simply reported as the ratio of adsorbed amounts of single-component gases. This selectivity is known as ideal adsorption selectivity and it represents the intrinsic separation capacity of a material based on adsorption. It has been showed that ideal adsorption selectivity may significantly differ from mixture adsorption selectivity when competition effects between two gas species become dominant during adsorption[116]. We computed both the ideal and mixture adsorption selectivities of MOFs using the data obtained from single-component and mixture GCMC simulations, respectively. Figure 4.4 compares adsorption selectivities calculated for an equimolar mixture at four different pressures 0.01, 1, 2, and 10 bar at 298 K with the ideal adsorption selectivities of the MOFs. All MOFs are CH_4 selective in adsorption as discussed before, therefore adsorption selectivities in Figure 4.4 are given as CH_4/He rather than He/CH_4. Results show that ideal and mixture adsorption selectivities are almost same at a pressure close to zero, 0.01 bar. The regression coefficient (R^2) between ideal and mixture

selectivities is 0.998 at 0.01 bar. The deviation between ideal and mixture adsorption selectivities increases as the pressure increases as shown in Figure 4.4. For example, the R^2 values are 0.85, 0.78, 0.70 for 1, 2, 10 bar, respectively. This deviation can be explained by the multi-component mixture effects which become dominant at high pressures. As the loading increases in the MOFs' pores, gas molecules compete with each other for the same adsorption sites. Adsorption favors CH_4 over He in the mixture and the more strongly adsorbed CH_4 molecules exclude the weakly adsorbed He molecules in the pores at high pressures. As a result, mixture adsorption selectivities for CH_4 over He become always higher than the ideal adsorption selectivities as shown in Figure 4.4. In other words, mixture adsorption selectivity computed at 2 bar for He/CH_4 mixture is less than the ideal adsorption selectivity. This is one reason of the lower membrane selectivities observed in Figure 4.3 compared to Figure 4.2.

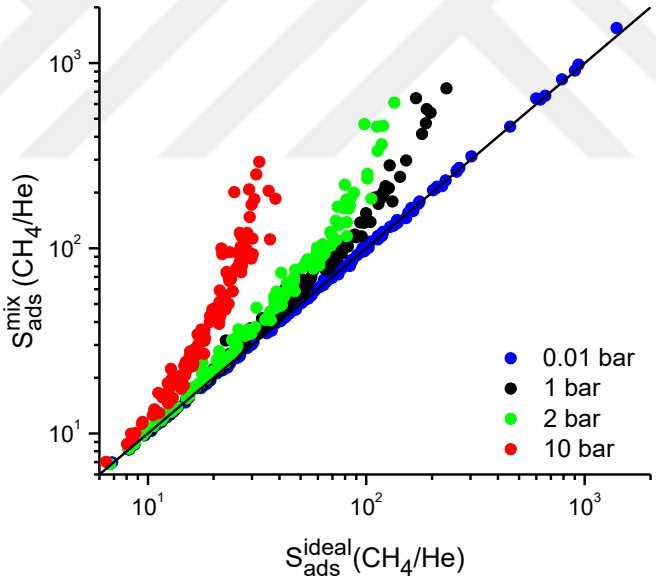

Figure 4.4. Comparison of ideal and mixture adsorption selectivities of MOFs at 0.01, 1, 2, 10 bar. Bulk composition of the mixture is equimolar. Selectivities are given for CH_4 over He since adsorption favors CH_4.

At that point one may think about the effect of composition of the gas mixtures on the results. Figure A.1 shows mixture adsorption selectivity results obtained for two mixtures having different bulk compositions, He/CH_4:50/50 and 4/96. Predicted adsorption selectivity of MOFs were found to be very similar for these two compositions under a wide range of pressure conditions, showing that composition of the feed mixture does not have a significant effect on the adsorption selectivity of the MOFs considered in this study. It is also important to note that we specifically considered 50/50 mixture throughout this manuscript rather than 4/96, the real industrial composition of He/CH_4 mixture.[7] When the He/CH_4:4/96 mixture was considered, the amount of He that must be loaded into a MOF to run the EMD simulations was significantly less than that of CH_4 due to the weak adsorption of He. If a weakly adsorbed component's loading is very low in a mixture compared to the strongly adsorbed one, the statistical accuracy of the EMD simulations significantly decreases. We used equimolar composition in order to get a reasonable He loading in the MOFs' pores compared to CH_4 so that diffusivities of gases can be computed with a high statistical accuracy using EMD.

Similar to adsorption, diffusion behavior of gases significantly changes when they are in a mixture compared to the case where they are alone. Figure 4.5 represents transport diffusivities of single-component gases and self-diffusivities of gas components in their binary mixtures which are all obtained from molecular simulations. When there is a mixture, both gases diffuse slower compared to their diffusion in the single-component case. Single-component He (CH_4) diffusivities were computed to be in the range of 2.68×10^{-4}-8.01×10^{-3} (3.92×10^{-7}-4.25×10^{-3}) cm^2/s whereas He (CH_4) diffusivities in binary mixtures were calculated to be in the range of 2.26×10^{-5}-4.05×10^{-3} (1.52×10^{-7}-1.77×10^{-3}) cm^2/s. This behavior can be attributed to the steric hindrance effects. In some MOFs, diffusion of CH_4 slightly increases since CH_4 molecules tend to diffuse faster in the presence of a smaller and lighter gas, He. In the cases where both of gas molecules slow down due to steric hindrance, the decrease is generally more pronounced for He since it diffuses much faster than CH_4. As a result of this, diffusion selectivity for He over

CH_4 generally gets smaller when gas molecules move together in the mixture. As shown in Table 4.1, mixture diffusion selectivity for He/CH_4 is less than the ideal diffusion selectivity for the MOFs. Since both adsorption selectivity and diffusion selectivity of MOFs for He/CH_4 decreases when a binary mixture is considered instead of the single-component gases, mixture membrane selectivities become less than the ideal membrane selectivities, supporting the results shown in Figures 4.2 and 4.3. For example, Table 4.1 shows that HUTZAX01 is a promising MOF membrane based on its ideal selectivity but it has a low selectivity for mixture separation. Ideal He/CH_4 adsorption (diffusion) selectivity of this MOF was computed as 0.025 (1140.68) whereas its mixture adsorption (diffusion) selectivity is 0.005 (776.19). As a result, the ideal selectivity of HUTZAX01 membrane, 29, was predicted to be significantly higher than its mixture selectivity, 4.25.

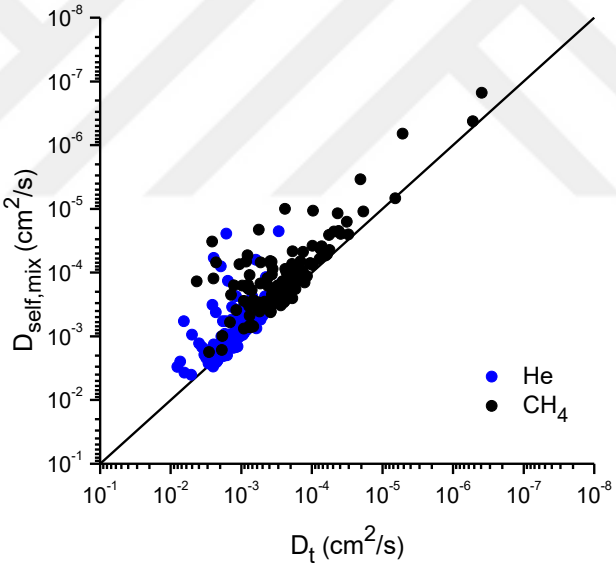

Figure 4.5. Comparison of transport diffusivities of gases in single-component case with the self-diffusivities of gases in a binary He/CH_4 mixture.

We focused on membrane-based He separation performances of MOFs so far. Computing both the adsorption selectivity and membrane selectivity of MOFs give us the opportunity to compare separation performances of these materials as adsorbents and membranes. For

example, GUPCUQ01, which has the highest membrane selectivity for He, 34.4 has a moderate adsorption selectivity of 21.74 for CH_4. This suggests that GUPCUQ01 is a promising membrane for selective separation of He from CH_4 but as an adsorbent it is moderately selective for CH_4, not for He. This result shows that a MOF with excellent properties as a membrane for He recovery may have less exciting properties as an adsorbent. A controversial example is PAQFIY. This MOF has the highest adsorption selectivity for CH_4/He mixture (610.82) among the MOFs considered in this work and in addition to this it exhibits high CH_4 selectivity (142.8) as a membrane. Therefore, this MOF can be considered as a promising material both as an adsorbent and as a membrane for selective separation of CH_4 from He. Overall, our results show that all the MOFs we considered are promising adsorbents for selective separation of CH_4 from He whereas a small number of them are promising membranes for selective separation of He from CH_4.

Our results also demonstrated that both selectivities and permeabilities of the MOFs we considered in this work are higher than those of the fabricated MOF membranes such as CuBTC, IRMOF-3, which were recently tested for He/CH_4 separation. It is important to note that only 139 selected MOFs were studied in this work and many other MOFs which may show better He recovery performance may exist in the database. The aim of this work was to introduce the computational methodology that can be further used to perform a large-scale material screening in order to identify the most promising materials for He/CH_4 separations before extensive experimental efforts. Finally, it is important to note that materials that we identified as promising membranes must be tested under real operating conditions and stability of the MOFs that will be used as membranes must be examined. We checked the stability information for GUPCUQ01, HUTZAX01 and PEHBIO since these three MOFs were identified to be promising for selective separation of He from CH_4. GUPCUQ01 was reported to have high thermo-stability up to 400 °C,[117] HUTZAX01 was reported to preserve its framework at high temperatures.[118] There was no any information reported on the stability of PEHBIO in the literature.

Chapter 5
The Effect of Charge Equilibration Methods on the Ranking of MOF Adsorbents

In this chapter, we investigated the effect of charge equilibration methods on the ranking of MOF adsorbents. Two different gas mixtures were studied; CO_2/CH_4 and CO_2/N_2. First, we showed that the IQEq method reported in literature was implemented properly. IQEq and QEq methods were then used to calculate adsorbent evaluation metrics and results were compared for the 10 best performing structures. Moreover, MOF rankings in terms of the adsorbent performance were discussed by calculating the correlation coefficients. The ability of the IQEq for reproducing the adsorption data calculated by the DDEC method was also investigated.

Wells et al.[30] reported single-component CO_2 adsorption data for 24 different MOFs which are optimized with quantum-based DFT calculations using the Siesta package.[30, 119] We validated our approach by computing the adsorption of CO_2 in 8 DFT-optimized MOFs at the operating conditions of 298 K, 0.1 and 1 bar, and using the cut-off of 12.5 Å as given in the IQEq paper.[30] MOF-74 structures were taken from the literature with the ab-initio derived force-fields.[120] ZIF-69, ZIF-68, ZIF-8, CuBTC, and MOF-177 were optimized with the freely available package cp2k.[121] MIL-47 structure was taken from the molecules library of RASPA.[84]

Figure 5.1 shows the CO_2 adsorption data (wt. %) of 8 different MOFs at two pressures. For both pressures, there is a reasonably good agreement between the values calculated in this thesis and the ones reported in the literature. The MOF-74 structures are the most

challenging MOFs to reproduce the adsorption data, because these structures are known to be very sensitive to the optimization package and the procedure. The variation is more visible at 0.1 bar as the electrostatic interactions are more pronounced at low pressures.

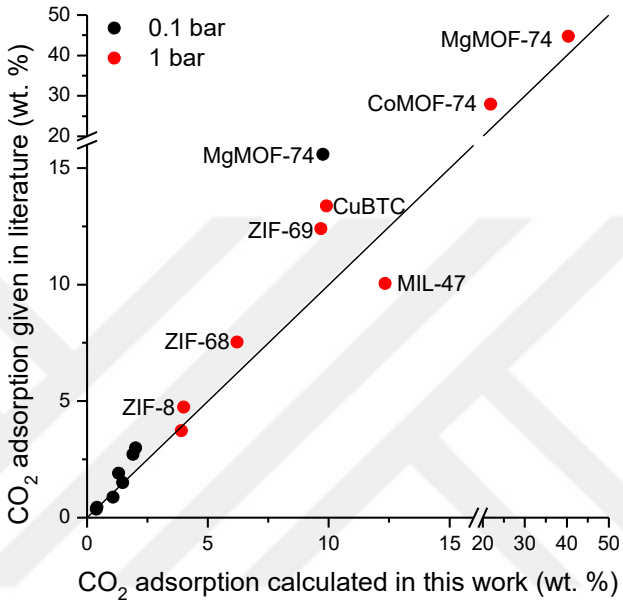

Figure 5.1. Validation showing that the IQEq method was applied correctly in this work. Black and red symbols are for 0.1 and 1 bar, respectively. Data on y-axis is taken from the literature.[30]

Motivated from this agreement, we predicted CO_2/CH_4 and CO_2/N_2 mixture adsorptions for 2244 structures (dataset construction can be found in Section 3.1.) Figures 5.2 and 5.3 compares the uptake data (mol/kg) of each gas molecule in CO_2/CH_4 and CO_2/N_2 mixtures computed using the IQEq and QEq methods. In Figure 5.2, The uptake values of CH_4 predicted by QEq are computed to be very similar to the ones predicted by IQEq. This situation is not valid for CO_2 and deviations are more visible between the values predicted by QEq and IQEq. This result can be attributed to the dominant effect of electrostatic interactions on the adsorption of quadrupolar molecules, such as CO_2 in contrast to nonpolar molecules such as CH_4.

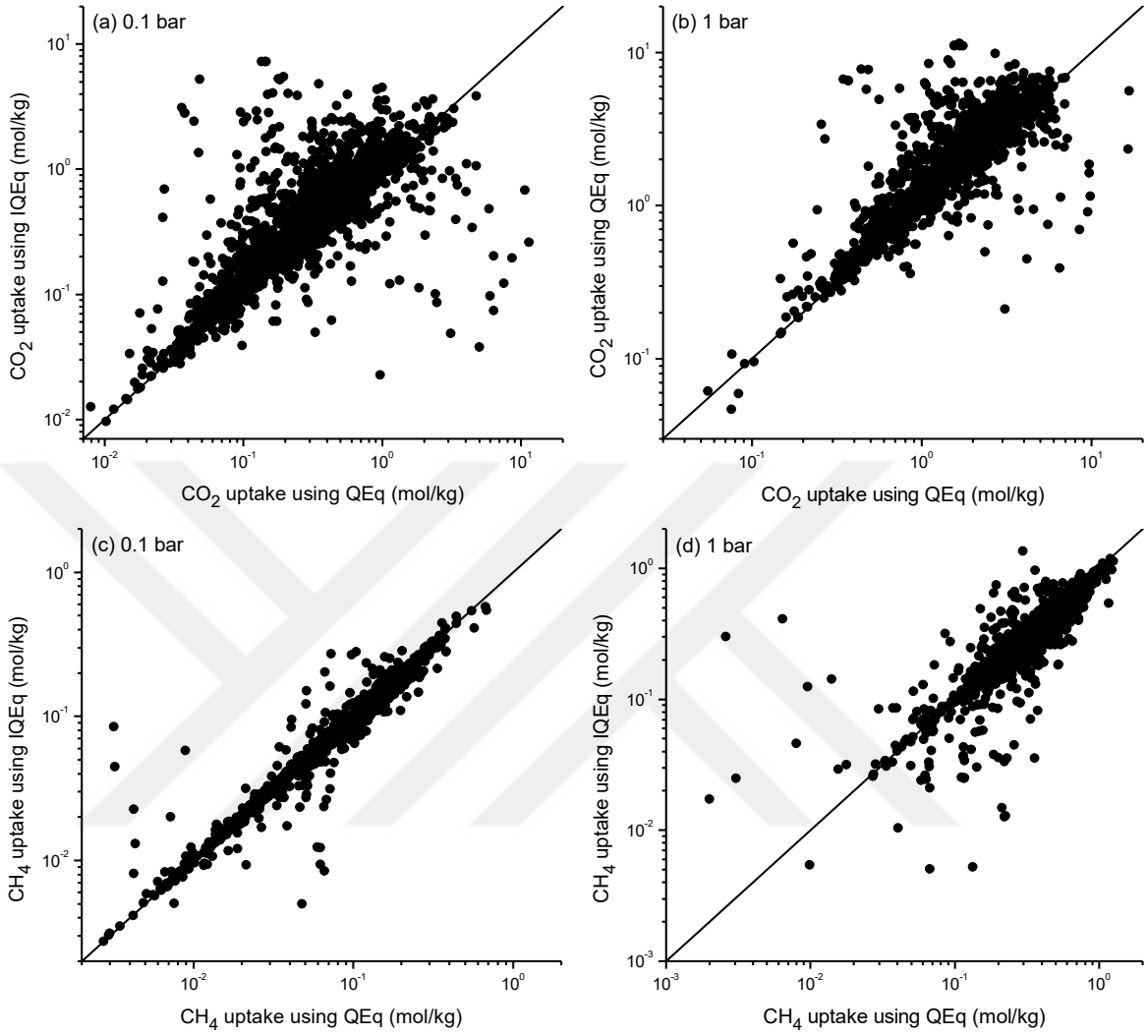

Figure 5.2. Comparison of CO_2 and CH_4 uptakes in MOFs predicted from simulations using IQEq and QEq methods. The composition of the CO_2/CH_4 mixture is equimolar.

Although both molecules in CO_2/N_2 mixture are polar, Figure 5.3 can be discussed as similar to the Figure 5.2. The effect of charge assignment method is more pronounced for CO_2 since CO_2 has a higher quadrupole moment than N_2.

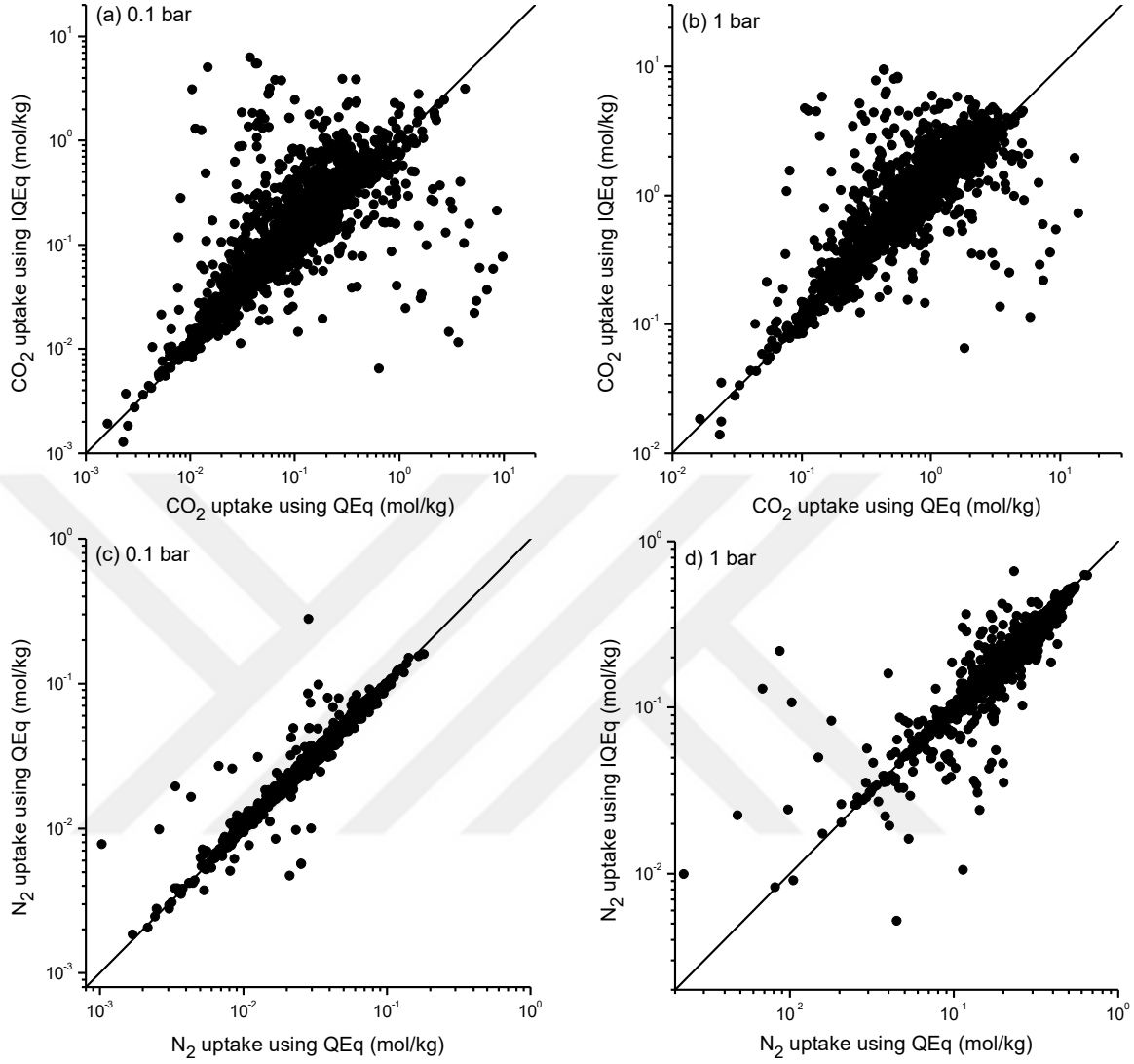

Figure 5.3. Comparison of CO_2 and N_2 uptakes in MOFs predicted from simulations using IQEq and QEq methods. The composition of the CO_2/N_2 mixture is 15/85.

The adsorption selectivities (CO_2/CH_4) of 2244 MOFs computed using the IQEq and QEq methods are compared in Figure 5.4. The selectivities calculated for each pressure using both methods are greater than 1 as expected. Due to its higher affinity to the atoms of an adsorbent as well as its polar nature which boosts the effect of electrostatic interactions, CO_2 is more selectively adsorbed in all MOFs compared to CH_4. Adsorption selectivities calculated using the IQEq method are generally greater than the ones calculated using

QEq. Considering the greater CO_2 uptakes predicted by the IQEq method and the similar CH_4 uptakes predicted by both methods, as shown in Figure 5.2, it is expected to see higher CO_2/CH_4 selectivity predictions by the IQEq method. The top 10 best performing MOFs identified using both charge assignment methods were also compared in terms of the adsorption selectivities. The adsorption selectivity of the top 10 MOFs that are identified using the IQEq are generally underestimated by the QEq for CO_2/CH_4 and vice versa. BUKSAD and MIDXON are the two materials that are in top 10 of IQEq and QEq, respectively and that draw attention regarding the variation between the adsorption selectivity values predicted by one another method. While BUKSAD is found to have a selectivity of 31.20 (2.07) by the IQEq (QEq), MIDXON is found to have a selectivity of 94.95 (29.21) by the QEq (IQEq) at 0.1 bar. SUTBIT is an example to materials for which the adsorption selectivity is calculated very similar by both methods at 0.1 and 1 bar.

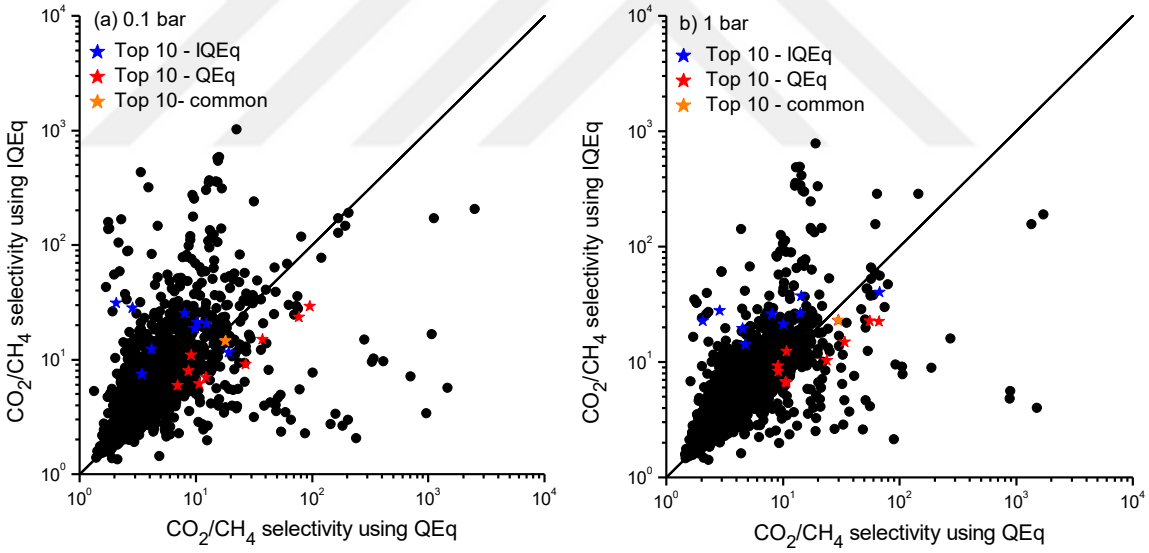

Figure 5.4. Comparison of adsorption selectivities at (a) 0.1 and (b) 1 bar predicted from the simulations using IQEq and QEq for the CO_2/CH_4 separation.

Figure 5.5 represents the adsorption selectivities computed for CO_2/N_2 using the two charge assignment methods. Selectivity values go up to 6000 in Figure 5.5 while this number was around 3000 in Figure 5.4. Distributions of the points on these two figures

are very similar. Adsorption selectivities computed using QEq are generally overestimated by the IQEq for CO_2/N_2 mixture. All selectivities are greater than 1 because CO_2 molecules are adsorbed more strongly due to their higher quadrupolar moment than N_2. In Figure 5.5, it is demonstrated that while all top 10 MOFs of the IQEq are underestimated by the QEq, some of the top 10 MOFs of QEq was found to have greater adsorption selectivities (CO_2/N_2) by the other method. For instance, RAVNAE is ranked as the best performing material by the QEq which calculates its adsorption selectivity as 84.46, but, IQEq claims this value as 228.27.

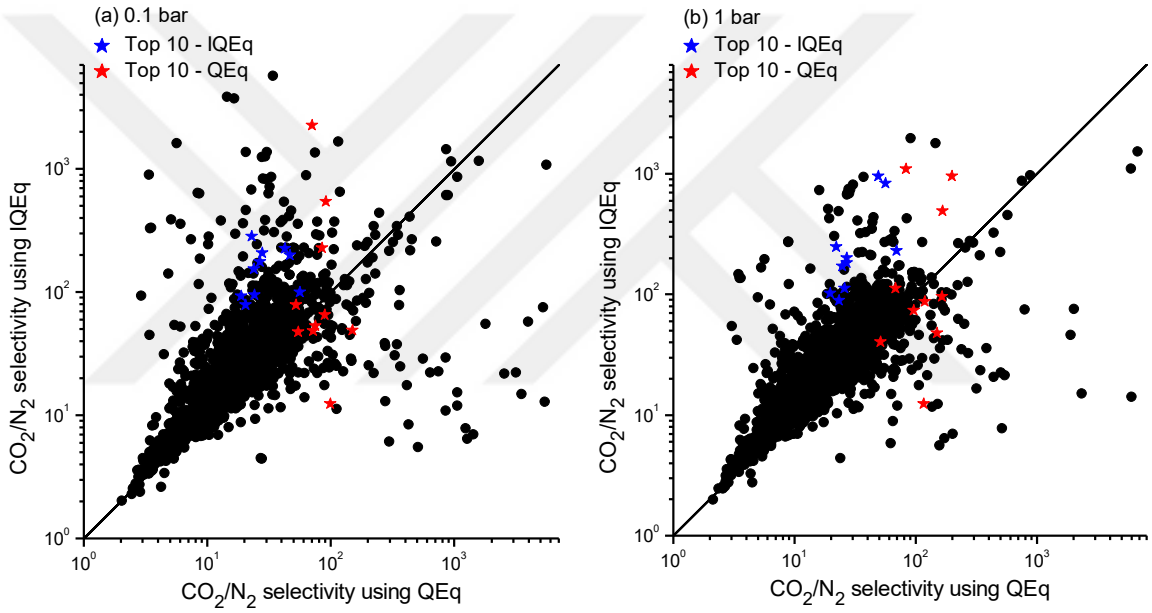

Figure 5.5. Comparison of adsorption selectivities at (a) 0.1 and (b) 1 bar predicted from the simulations using IQEq and QEq for the CO_2/N_2 separation.

It is important to examine the predictions for the top performing materials to understand the effect of charges assignment methods in high-throughput computational screening. Top 10 materials were identified as MOFs with R%>85%. Thus, regenerability of 2244 materials were computed first and then the materials with R% lower than 85 were eliminated. APS of the entire materials was ranked in an ascending order and the first 10 MOFs were named as the best performing adsorbents. This procedure was repeated for

both mixtures using the two charge assignment methods so that we have 4 different list at the end.

All adsorbent evaluation metrics calculated for the top 10 best performing materials identified using each method are given in Tables 5.1 and 5.2 for CO_2/CH_4 and CO_2/N_2 mixtures, respectively. Table 5.1 shows that there is only one common MOF between the two lists created using the IQEq and QEq, which is LUVLUJ. However, in Table 5.2 demonstrates that the top 10 MOFs identified for the CO_2/N_2 mixture are totally different in the use of IQEq and QEq.

Figure 5.6 and 5.7 are to compare the working capacities calculated by the IQEq and QEq methods. Except a small group of materials, working capacities are in a good agreement for both methods and mixtures. Even if the CO_2 uptakes calculated by the two methods have large variations, the increases in the calculated uptakes by both method when pressure increases from 0.1 to 1 bar are close to each other so that the working capacities can be calculated similarly. Being the only common MOF present in the both top 10 list, LUVLUJ, is found to have 2.85 and 3.15 mol/kg of working capacity by IQEq and QEq, respectively, for CO_2/CH_4 separation. Similarly, as three of the top 10 identified by QEq, namely SUTBIT, CIFCEB, and FIRMUQ have very close working capacities calculated by each method. However, there are also materials for which working capacities are computed to be very different by each method. BUKSAD is a material that is in top 10 of IQEq. While BUKSAD is found to have a working capacity of 2.98 mol/kg by the IQEq, this value is calculated as 0.23 by the QEq. Similar discussion is valid for CO_2/N_2 separation. The range of working capacities demonstrated in Figure 5.7 is very similar to the range of those calculated for CO_2/CH_4 separation. The working capacities of the top 10 best performing MOFs determined using the IQEq are always underestimated when the QEq method is used. Being one of the top 10 MOFs determined by the IQEq, ZAZBUZ has a working capacity of 3.05 mol/kg based on the IQEq which is calculated as 0.98 mol/kg based on the QEq.

Table 5.1. Adsorbent evaluation metrics of top 10 MOFs for CO_2/CH_4 mixture.

	Top 10 - IQEq	R (%)	APS (mol/kg)	CO_2/CH_4 selectivity at 0.1 bar	CO_2/CH_4 selectivity at 1 bar	ΔN_{CO2} (mol/kg)	R (%) using QEq	APS using QEq (mol/kg)	CO_2/CH_4 selectivity at 0.1 bar using QEq	CO_2/CH_4 selectivity at 1 bar using QEq	ΔN_{CO2} using QEq (mol/kg)
1	IJEFUZ	90.17	136.94	20.59	26.49	5.17	90.22	42.37	12.34	14.04	3.02
2	YONXEE	88.34	121.98	28.32	27.94	4.37	89.72	1.46	2.84	2.88	0.51
3	WOQTUT	87.67	118.04	25.35	26.12	4.52	89.70	13.76	7.98	8.04	1.71
4	GUKYUI	85.10	112.76	11.54	40.52	2.78	79.16	195.03	19.12	67.02	2.91
5	SINKOR	87.18	108.35	21.15	37.54	2.89	88.77	24.53	10.29	14.38	1.71
6	DAWWEF	92.25	86.97	12.34	19.61	4.43	90.56	5.24	4.12	4.49	1.17
7	AGAWUA	86.63	84.06	7.52	14.27	5.89	87.12	13.80	3.43	4.72	2.92
8	KOSKIO	88.91	82.24	18.67	21.24	3.87	88.90	20.69	9.85	10.01	2.07
9	BUKSAD	87.91	68.13	31.20	22.84	2.98	89.78	0.47	2.07	2.04	0.23
10	LUVLUJ	87.52	65.90	14.60	23.10	2.85	86.37	93.63	18.01	29.72	3.15
	Top 10 - QEq	R (%)	APS (mol/kg)	CO_2/CH_4 selectivity at 0.1 bar	CO_2/CH_4 selectivity at 1 bar	ΔN_{CO2} (mol/kg)	R (%) using IQEq	APS using IQEq (mol/kg)	CO_2/CH_4 selectivity at 0.1 bar using IQEq	CO_2/CH_4 selectivity at 1 bar using IQEq	ΔN_{CO2} using IQEq (mol/kg)
1	YEMMAF	84.88	184.33	76.84	55.68	3.31	90.63	37.00	23.41	22.77	1.62
2	MIDXON	88.44	145.07	94.95	66.40	2.18	87.81	14.82	29.21	22.60	0.66
3	LUVLUJ	86.37	93.63	18.01	29.72	3.15	87.52	65.90	14.60	23.10	2.85
4	KOSLUB	85.11	93.28	26.84	23.79	3.92	90.67	24.09	9.09	10.36	2.33
5	QOVDAH	89.85	83.02	37.37	33.79	2.46	90.50	16.04	15.06	14.91	1.08
6	CIFCEB	88.93	54.80	6.92	9.15	5.99	90.42	51.38	5.93	8.35	6.15
7	FIRMUQ	89.29	51.82	9.08	10.73	4.83	88.37	65.80	10.95	12.46	5.28
8	WONZIJ	85.52	48.36	12.11	10.75	4.50	87.45	20.41	7.03	6.65	3.07
9	SUTBIT	88.16	47.50	8.61	9.02	5.26	89.41	50.51	8.02	9.32	5.42
10	SIXWED	86.29	47.06	10.73	10.55	4.46	89.21	22.82	6.13	6.77	3.37

Table 5.2. Adsorbent evaluation metrics of top 10 MOFs for CO_2/N_2 mixture.

	Top 10 - IQEq	R (%)	APS (mol/kg)	CO_2/N_2 selectivity at 0.1 bar	CO_2/N_2 selectivity at 1 bar	ΔN_{CO2} (mol/kg)	R (%) using QEq	APS using QEq (mol/kg)	CO_2/N_2 selectivity at 0.1 bar using QEq	CO_2/N_2 selectivity at 1 bar using QEq	ΔN_{CO2} using QEq (mol/kg)
1	YUCZOM	85.07	4259.97	226.41	961.79	4.43	88.02	51.75	42.24	48.84	1.06
2	FIFNUE	86.19	3677.38	200.39	839.79	4.38	88.08	66.49	46.35	55.85	1.19
3	MOYMET	84.64	907.86	285.48	247.57	3.67	89.46	8.98	22.72	22.06	0.41
4	FIFPAM	89.00	612.77	99.90	230.04	2.66	88.04	91.73	56.00	69.41	1.32
5	XESKUD	89.89	489.54	177.25	201.56	2.43	89.72	8.24	26.71	26.86	0.31
6	REZXIE	84.70	467.02	208.10	184.15	2.54	88.72	11.18	27.85	26.95	0.41
7	HOWRES	89.19	461.26	94.74	112.52	4.10	89.91	24.76	24.12	25.71	0.96
8	SINKUX	86.54	328.89	155.04	172.29	1.91	89.43	8.82	23.87	24.68	0.36
9	ZAZBUZ	85.72	273.44	78.97	89.52	3.05	88.26	22.57	20.45	23.05	0.98
10	WUFXAY	88.31	270.62	93.04	102.10	2.65	89.82	11.15	18.66	19.65	0.57
	Top 10 - QEq	R (%)	APS (mol/kg)	CO_2/N_2 selectivity at 0.1 bar	CO_2/N_2 selectivity at 1 bar	ΔN_{CO2} (mol/kg)	R (%) using IQEq	APS using IQEq (mol/kg)	CO_2/N_2 selectivity at 0.1 bar using IQEq	CO_2/N_2 selectivity at 1 bar using IQEq	ΔN_{CO2} using IQEq (mol/kg)
1	RAVNAE	86.83	343.38	84.46	164.87	2.08	80.95	1542.35	228.27	494.90	3.12
2	HISJIE	89.91	330.50	90.64	197.68	1.67	61.53	1616.41	543.70	961.59	1.68
3	GUKYUI	90.42	326.31	71.89	162.96	2.00	91.30	144.28	48.76	96.66	1.49
4	CUSDIE	88.24	304.44	98.52	115.44	2.64	89.14	3.92	12.45	12.41	0.32
5	AFEJOK	85.02	286.08	74.66	95.43	3.00	87.47	197.11	53.37	73.80	2.67
6	YEMMAF	89.35	234.71	148.40	149.44	1.57	89.46	22.61	49.13	47.88	0.47
7	VUNYAF	85.27	229.41	88.88	118.11	1.94	87.17	148.53	65.94	87.63	1.69
8	CUCKIV	86.25	148.60	70.17	82.28	1.81	16.76	862.98	2277.73	1099.99	0.78
9	UBIPAY	85.80	144.83	52.01	67.62	2.14	84.46	322.57	78.93	112.65	2.86
10	KINNEC	84.88	129.98	54.18	51.17	2.54	84.16	82.30	47.46	40.48	2.03

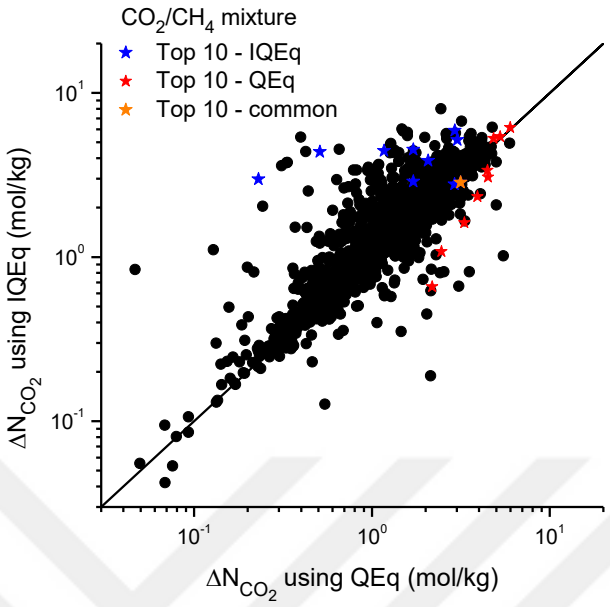

Figure 5.6. Comparison of working capacities predicted from the simulations using IQEq and QEq for the CO_2/CH_4 separation.

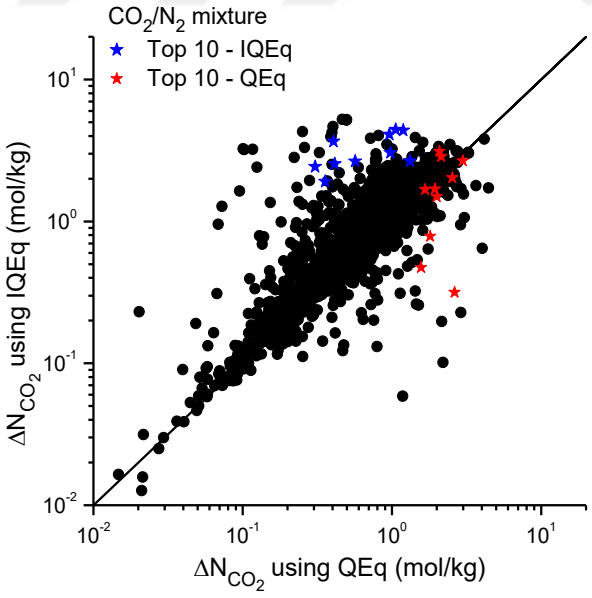

Figure 5.7. Comparison of the working capacities predicted from the simulations using IQEq and QEq for the CO_2/N_2 separation.

APS is an adsorbent evaluation metric and calculated as the multiplication of working capacity and the adsorption selectivity at the adsorption pressure. In Figure 5.8 and 5.9, the IQEq and QEq methods are compared for APSs. Working capacity and adsorption selectivities are the multiplying factors of APS. Because the adsorption selectivities calculated by the QEq at 1 bar overpredicted the ones computed by the IQEq and the working capacity values calculated by those two methods are moderately similar, large variations inherently occur between the APS values calculated based on the atomic partial charges assigned with the IQEq and QEq methods. Adsorption selectivity (at 1 bar) and working capacity of BUKSAD were calculated by the QEq as 2.04 and 0.23 mol/kg, respectively. However, due to the adsorption selectivity and working capacity values that are 11.2 and 13 times higher than the values of those calculated by the QEq. APS of this material is calculated by QEq becomes 68.13, 145 times higher than the value calculated by QEq. Another example can be given from Figure 5.9. HISJIE is one of the top 10 best performing MOFs for CO_2/N_2 separation as identified using the QEq. Working capacity calculated for this MOF is the same when either of the methods is used, 1.67 mol/kg. However, APS values computed for HISJIE are substantially different depending on the method used. While APS of this MOF is calculated as 330.50 using the QEq, this number reaches 1616.41 when the IQEq is used as the charge assignment method.

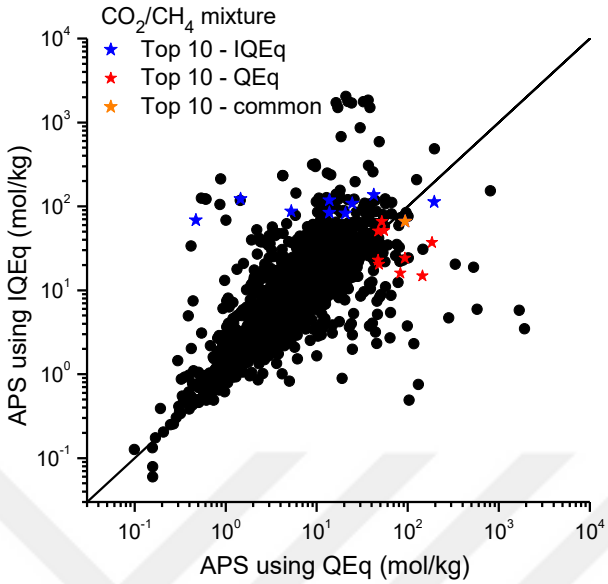

Figure 5.8. Comparison of the adsorbent selection parameters predicted from the simulations using IQEq and QEq for the CO_2/CH_4 separation.

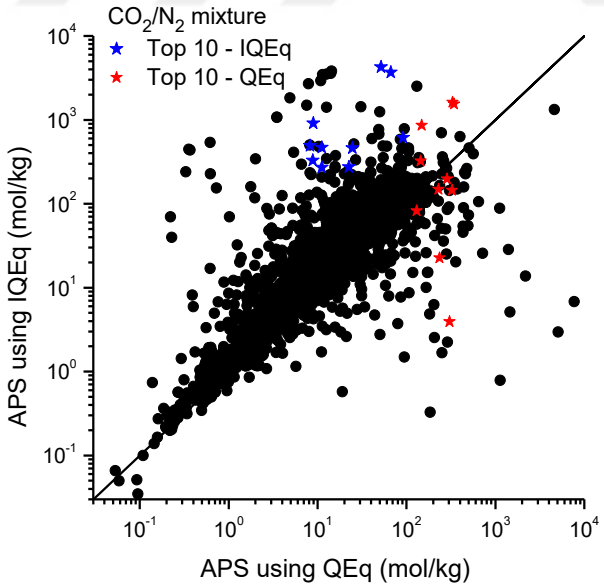

Figure 5.9. Comparison of adsorbent selection parameters predicted from the simulations using IQEq and QEq for the CO_2/N_2 separation.

Finally, the last adsorbent evaluation metrics, regenerability, was compared using the values which were calculated based on the partial charges computed with the IQEq and QEq methods. In Figure 5.10 and 5.11, red area consists of the MOFs for which the R% is calculated to be greater than 85% (the desired R%) by QEq, while blue area shows the materials which are predicted to have R%>85% by IQEq. The percentage of the MOFs with high regenerability (>85%) in the dataset (2244 structures) is found to be different for each method and each separation. In Figure 5.10 (5.11), while 1177 (1683) materials out of 2244 have R%>85% based on the QEq method, this number decreased to 999 (1542) when the IQEq method is used. Considering the procedure to rank the MOFs based on their adsorbent performance, it can be stated that the regenerability has a major role. A structure which is not identified as regenerable by a method may be identified as a material with high regenerability by another. This is an unfortunate contradiction which can cause a high selective material to be improperly ignored during a high-throughput computational screening. For instance, for CO_2/CH_4 mixture, 225 (19%) of 1177 materials found to have R%>85% by the QEq is not considered by IQEq in the performance rankings due to R%<85%. Only 934 out of 2244 materials are calculated to have R% >85% by both methods. However, this number increased to 1468 in the case of CO_2/N_2, which means that 65% of the 2244 materials in dataset is involved in the ranking of the best performing MOFs with R%>85% for both charge assignment methods.

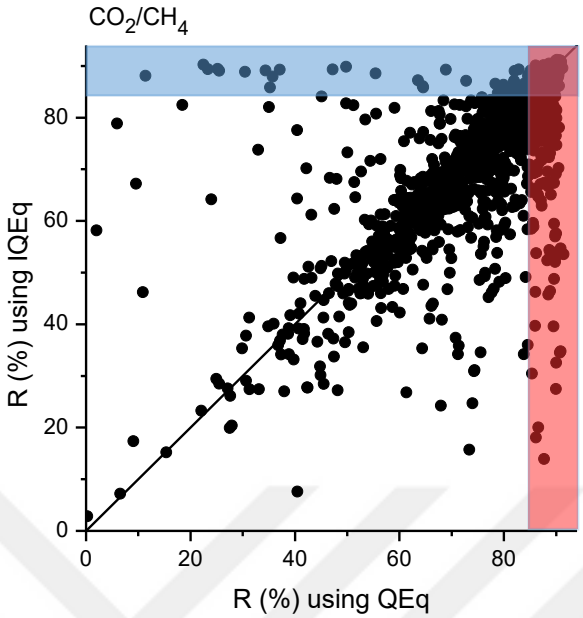

Figure 5.10. Comparison of the regenerabilities predicted from the simulations using IQEq and QEq for the CO_2/CH_4 separation.

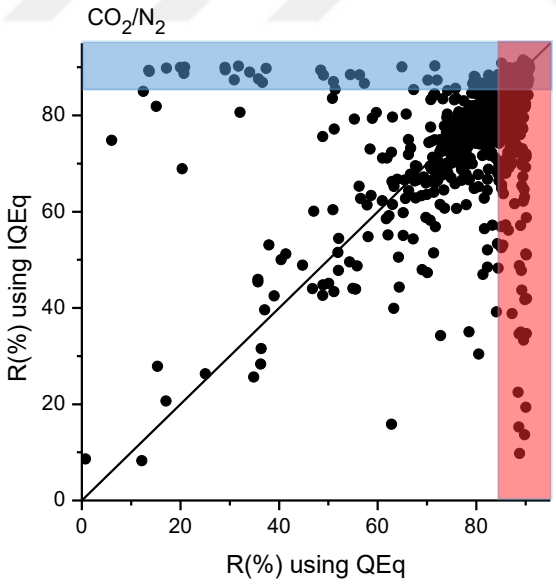

Figure 5.11. Comparison of the regenerabilities predicted from the simulations using IQEq and QEq for the CO_2/N_2 separation.

After comparing the IQEq and QEq methods in the basis of each adsorbent evaluation metrics, now each method can be separately investigated in detail. Figure 5.12 and 5.13 show the regenerability of MOF adsorbents as a function of adsorption selectivity. All points on the graphs represent the MOFs with R%>85%. Figure 5.12 consists of the results calculated based on the IQEq. Top 10 best performing MOFs identified based on the QEq calculations are found to have R% values greater than 85. In Figures 5.12(a) and 5.12(b), we see that adsorption selectivity does not give an idea about the best performing MOFs because a material with a very high selectivity might not be in one of the best adsorbents for CO_2/CH_4 due to low R% or ΔN. For instance, MIDXON and YONXEE are the two materials with very similar adsorption selectivities at 0.1 bar calculated using IQEq, 29.21 and 28.32, respectively, and the regenerability of both materials are greater than 85%. However, MIDXON ranks as the 155th while YONXEE is identified as the top performing adsorbent when the electrostatic potential of the adsorbents was produced using the IQEq. Even if the range of R% values are same for both methods, the range of the adsorption selectivity values calculated based on the QEq is broader and can go up to 90 as can be seen in Figures 5.12(c) and 5.12(d). Same discussion can be made by looking at Figure 5.13. We can still say that the range of R% values are very similar for both methods and even for both mixtures. The adsorption values calculated at 0.1 or 1 bar by using the IQEq method shift to the left when the QEq is used. The points located on Figure 5.13(a) and 5.13(b) have their maximum adsorption selectivity values around 200 and 800, respectively, these numbers decreased to around 90 on Figure 5.13(c) and 5.13(d), respectively. Herein, we can give an example proving that higher selectivity is not enough to make a MOF better performing than the other even if the R% are almost the same for the two. In Figure 5.13(d), TIXVON and SOCFUM are two materials with very similar R% computed using the QEq method, 85.92 and 85.86. Adsorption selectivities of these MOFs at 1 bar computed using the QEq method, 42.39 and 73.46, respectively. However, while the rank of TIXVON is 15th, that of SOCFUM is 34th.

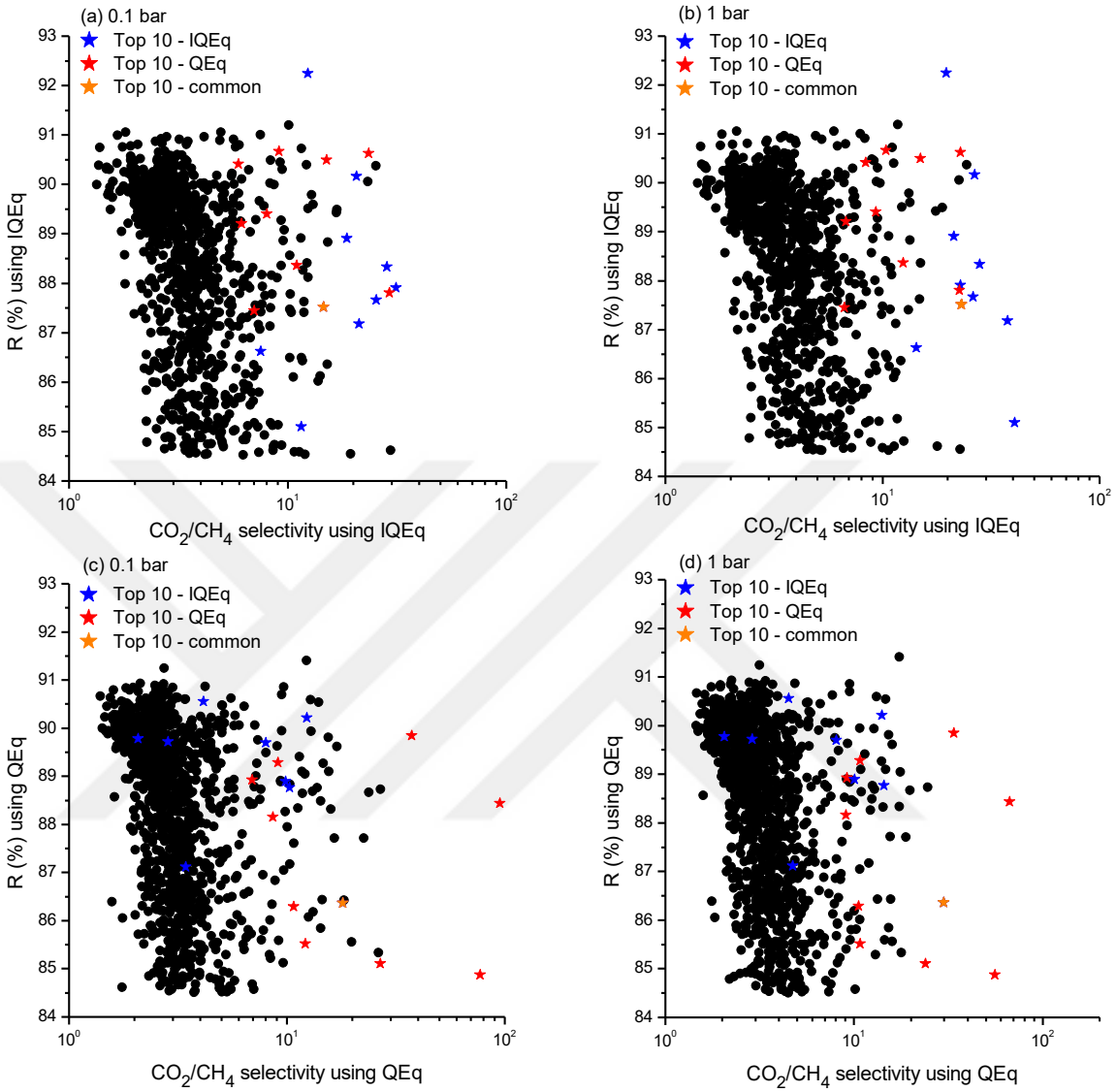

Figure 5.12. Regenerability and adsorption selectivity (CO_2/CH_4) of the MOF adsorbents with the regenerability greater than 85%: Results were calculated using (a) IQEq at 0.1 bar, (b) IQEq at 1 bar, (c) QEq at 0.1 bar, (d) QEq at 1 bar.

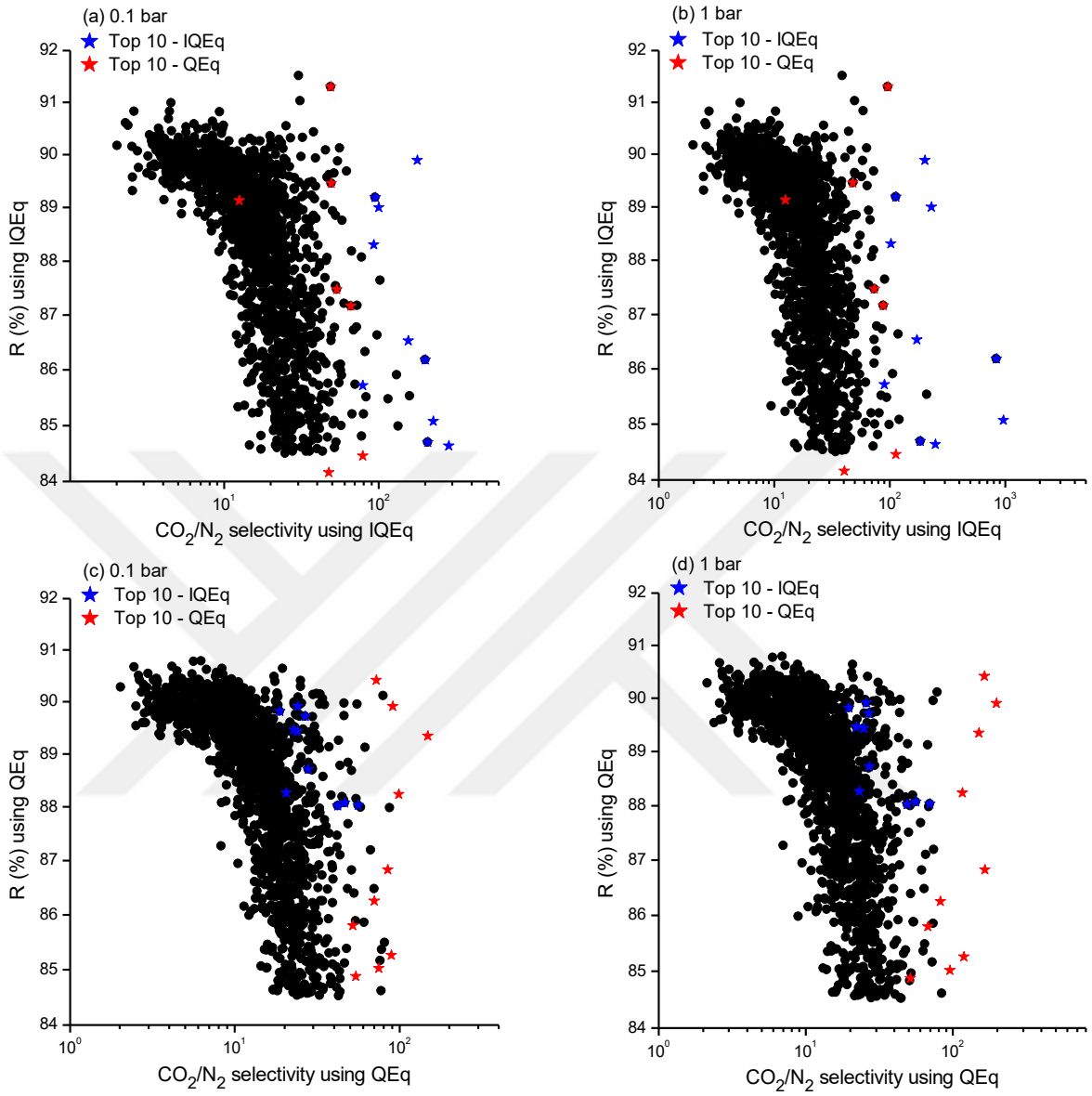

Figure 5.13. Regenerability and adsorption selectivity (CO_2/N_2) of the MOF adsorbents with the regenerability greater than 85%: Results were calculated using (a) IQEq at 0.1 bar, (b) IQEq at 1 bar, (c) QEq at 0.1 bar, (d) QEq at 1 bar.

Figure 5.14 and 5.15 represent R% as function of APS for CO_2/CH_4 and CO_2/N_2 mixtures, respectively. In both figures, APS and R% ranges are similar for the cases where different charge equilibration methods are employed. As the top materials are identified among the MOFs having R% values greater than 85 by sorting the APS values in ascending order, R vs APS graph is supposed to give an idea about the top performing materials. For both CO_2/CH_4 and CO_2/N_2 mixtures, top 10 best performing adsorbent materials are located on right side of the graph for each method. The only noticeable difference on Figure 5.15 is that the APS values computed using the IQEq method spread in a broader range. To investigate the difference/similarity between the rankings of the top 10 materials which were predicted from the simulations using the IQEq and QEq, we should look at the positions of those materials located on the graphs. Figure 5.16 and 5.17 visualize the data in Table 5.1 by locating how the rankings of the top 10 materials identified using one method changes when the another is used.

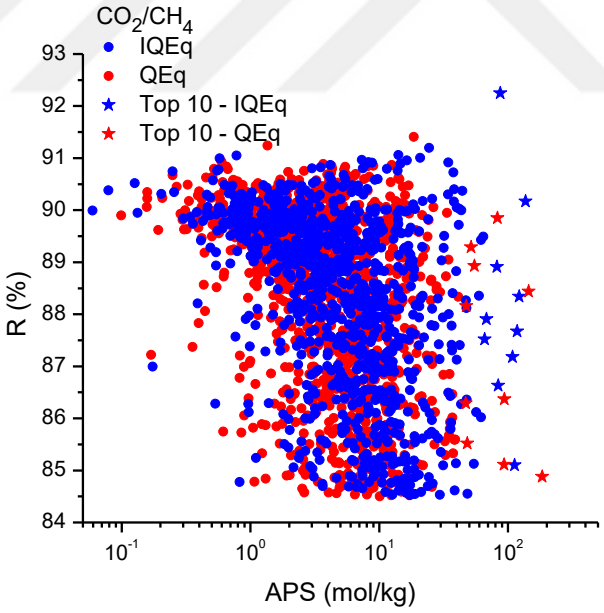

Figure 5.14. Regenerability and adsorbent selection parameter of the MOF adsorbents with the regenerability greater than 85% for CO_2/CH_4.

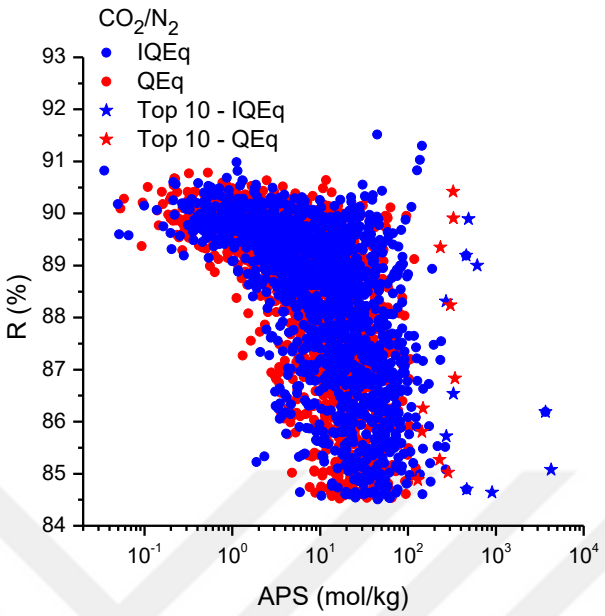

Figure 5.15. Regenerability and adsorbent selection parameter of the MOF adsorbents with the regenerability greater than 85% for CO_2/N_2.

Previous figures provided an idea about the variation between the values of adsorbent selection metrics predicted for the top materials using the two different charge assignment methods. We also showed that identity of materials that can be considered as potential adsorbents might be very different based one the methods used. However, those figures did not give any information about how the ranking order of a material in top 10 list would change depending on the method used. Figures 5.16 and 5.17 demonstrate the regenerability of MOFs as function of APS, but, they differ from Figures 5.14 and 5.15 by representing the top 10 materials with their ranking order in the corresponding lists as label on the graphs.

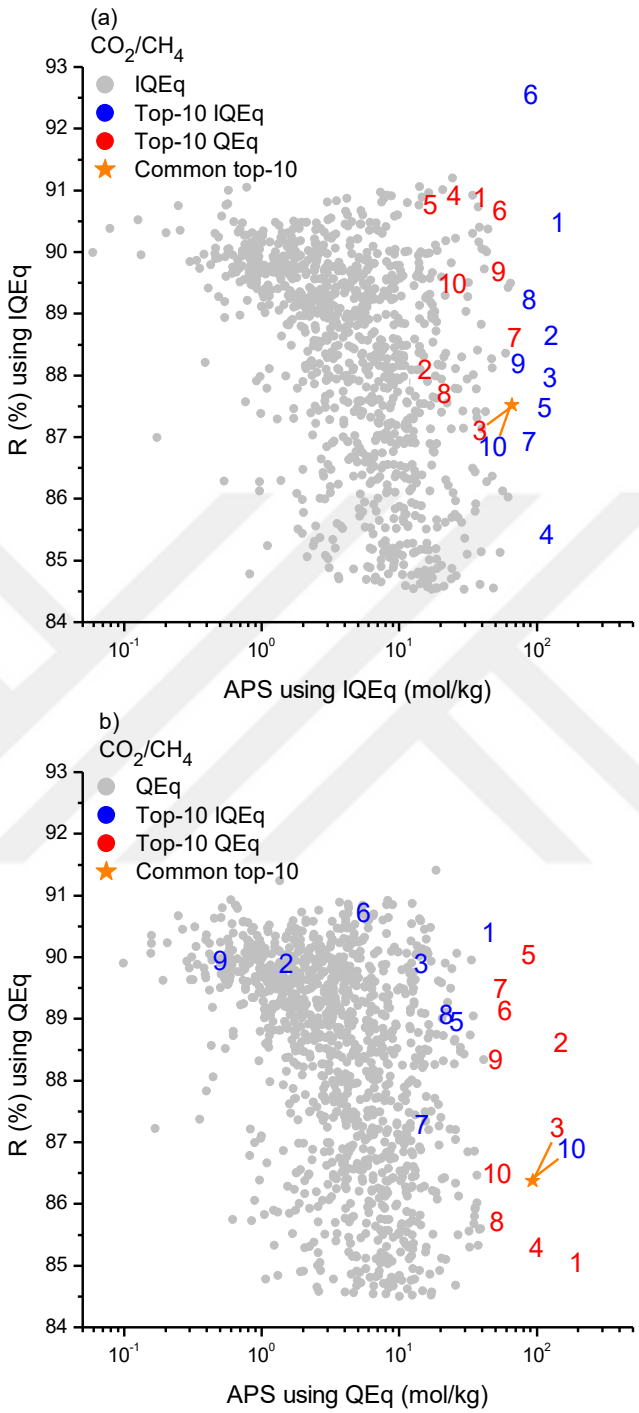

Figure 5.16. Regenerability and adsorbent selection parameter of the MOF adsorbents. MOFs with R%>85% are shown for CO_2/CH_4 separation. Materials in the top 10 lists were colored and numbered based on their ranking orders in (a) IQEq and (b) QEq.

The important result from Figure 5.16(a) is that even the 2nd and the 10th ranked materials identified by the QEq were found to show a very similar performance once their position corresponding to x-axis are considered. In Figure 5.16(b), it is shown that the 4th ranked material in the top 10 list created using the IQEq is not involved in that figure due to its low regenerability (79.16) as calculated by the QEq. A non-trivial result that draws attention from Figure 5.16(b) is the location of 2nd and 9th best performing MOFs identified by the IQEq. Even though these MOFs were identified as good candidates using the IQEq, QEq-based results locate them in the left side of the figure. Similar examples can be given for CO_2/N_2 mixture as well. In Figure 5.17(a), 5 materials of the top 10 list created based on the QEq are not present due to their undesired regenerability computed from the simulations based on the IQEq. Also, the 4th ranked material of the top 10 list created based on the QEq is regarded with a lower separation performance by the IQEq and this MOF is located almost in the middle of the graph. However, this investigation was done only for the best performing MOF adsorbents. Since the aim of this work is to compare the IQEq and QEq in terms of the rankings created depending on the adsorbent selection metrics, considering the whole dataset might be instrumental regardless of the regenerability percentage.

In order to investigate the similarity of the ranking of MOFs when different charge assignment methods were used, we computed the Spearman's ranking correlation coefficients (SRCC). Correlation between the two sets of ranking lists is quantified with a number in a range from -1 to 1. As the coefficient goes towards 1, similarity between the lists increases. In Table 5.3, calculated SRCC values for the two sets of ranking lists can be seen. MOFs were sorted on their adsorption selectivity at 0.1 and 1 bar, working capacity, regenerability, and APS in an ascending order for each charge assignment method and then the correlations between the paired lists were calculated.

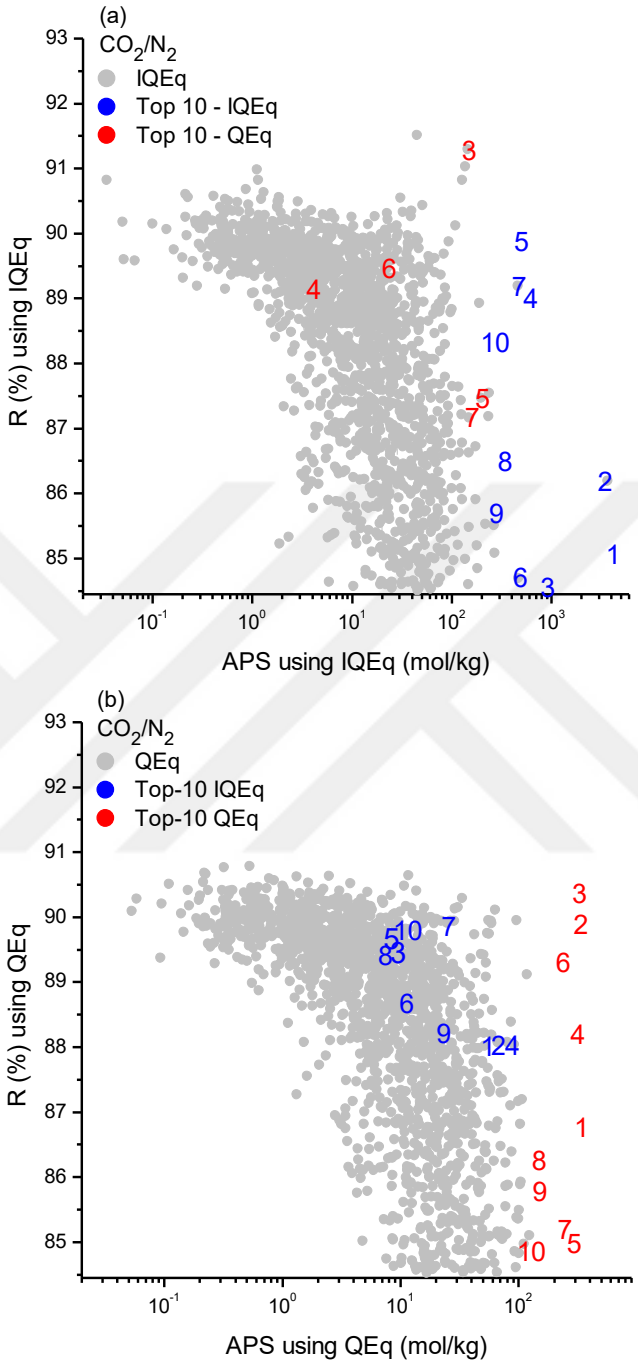

Figure 5.17. Regenerability and adsorbent selection parameter of the MOF adsorbents. MOFs with R%>85% are shown for CO_2/N_2 separation. Materials in the top 10 lists were colored and numbered based on their ranking orders in (a) IQEq and (b) QEq.

Table 5.3. The Spearman's ranking correlation coefficient (SRCC) between the IQEq-based and QEq-based rankings of 2244 MOFs.

	CO_2/CH_4	**CO_2/N_2**
Selectivity at 1 bar	0.73	0.80
Selectivity at 0.1 bar	0.76	0.82
ΔN_{CO2} (mol/kg)	0.87	0.84
APS (mol/kg)	0.79	0.81
R (%)	0.85	0.82

Table 5.3 shows that all SRCC values are greater than 0.7. Correlation coefficients between the rankings are generally higher for CO_2/N_2 mixture, equal to/greater than 0.8. It means that the calculation results obtained from the simulations where the IQEq and QEq methods are used to model electrostatic interactions compromise better for CO_2/N_2 mixture. The SRCC quantifying the similarity between the two rankings based on regenerability is 0.85, which can be regarded as a good coefficient considering the size of the dataset and the major role of this metric in the selection of the top performing materials.

In the original paper of IQEq, it is reported that the IQEq provides a better estimation of the ESP than the other charge equilibration methods used in the work, QEq as implemented also in this thesis. The authors also stated that the better estimated ESP leads to more accurate predictions for CO_2 adsorption than the other charge equilibration can achieve. Inspiring from this claim, it would be a good practice to compare the IQEq method to a method known as more accurate, DDEC (density derived electrostatic and chemical) charges. For this aim, we used 355 MOFs from CoRE-MOF database consisting of 2500+ optimized structures with already assigned DDEC charges. IQEq charges were assigned to the atoms of these 355 optimized MOFs and then adsorption selectivities and CO_2 uptakes were calculated at 0.1 and 1 bar for both CO_2/CH_4 and CO_2/N_2 mixtures. At that point, it may be thought the comparison of calculation results

obtained for the optimized structures for which the partial atomic charges were assigned using IQEq may be impractical considering all previous calculations were carried out for non-optimized structures. All MOF structures used in this work are experimental rather than hypothetical. The coordinates of the atoms in a MOF would stay unchanged after an energy optimization because the crystal structures were taken from the synthesized MOF by using XRD. Thus, we did not perform simulations for non-optimized structures with IQEq charges. The calculation results of the optimized structures obtained using IQEq in Figures 5.18 and 5.19 can be considered as the same with those of non-optimized structures. Figures 5.18 and 5.19 represent the CO_2 uptakes and Figures 5.18 and 5.19 show the adsorption selectivity data which were computed through the simulations based on different charge assignment methods at 0.1 and 1 bar, for CO_2/CH_4 and CO_2/N_2 mixtures, respectively. Many materials have large variations for CO_2 uptake and adsorption selectivity results when different charge equilibration methods are used. The variations in Figures 5.18(a) and 5.18(b) are more pronounced in the latter due to the higher pressure that reveals the effect of partial atomic charges. Similar discussion is valid for Figures 5.20(a) and 5.20(b).

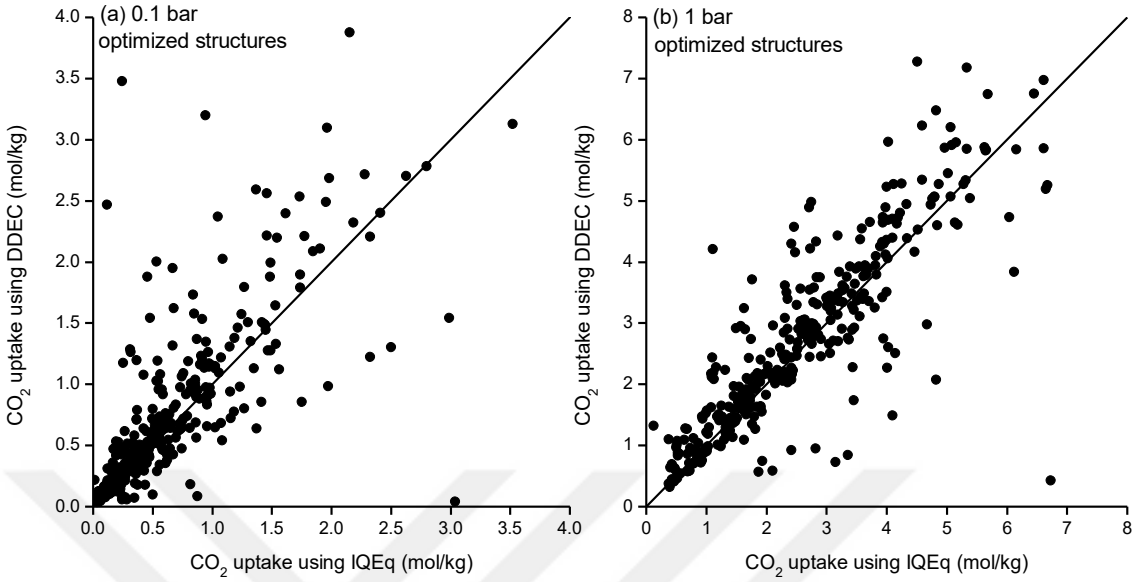

Figure 5.18. Comparison of CO_2 uptakes predicted from the simulations using IQEq and DDEC for the CO_2/CH_4 separation. Results were obtained at (a) 0.1 bar, (b) 1 bar.

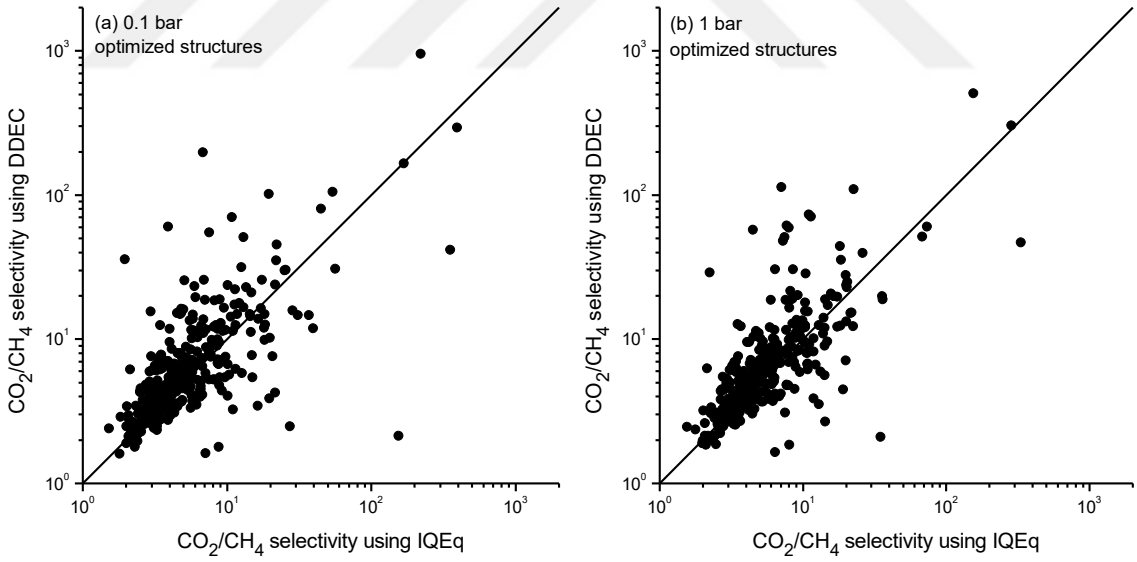

Figure 5.19. Comparison of CO_2/CH_4 selectivities predicted from the simulations using IQEq and DDEC. Results were obtained at (a) 0.1 bar, (b) 1 bar.

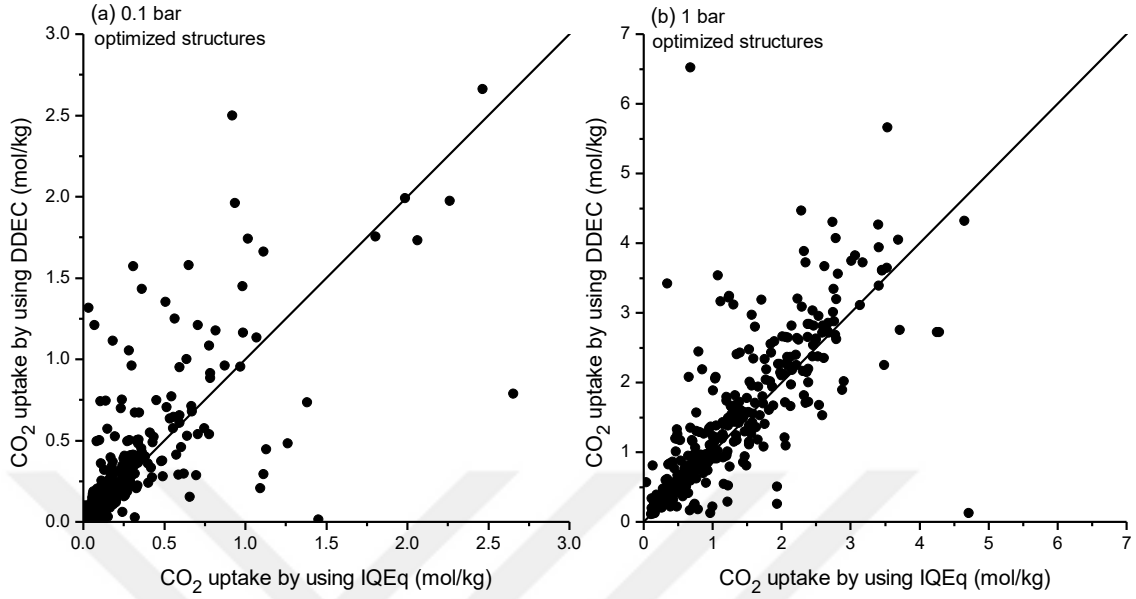

Figure 5.20. Comparison of CO_2 uptakes predicted from the simulations using IQEq and DDEC for the CO_2/N_2 separation. Results were obtained at (a) 0.1 bar, (b) 1 bar.

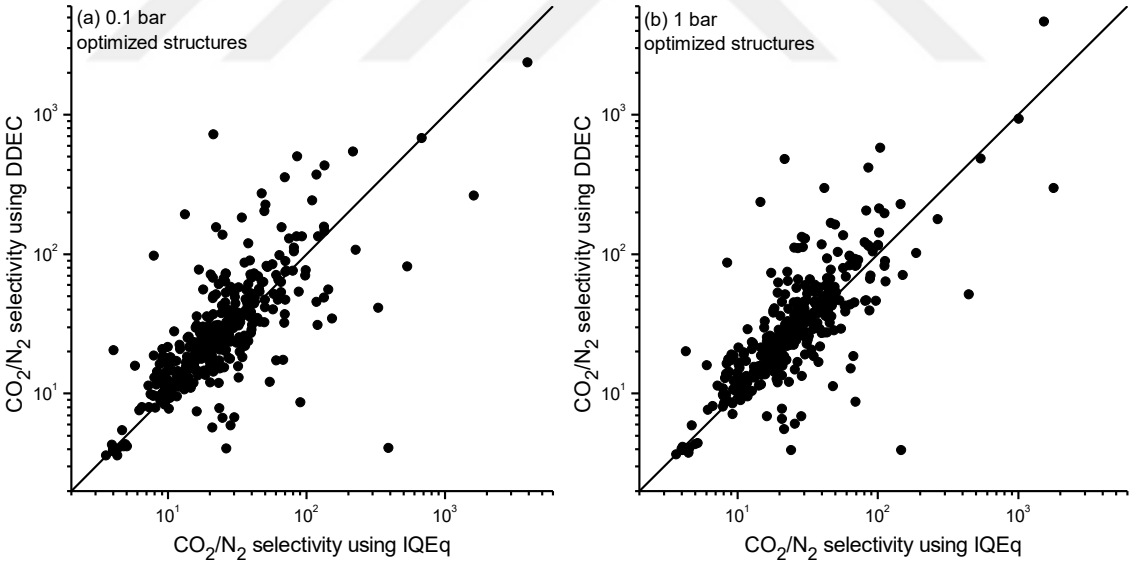

Figure 5.21. Comparison of CO_2/N_2 selectivities predicted from the simulations using IQEq and DDEC. Results were obtained at (a) 0.1 bar, (b) 1 bar.

Figures 5.19 and 5.21 showed that adsorption selectivities calculated by using DDEC and IQEq methods may have differ from each other significantly. Considering that the aim of this work is to compare the charge assignment methods in the sense of MOF rankings, it is important to examine the similarity between the rankings. For that reason, we ranked the 355 MOFs based on each adsorbent evaluation metric in ascending order and obtained two sets of rankings from DDEC-based and IQEq-based results. Table 5.4 demonstrates the SRCC quantifying the similarity between each two sets of rankings for CO_2/CH_4 and CO_2/N_2 separations.

Table 5.4. The Spearman's ranking correlation coefficient (SRCC) between the IQEq-based and DDEC-based rankings of 355 MOFs.

	CO_2/CH_4	**CO_2/N_2**
Selectivity at 1 bar	0.71	0.76
Selectivity at 0.1 bar	0.75	0.78
ΔN_{CO2} (mol/kg)	0.89	0.84
APS (mol/kg)	0.75	0.80
R (%)	0.89	0.86

Results from Table 5.4 show that even for the adsorption selectivity metrics, we have good correlation coefficients (0.71-0.78). For the working capacity, SRCC is 0.89 and 0.84 for CO_2/CH_4 and CO_2/N_2 separations, respectively. Similarity between the rankings based on APS, which is a highly effective metric on the decision of best performing MOF adsorbents, is also satisfying. The highest coefficient is attained for the regenerability basis with 0.89 and 0.86 for CO_2/CH_4 and CO_2/N_2 separations, respectively. To go one step further, we examined the performance of IQEq method in predicting the first 20 MOFs of DDEC rankings. Table 5.5 shows the rankings only for first 20 MOFs based on each of four adsorbent evaluation metrics.

Table 5.5. Ranking of top 20 MOFs based on four adsorbent evaluation metrics and charge assignment methods for CO_2/CH_4 separation.

CO_2/CH_4 selectivity at 0.1 bar				**CO_2/CH_4 selectivity at 1 bar**				**ΔN_{CO2} (mol/kg)**				**APS (mol/kg)**				**R (%)**			
using DDEC		using IQEq		using DDEC		using IQEq		using DDEC		using IQEq		using DDEC		using IQEq		using DDEC		using IQEq	
1	FUDQIF	2	RIFQUT	1	FUDQIF	14	QOKCID	1	WUHJIT	9	XINFUW	1	LOBHAM	2	BAXSIE	1	DAWWEF	1	DAWWEF
2	RIFQUT	13	QOKCID	2	BAXSIE	2	BAXSIE	2	DABWUA	3	QUQFIS	2	BAXSIE	349	MIBQAR	2	IDIWOH	4	EXEQII
3	VEQBID	1	FUDQIF	3	VEQBID	1	FUDQIF	3	QUQFIS	47	SUTBIT	3	SEHZUB	15	HEBJAB	3	KEWZOD	6	HAFVUH
4	BAXSIE	4	BAXSIE	4	SEHZUB	8	RIFQUT	4	WAMRIN01	7	GINLIA	4	VEQBID	162	DAWWEF	4	EXEQII	9	FEHCOM
5	GEDDAW	342	MIBQAR	5	FIPWOS	11	HEBJAB	5	LOBHAM	25	DEYVUA	5	OLUCAZ	44	VASKOR	5	VACFUB01	8	IDIWOH01
6	SEHZUB	17	HEBJAB	6	OLUCAZ	34	VASKOR	6	BUKMUQ	14	LUFNAC01	6	DABWUA	7	OKILEA	6	HAFVUH	86	REGREC
7	OKILEA	5	GEDDAW	7	CAYDEN	29	QUTTII	7	GINLIA	11	LUFNAC04	7	OKILEA	32	XINFUW	7	VACFUB	29	IBICAZ
8	FIPWOS	7	OKILEA	8	RIFQUT	343	MIBQAR	8	BONMEX	12	LUFNAC02	8	WUHJIT	38	QUTTII	8	IDIWOH01	12	IXOFEH
9	LOBHAM	66	YARSAN	9	CAYGIU	16	OKILEA	9	XINFUW	19	IXAJUN	9	NARTIL	40	SEQSOY	9	FEHCOM	7	VACFUB
10	OLUCAZ	50	QUTTII	10	LOBHAM	4	SEHZUB	10	LUFNAC03	16	WAMRIN02	10	UBIPAY	41	FEXCES	10	TEDGOA	5	VACFUB01
11	MULQOA	49	MUWQEB	11	HEBJAB	59	WECFAN	11	LUFNAC04	10	LUFNAC03	11	MOYMET	22	XOHLEM01	11	LAWGEW	123	DABWUA
12	MICDEJ	40	VASKOR	12	CAYDIR	43	LETROT	12	LUFNAC02	4	WAMRIN01	12	CAYGIU	3	SEHZUB	12	IXOFEH	10	TEDGOA
13	QOKCID	325	KIGCEK	13	CAYDOX06	44	QAQSAD	13	LUFNAC05	175	DAWWEF	13	WEMGAY	21	XOHLEM	13	SENWAL	31	IBICON
14	FABFOF	18	XOHLEM	14	QOKCID	23	GEDDAW	14	LUFNAC01	26	SEQSOY	14	CAYDEN	11	MOYMET	14	PEVQAK	161	FABFOF
15	MOYMET	19	XOHLEM01	15	NARTIL	25	XOHLEM01	15	UWELIS	15	UWELIS	15	HEBJAB	10	UBIPAY	15	SAHYOQ03	2	IDIWOH
16	IXURAV	12	MICDEJ	16	OKILEA	49	YARSAN	16	WAMRIN02	6	BUKMUQ	16	WAMRIN01	254	CIDKUX	16	IBICED	3	KEWZOD
17	HEBJAB	15	MOYMET	17	UBIPAY	24	XOHLEM	17	HAMJOW	13	LUFNAC05	17	MULQOA	23	GEDDAW	17	XEBHOC	64	OJICUG
18	XOHLEM	228	CIDKUX	18	MULQOA	132	DAWWEF	18	FAHFUR	8	BONMEX	18	BUKMUQ	59	QAQSAD	18	IBICUT	16	IBICED
19	XOHLEM01	23	RUVMAX	19	WEMGAY	22	MOYMET	19	IXAJUN	31	FEXCES	19	CAYDIR	27	LUFNAC05	19	PEVQEO	34	RAPYUE
20	WEMNAF	108	WECFAN	20	FABFOF	235	CIDKUX	20	KALGAH	22	BAKJII	20	CAYDOX06	24	GINLIA	20	XAWVUN	52	BEPMIU

Table 5.6. Ranking of top 20 MOFs based on four adsorbent evaluation metrics and charge assignment methods for CO_2/N_2 separation.

CO_2/N_2 selectivity at 0.1 bar				**CO_2/N_2 selectivity at 1 bar**				**ΔN_{CO2} (mol/kg)**				**APS (mol/kg)**				**R (%)**			
using DDEC		using IQEq		using DDEC		using IQEq		using DDEC		using IQEq		using DDEC		using IQEq		using DDEC		using IQEq	
1	FUDQIF	2	RIFQUT	1	FUDQIF	8	QOKCID	1	LOBHAM	349	MIBQAR16	1	BAXSIE	1	BAXSIE	1	VUSKAW	107	OJICUG
2	RIFQUT	1	FUDQIF	2	BAXSIE	1	FUDQIF	2	WEMGAY	38	SEQSOY	2	LOBHAM	104	WECFAN	2	IXOFEH	31	DAWWEF
3	VEQBID	11	QOKCID	3	FIPWOS	2	BAXSIE	3	UBIPAY	41	FEXCES	3	SEHZUB	351	MIBQAR16	3	IBICON	22	EDUSIF
4	BAXSIE	4	BAXSIE	4	RIFQUT	4	RIFQUT	4	WAMRIN02	3	UBIPAY	4	VEQBID	16	HEBJAB	4	MIBQAR	163	FABFOF
5	OKILEA	38	YARSAN	5	VEQBID	73	WECFAN	5	WAMRIN01	7	GINLIA	5	OLUCAZ	37	QOKCID	5	TEDGOA	162	HIFTOG
6	FIPWOS	348	MIBQAR16	6	SEHZUB	14	HEBJAB	6	WUHJIT	19	CENPUI	6	UBIPAY	53	QUTTII	6	BEPYIG	4	MIBQAR
7	GEDDAW	99	WECFAN	7	OLUCAZ	32	YARSAN	7	GINLIA	16	XOHLEM	7	OKILEA	18	FUDQIF	7	BEPLUF	87	BEPMIU
8	MICDEJ	29	HEBJAB	8	QOKCID	48	QUTTII	8	OKILEA	15	XOHLEM01	8	WEMGAY	7	OKILEA	8	SAHYOQ05	58	IBICUT
9	SEHZUB	5	OKILEA	9	LOBHAM	352	MIBQAR16	9	DABWUA	32	LUFNAC04	9	FIPWOS	6	UBIPAY	9	KEFBOO	6	BEPYIG
10	MULQOA	121	MUWQEB	10	OKILEA	10	OKILEA	10	SEHZUB	2	WEMGAY	10	WEMNAF	21	ADIQEL	10	BUWGEG	41	XEBHOC
11	QOKCID	68	QUTTII	11	IXURAV	57	VASKOR	11	PORVUO	14	PURJES	11	XOHLEM01	12	XOHLEM	11	VACFUB	72	TEDHAN
12	IXURAV	21	RUVMAX	12	FIPWUY	38	ADIQEL	12	HAFVOB	20	ADIQEL	12	XOHLEM	11	XOHLEM01	12	IDIWOH	48	VACFUB01
13	YEGCUJ	7	GEDDAW	13	UBIPAY	42	LETROT	13	BONMEX	81	DEYVUA	13	FIPWUY	69	SEQSOY	13	DIDDOK	53	PEVQAK
14	VICYUD	17	XOHLEM	14	HEBJAB	13	UBIPAY	14	PURJES	11	PORVUO	14	AVIMOI	70	FEXCES	14	SAHYOQ03	5	TEDGOA
15	LOBHAM	18	XOHLEM01	15	WEMGAY	3	FIPWOS	15	XOHLEM01	4	WAMRIN02	15	NARTIL	17	RUVMAX	15	GALCAZ	23	IDIWOH01
16	OLUCAZ	82	FEXCES	16	WEMNAF	17	OJIWIO	16	XOHLEM	26	RUVMAX	16	HEBJAB	79	VASKOR	16	SENWAL	37	KEWZOD
17	XOHLEM	23	YARKEJ	17	OJIWIO	11	IXURAV	17	BORBEQ	18	QUQFIS	17	RUVMAX	14	AVIMOI	17	DABWUA	11	VACFUB
18	XOHLEM01	133	LUFNAC04	18	NARTIL	23	XOHLEM	18	QUQFIS	23	LUFNAC01	18	FUDQIF	25	CENPUI	18	PEVQEO	12	IDIWOH
19	NERSUA	91	SEQSOY	19	CAYGIU	25	XOHLEM01	19	CENPUI	12	HAFVOB	19	VICYUD	9	FIPWOS	19	LAWGEW	52	IBIDAA
20	FIPWUY	8	MICDEJ	20	CAYDEN	84	TONBII	20	ADIQEL	29	LUFNAC03	20	MULQOA	64	QAQSAD	20	FAZPED	1	VUSKAW

Tables 5.5 and 5.6 shows the results of adsorbent evaluating metrics for the top 20 MOFs for CO_2/N_2 and CO_2/CH_4 separations, respectively. Here, it should be reminded that all results given in these tables were produced from the simulations that were performed for the optimized structures. For each ranking list, 20 MOFs are listed together with their rank in the corresponding list. The MOFs ranked in the list established using the DDEC were numbered from 1 to 20. Then, each MOF in the list created using IQEq was found in the list of DDEC and then given a number next to it depending on the rank of this MOF in the list based on DDEC method. The greatest number of common MOFs found in the sets of rankings is for the working capacity. 12 of the 20 MOFs ranked by using IQEq method are also included in the ranking list based on the DDEC method. For instance, UBIPAY is a MOF which was identified as the 9th best performing MOF adsorbent for CO_2/N_2 separation based on the simulations performed using non-optimized structure and the QEq. UBIPAY is ranked 3rd based on the DDEC and 4th based on the IQEq method, which can be regarded as a good estimation. The working capacity of this MOF was computed as 3.49 (2.86) mol/kg based on the simulations performed for the optimized structures and the DDEC (IQEq) method. Considering that the exact same working capacity was computed by using the IQEq and the non-optimized structure (2.86 mol/kg) and that UBIPAY was successfully covered in the top 4 MOFs of both DDEC and IQEq-based ranking lists in Table 5.5, the value computed based on the QEq method, 2.14 mol/kg, can be regarded as a bad estimation.

In Table 5.5, it is seen that 9 and 10 MOFs are common in the set of rankings based on adsorption selectivities at 0.1 and 1 bar, respectively. When further investigated, we see that the 3 of these common MOFs are located in the top 4 rows, which seems promising for the use of charge equilibration methods in the screening studies. For the metric of APS, we cannot give a similar example, because the ranking number of 2nd and 3rd MOF of the IQEq-based list was found to be 104 and 351 in the list created based on the DDEC method. However, the top MOF of two sets of rankings is the same, namely BAXSIE.

Similar examples can be given for Table 5.6 as well. Results from Table 5.6 shows that there are 11 common MOFs in two sets of rankings based on the adsorption selectivities at 0.1 bar. Moreover, 1st, 2nd, and the 4th MOFs in the list of DDEC is present in the top 4 MOFs identified by using IQEq. For working capacity, the highest number of common MOFs were attained with 14. Regenerability metric follows working capacity with 12 common MOFs. For regenerability, the top MOF is the same for both DDEC-based and IQEq-based lists, DAWWEF, which was identified as the 6th best performing MOF adsorbent for CO_2/CH_4 separation based on the simulations performed with the non-optimized structures. The APS value for this MOF was found to be 86.97 mol/kg when the simulations were performed for the non-optimized structure and based on the IQEq method. The APS value is calculated as 88.60 mol/kg for DAWWEF once the optimized structure was used. These two APS values are very similar regardless of the optimization. However, the APS value for DAWWEF was computed as 13.49 mol/kg which can be regarded as significantly different considering the effect of APS on the adsorbent separation performance rankings of MOFs. SUTBIT is another material that can be examined referring to the simulation results produced by using the non-optimized structures. For CO_2/CH_4 separation, SUTBIT was identified as the 9th best performing MOF based on the QEq method. Working capacity of SUTBIT was computed to be 5.26 and 5.42 mol/kg as very similar to each other. However, this MOF was ranked 47th in the lists created using the DDEC method based on the working capacity. The working capacity values calculated using DDEC method was 3.41 and this number was predicted by IQEq method as 5.45 for the optimized structure.

In general, the number of common MOFs identified based on the four adsorbent evaluation metrics is quite satisfying for either CO_2/CH_4 or CO_2/N_2 separation. The results support the idea of using charge equilibration methods for screening purposes. In our investigation on the 355 optimized MOFs, we saw that the IQEq method is quite successful in predicting the top 3 MOFs identified by the DDEC especially for the adsorption selectivity-based ranking.

Chapter 6
Conclusions and Outlook

In the first chapter of this work, we performed atomically-detailed GCMC and EMD simulations to predict the membrane-based separation performances of 139 different MOFs for He/CH_4 separation. Adsorption always favors CH_4 over He in all MOFs while diffusion favors He. When the adsorption selectivity dominates the diffusion selectivity, MOFs become CH_4 selective membranes. In a small number of materials, high adsorption selectivity of MOFs towards CH_4 is compensated by the high diffusion selectivity towards He because strongly adsorbed CH_4 molecules diffuse more slowly than the weakly adsorbed He molecules. These MOFs namely, GUPCUQ01, HUTZAX01 and PEHBIO, were identified to be He selective in addition to their high He permeabilities. He selectivity of MOF membranes were found to be generally lower than that of most polymeric membranes but He permeabilities of MOF membranes were predicted to be significantly higher than those of polymeric membranes and zeolite membranes. Considering the fact that most of the traditional membrane materials suffer from low He permeabilities, identification of the three MOF membranes that combine high He selectivity and high He permeability is important. Our results suggest that MOFs can be strong alternatives to polymers and zeolites in membrane-based He/CH_4 separations. We also compared the ideal and mixture selectivities of MOF membranes using both the single-component gas permeation data and mixture permeation data. Results showed that ideal selectivities can significantly overestimate the mixture selectivities, which suggests that computational studies should focus on simulations of gas mixtures to predict the real separation performance of membranes. Considering the large versatility in chemistries,

topologies and physical properties of MOFs, it is always challenging to give firm guidelines about the physical/chemical/structural characteristics of MOFs that make a good membrane for target gas separations. Based on the results of this study, we can provide some insights into MOF series that are worthy of future membrane research: All the MOFs are CH_4 selective in adsorption and diffusion selectivity determines the overall performance of the MOF membrane. In order to have a He selective membrane, diffusion of CH_4 should be very slow compared to that of He. MOFs with limiting pore diameters close to the kinetic diameter of CH_4 generally exhibit high diffusion selectivity for He. In fact, these MOFs (for example, GUPCUQ01, HUTZAX01 and PEHBIO) are the most promising membranes for highly selective separation of He from CH_4. MOFs with LPDs between 3.8–4 Å leads to diffusion selectivities towards He generally greater than 30, which can overcompensate the adsorption selectivities towards CH_4. In other words, one can roughly identify the highly He/CH_4 selective MOF membranes by screening the materials based on the pore diameters. An approach for large-pored MOFs can be tailoring the pore sizes of MOFs such as incorporation of guest molecules (i.e. ionic liquids, dye molecules) to narrow down the pore diameter to limit the diffusion of CH_4. These are the conclusions of molecular simulations performed only for 139 different MOF structures. Relations between structure and performance of MOFs are often too complex and require more materials to obtain clear fundamental insights into how structural properties relate to the gas separation performance of MOFs. Results of this work will be a guide for future computational studies to screen larger numbers of MOFs as membranes and trigger experimental studies to further investigate the MOFs that are identified to be highly promising for He/CH_4 separation. Finally, this work thoroughly focused on He separation from CH_4. Considering the equal importance of He recovery from the nitrogen rejection unit, studies that investigate He/N_2 separation potentials of MOF membranes would be also useful for the future application of these new materials

In the second part of this thesis, the effects of using different charge equilibration methods, IQEq and QEq, on the ranking of MOF adsorbents for CO_2/N_2 and CO_2/CH_4

separations were investigated. The choice of the charge assignment method was found to have a more pronounced effect on the simulated CO_2 uptakes due to the quadrupolar nature of this molecule. Four different adsorbent evaluation metrics of MOFs, namely, adsorption selectivity, working capacity, regenerability, and adsorbent performance score, were calculated using the simulations based on IQEq and QEq. IQEq method was found to have a tendency to overestimate the selectivity and APSs of MOFs compared to the QEq method. We ranked the MOF adsorbents based on evaluation metrics (MOFs having R%>85% were ranked based on their APSs) and identified the top 10 best MOFs for each gas separations

Results show that for CO_2/CH_4 separation, there is only one common MOF in the two sets of top 10 best performing MOF adsorbents established using the IQEq and QEq, while there is no common MOF in the top 10 MOF lists of CO_2/N_2 separation. Moreover, a MOF among the top 10 best list identified using the IQEq may not even have R%>85% based on the simulations using the QEq method, which prevents this MOF from being a potential adsorbent. This result is very significant because R% plays a major role in determining the best performing MOFs. Thus, a MOF identified as a candidate based on a charge assignment method might be identified as unpractical based on another method, showing the importance of election of the appropriate charge assignment methods prior to screening materials using molecular simulations. The calculated correlation factors (SRCC) quantifying the similarity on R% predicted from two different sets of simulations using different charge assignment methods were found to be 0.85 (0.82) for CO_2/CH_4 (CO_2/N_2) separations, which can be accepted as a moderately good coefficient considering the size of the dataset and the significance of this metric on the material choice. The correlation coefficients between the two sets of MOF rankings created by using the IQEq and QEq methods based on the four adsorbent evaluation metrics show that the rankings created by using the two methods have better similarity for CO_2/N_2 mixture.

Here, we should give details about the assumptions made during our simulations. First of all, MOF structures were assumed to be rigid which avoids the effect of flexibility on adsorption or diffusion. In simulations, we do not account for the stability problem of MOFs under a high pressure or temperature. However, we checked the chemical and mechanical stability of the promising MOFs from the experimental synthesis articles of these MOFs in the literature. Additionally, there might be some solvent molecules left inside the pores of the MOFs structures. These impurities present in the crystal file of the MOFs must be handled since they might cause a blockage for the pores. However, blockage of a pore has a more pronounced effect on the diffusion. Purification of a MOF crystal data file by removing all the solvent molecules or the ionic compounds which ensure the zero charge on the system is not always a simple and straight-forward procedure even if there are shared python scripts in the literature. Removing a solvent molecule or an ionic compound must be done wisely as the electrostatic potential and the porosity of this material may be affected enormously. Once a MOF is identified as promising membrane or adsorbent, the crystal structure of this MOF must be rechecked for further examination, and new simulations must be performed in case a purification, structure relaxation (due to the collapsing effect of the solvent removal), and accounting the flexibility is needed based on the screening purpose.

In the literature, it was reported that the IQEq method was better for the estimation of CO_2 adsorption than the other approximate charge equilibration methods. We tested this claim by comparing the CO_2 uptake and the CO_2 adsorption selectivity results computed using the IQEq method with the ones computed by using the a more accurate density functional theory (DFT)-based method, DDEC. Our results showed that there are large deviations between the values calculated form these two methods. This result is not surprising because the DDEC method was repeatedly stated to be a more accurate charge assignment method in the literature due to its quantum mechanical background. However, DFT-based methods are highly computationally demanding which makes charge equilibration methods to draw attention for the high-throughput screening of large

number of materials. Although the adsorption selectivity values calculated using DDEC and IQEq might be very different than each other, the similarity between the MOF rankings based on the adsorption selectivity is critical. The SRCCs quantifying the similarity between the two sets of MOF rankings based on the regenerability are 0.89 (0.86) for CO_2/CH_4 (CO_2/N_2). Even if the SRCC coefficients based on the adsorption selectivities change in the range of 0.71-0.78 for both mixtures, having 6-12 common MOFs in the top 20 MOFs of each ranking supports the idea of using IQEq method in screening studies instead of the computationally demanding DDEC method. The high correlation coefficients indicate that it might be a good strategy to start a high-throughput computational screening study with the IQEq and continue with a narrowed list of MOFs by using the DDEC method. Since identifying a charge assignment method as the best one is not a straight-forward and a simple task, the user should choose a method wisely depending on the screening purpose. Finally, this study focused only on the comparison of different charge assignment methods in the sense of MOF rankings constructed by using different adsorbent selection metrics for CO_2/N_2 and CO_2/CH_4, rather than the identifying the best one between these two methods. Results of this work will be a guide for future computational studies to screen larger numbers of MOFs as adsorbents for the separation of quadrupolar molecules.

BIBLIOGRAPHY

1. Rufford, T. E.; Chan, K. I.; Huang, S. H.; May, E. F., A review of conventional and emerging process technologies for the recovery of helium from natural gas. *Adsorption Science & Technology* 2014, *32* (1), 49-72.

2. Haussinger, P.; Glathaar, R.; Rhode, W.; Kick, H.; Benkmann, C.; Weber, J.; Wunschel, H.-J.; Stenke, V.; Leicht, E.; Stenger, H., Noble Gases. In *Ullmann's Encyclopedia of Industrial Chemistry*, John Wiley and Sons: Hoboken, NJ, USA, 2011; pp 392–448.

3. Clarke, R.; Nuttall, W.; Glowacki, B., Endangered helium: Bursting the myth. *The Chemical Engineer, Institution of Chemical Engineers, Rugby, UK* 2013, pp. 32–36.

4. Hu, W.; Wu, X.; Li, Z.; Yang, J., Helium separation via porous silicene based ultimate membrane. *Nanoscale* 2013, *5* (19), 9062-9066.

5. Schlatter, T. W., Atmospheric composition and vertical structure. *Earth System Research Laboratory, National Oceanic and Atmospheric Administration, Boulder, CO, USA* 2009.

6. Scholes, C. A.; Ghosh, U. K., Review of Membranes for Helium Separation and Purification. *Membranes* 2017, *7* (1), 9.

7. Scholes, C. A.; Ghosh, U., Helium separation through polymeric membranes: selectivity targets. *Journal of Membrane Science* 2016, *520*, 221-230.

8. Towler, G.; Sinnott, R. K., *Chemical engineering design: principles, practice and economics of plant and process design*. Elsevier: 2012.

9. Stock, N.; Biswas, S., Synthesis of metal-organic frameworks (MOFs): routes to various MOF topologies, morphologies, and composites. *Chemical reviews* 2011, *112* (2), 933-969.

10. Allen, F. H., The Cambridge Structural Database: a quarter of a million crystal structures and rising. *Acta Crystallographica Section B: Structural Science* 2002, *58* (3), 380-388.

11. Basdogan, Y.; Keskin, S., Simulation and modelling of MOFs for hydrogen storage. *CrystEngComm* 2015, *17* (2), 261-275.

12. Keskin, S.; van Heest, T. M.; Sholl, D. S., Can Metal–Organic Framework Materials Play a Useful Role in Large-Scale Carbon Dioxide Separations? *ChemSusChem* 2010, *3* (8), 879-891.

13. Kuppler, R. J.; Timmons, D. J.; Fang, Q.-R.; Li, J.-R.; Makal, T. A.; Young, M. D.; Yuan, D.; Zhao, D.; Zhuang, W.; Zhou, H.-C., Potential applications of metal-organic frameworks. *Coordination Chemistry Reviews* 2009, *253* (23-24), 3042-3066.

14. Furukawa, H.; Cordova, K. E.; O'Keeffe, M.; Yaghi, O. M., The chemistry and applications of metal-organic frameworks. *Science* 2013, *341* (6149), 1230444.

15. Argueta, E.; Shaji, J.; Gopalan, A.; Liao, P.; Snurr, R. Q.; Gomez-Gualdron, D. A., Molecular building block-based electronic charges for high-throughput screening of MOFs for adsorption applications. *Journal of chemical theory and computation* 2017.

16. Frenkel, D.; Smit, B., Monte Carlo Simulations in Various Ensembles. In *Understanding Molecular Simulation*, 2nd ed.; Academic Press San Diego, CA, 2002; p 111−137.

17. Hamad, S.; Balestra, S. R.; Bueno-Perez, R.; Calero, S.; Ruiz-Salvador, A. R., Atomic charges for modeling metal–organic frameworks: Why and how. *Journal of Solid State Chemistry* 2015, *223*, 144-151.

18. Wilmer, C. E.; Leaf, M.; Lee, C. Y.; Farha, O. K.; Hauser, B. G.; Hupp, J. T.; Snurr, R. Q., Large-scale screening of hypothetical metal–organic frameworks. *Nature Chemistry* 2012, *4* (2), 83.

19. Erucar, I.; Keskin, S., Computational assessment of MOF membranes for CH_4/H_2 separations. *Journal of Membrane Science* 2016, *514*, 313-321.

20. Yang, Q.; Zhong, C.; Chen, J.-F., Computational study of CO_2 storage in metal− organic frameworks. *The Journal of Physical Chemistry C* 2008, *112* (5), 1562-1569.

21. Liu, B.; Smit, B., Comparative molecular simulation study of CO_2/N_2 and CH_4/N_2 separation in zeolites and metal− organic frameworks. *Langmuir* 2009, *25* (10), 5918-5926.

22. Erucar, I.; Keskin, S., Computational modeling of bio-MOFs for CO_2/CH_4 separations. *Chemical Engineering Science* 2015, *130*, 120-128.

23. Fracaroli, A. M.; Furukawa, H.; Suzuki, M.; Dodd, M.; Okajima, S.; Gándara, F.; Reimer, J. A.; Yaghi, O. M., Metal–Organic Frameworks with Precisely Designed Interior for Carbon Dioxide Capture in the Presence of Water. *Journal of the American Chemical Society* 2014, *136* (25), 8863-8866.

24. Campaná, C.; Mussard, B.; Woo, T. K., Electrostatic potential derived atomic charges for periodic systems using a modified error functional. *Journal of chemical theory and computation* 2009, *5* (10), 2866-2878.

25. Manz, T. A.; Sholl, D. S., Improved atoms-in-molecule charge partitioning functional for simultaneously reproducing the electrostatic potential and chemical states in periodic and nonperiodic materials. *Journal of chemical theory and computation* 2012, *8* (8), 2844-2867.

26. Mulliken, R. S., Electronic population analysis on LCAO–MO molecular wave functions. I. *The Journal of Chemical Physics* 1955, *23* (10), 1833-1840.

27. Rappe, A. K.; Goddard, W. A., Charge equilibration for molecular dynamics simulations. *The Journal of Physical Chemistry* 1991, *95* (8), 3358-3363.

28. Ramachandran, S.; Lenz, T.; Skiff, W.; Rappe, A., Toward an understanding of zeolite Y as a cracking catalyst with the use of periodic charge equilibration. *The Journal of Physical Chemistry* 1996, *100* (14), 5898-5907.

29. Wilmer, C. E.; Kim, K. C.; Snurr, R. Q., An Extended Charge Equilibration Method. *The Journal of Physical Chemistry Letters* 2012, *3* (17), 2506-2511.

30. Wells, B. A.; De Bruin-Dickason, C.; Chaffee, A. L., Charge equilibration based on atomic ionization in metal–organic frameworks. *The Journal of Physical Chemistry C* 2014, *119* (1), 456-466.

31. Kadantsev, E. S.; Boyd, P. G.; Daff, T. D.; Woo, T. K., Fast and accurate electrostatics in metal organic frameworks with a robust charge equilibration parameterization for high-throughput virtual screening of gas adsorption. *The Journal of Physical Chemistry Letters* 2013, *4* (18), 3056-3061.

32. Khan, N. A.; Hasan, Z.; Jhung, S. H., Adsorptive removal of hazardous materials using metal-organic frameworks (MOFs): a review. *Journal of hazardous materials* 2013, *244*, 444-456.

33. Qiu, S.; Xue, M.; Zhu, G., Metal–organic framework membranes: from synthesis to separation application. *Chemical Society Reviews* 2014, *43* (16), 6116-6140.

34. Colón, Y. J.; Snurr, R. Q., High-throughput computational screening of metal–organic frameworks. *Chemical Society Reviews* 2014, *43* (16), 5735-5749.

35. Krishna, R.; Van Baten, J., Using molecular simulations for screening of zeolites for separation of CO_2/CH_4 mixtures. *Chemical Engineering Journal* 2007, *133* (1-3), 121-131.

36. Babarao, R.; Jiang, J.; Sandler, S. I., Molecular simulations for adsorptive separation of CO_2/CH_4 mixture in metal-exposed, catenated, and charged metal− organic frameworks. *Langmuir* 2008, *25* (9), 5239-5247.

37. Liu, J.; Keskin, S.; Sholl, D. S.; Johnson, J. K., Molecular simulations and theoretical predictions for adsorption and diffusion of CH_4/H_2 and CO_2/CH_4 mixtures in ZIFs. *The Journal of Physical Chemistry C* 2011, *115* (25), 12560-12566.

38. Sumer, Z.; Keskin, S., Computational Screening of MOF-Based Mixed Matrix Membranes for CO_2/N_2 Separations. *Journal of Nanomaterials* 2016, *2016*.

39. Keskin, S.; Sholl, D. S., Assessment of a Metal−Organic Framework Membrane for Gas Separations Using Atomically Detailed Calculations: CO_2, CH_4, N_2, H_2 Mixtures in MOF-5. *Industrial & Engineering Chemistry Research* 2009, *48* (2), 914-922.

40. Battisti, A.; Taioli, S.; Garberoglio, G., Zeolitic imidazolate frameworks for separation of binary mixtures of CO_2, CH_4, N_2 and H_2: A computer simulation investigation. *Microporous and Mesoporous Materials* 2011, *143* (1), 46-53.

41. Haldoupis, E.; Nair, S.; Sholl, D. S., Finding MOFs for highly selective CO_2/N_2 adsorption using materials screening based on efficient assignment of atomic point charges. *Journal of the American Chemical Society* 2012, *134* (9), 4313-4323.

42. Liu, B.; Smit, B., Molecular simulation studies of separation of CO_2/N_2, CO_2/CH_4, and CH_4/N_2 by ZIFs. *The Journal of Physical Chemistry C* 2010, *114* (18), 8515-8522.

43. Krishna, R.; van Baten, J. M., Comment on comparative molecular simulation study of CO_2/N_2 and CH_4/N_2 separation in zeolites and metal− organic frameworks. *Langmuir* 2009, *26* (4), 2975-2978.

44. Wu, D.; Wang, C.; Liu, B.; Liu, D.; Yang, Q.; Zhong, C., Large-scale computational screening of metal-organic frameworks for CH_4/H_2 separation. *AIChE Journal* 2012, *58* (7), 2078-2084.

45. Guo, H.-c.; Shi, F.; Ma, Z.-f.; Liu, X.-q., Molecular simulation for adsorption and separation of CH_4/H_2 in zeolitic imidazolate frameworks. *The Journal of Physical Chemistry C* 2010, *114* (28), 12158-12165.

46. Keskin, S., Molecular simulation study of CH_4/H_2 mixture separations using metal organic framework membranes and composites. *The Journal of Physical Chemistry C* 2010, *114* (30), 13047-13054.

47. Altintas, C.; Erucar, I.; Keskin, S., High-Throughput Computational Screening of the Metal Organic Framework Database for CH_4/H_2 Separations. *ACS applied materials & interfaces* 2018, *10* (4), 3668-3679.

48. Sumer, Z.; Keskin, S., Adsorption-and Membrane-Based CH_4/N_2 Separation Performances of MOFs. *Industrial & Engineering Chemistry Research* 2017, *56* (30), 8713-8722.

49. Valenzano, L.; Civalleri, B.; Chavan, S.; Palomino, G. T.; Areán, C. O.; Bordiga, S., Computational and Experimental Studies on the Adsorption of CO, N_2, and CO_2 on Mg-MOF-74. *The Journal of Physical Chemistry C* 2010, *114* (25), 11185-11191.

50. Zheng, C.; Liu, D.; Yang, Q.; Zhong, C.; Mi, J., Computational study on the influences of framework charges on CO_2 uptake in metal− organic frameworks. *Industrial & Engineering Chemistry Research* 2009, *48* (23), 10479-10484.

51. Sagara, T.; Klassen, J.; Ganz, E., Computational study of hydrogen binding by metal-organic framework-5. *The Journal of chemical physics* 2004, *121* (24), 12543-12547.

52. Yang, S. J.; Kim, T.; Im, J. H.; Kim, Y. S.; Lee, K.; Jung, H.; Park, C. R., MOF-derived hierarchically porous carbon with exceptional porosity and hydrogen storage capacity. *Chemistry of Materials* 2012, *24* (3), 464-470.

53. Klontzas, E.; Mavrandonakis, A.; Tylianakis, E.; Froudakis, G. E., Improving hydrogen storage capacity of MOF by functionalization of the organic linker with lithium atoms. *Nano letters* 2008, *8* (6), 1572-1576.

54. Yang, Q.; Zhong, C., Understanding Hydrogen Adsorption in Metal−Organic Frameworks with Open Metal Sites: A Computational Study. *The Journal of Physical Chemistry B* 2006, *110* (2), 655-658.

55. Ranjan, R.; Tsapatsis, M., Microporous metal organic framework membrane on porous support using the seeded growth method. *Chemistry of Materials* 2009, *21* (20), 4920-4924.

56. Takamizawa, S.; Takasaki, Y.; Miyake, R., Single-crystal membrane for anisotropic and efficient gas permeation. *Journal of the American Chemical Society* 2010, *132* (9), 2862-2863.

57. Yoo, Y.; Varela-Guerrero, V.; Jeong, H.-K., Isoreticular metal− organic frameworks and their membranes with enhanced crack resistance and moisture stability by surfactant-assisted drying. *Langmuir* 2011, *27* (6), 2652-2657.

58. Zhao, Z.; Ma, X.; Li, Z.; Lin, Y., Synthesis, characterization and gas transport properties of MOF-5 membranes. *Journal of membrane science* 2011, *382* (1), 82-90.

59. Cao, F.; Zhang, C.; Xiao, Y.; Huang, H.; Zhang, W.; Liu, D.; Zhong, C.; Yang, Q.; Yang, Z.; Lu, X., Helium recovery by a Cu-BTC metal–organic-framework membrane. *Industrial & Engineering Chemistry Research* 2012, *51* (34), 11274-11278.

60. Hara, N.; Yoshimune, M.; Negishi, H.; Haraya, K.; Hara, S.; Yamaguchi, T., Diffusive separation of propylene/propane with ZIF-8 membranes. *Journal of Membrane Science* 2014, *450*, 215-223.

61. Kasik, A.; Dong, X.; Lin, Y., Synthesis and stability of zeolitic imidazolate framework-68 membranes. *Microporous and Mesoporous Materials* 2015, *204*, 99-105.

62. Mayo, S. L.; Olafson, B. D.; Goddard, W. A., DREIDING: a generic force field for molecular simulations. *J. phys. Chem* 1990, *94* (26), 8897-8909.

63. Rappé, A. K.; Casewit, C. J.; Colwell, K.; Goddard Iii, W.; Skiff, W., UFF, a full periodic table force field for molecular mechanics and molecular dynamics simulations. *Journal of the American chemical society* 1992, *114* (25), 10024-10035.

64. Martin, M. G.; Siepmann, J. I., Transferable Potentials for Phase Equilibria. 1. United-Atom Description of n-Alkanes. *The Journal of Physical Chemistry B* 1998, *102* (14), 2569-2577.

65. Allen, M. P.; Tildesley, D. J., *Computer simulation of liquids*. Oxford university press: 2017.

66. Jorgensen, W. L., Optimized intermolecular potential functions for liquid alcohols. *The Journal of Physical Chemistry* 1986, *90* (7), 1276-1284.

67. Watanabe, T.; Sholl, D. S., Accelerating applications of metal–organic frameworks for gas adsorption and separation by computational screening of materials. *Langmuir* 2012, *28* (40), 14114-14128.

68. Qiao, Z.; Zhang, K.; Jiang, J., In silico screening of 4764 computation-ready, experimental metal–organic frameworks for CO_2 separation. *Journal of Materials Chemistry A* 2016, *4* (6), 2105-2114.

69. Nazarian, D.; Camp, J. S.; Sholl, D. S., A Comprehensive Set of High-Quality Point Charges for Simulations of Metal–Organic Frameworks. *Chemistry of Materials* 2016, *28* (3), 785-793.

70. Wu, D.; Yang, Q.; Zhong, C.; Liu, D.; Huang, H.; Zhang, W.; Maurin, G., Revealing the structure–property relationships of metal–organic frameworks for CO_2 capture from flue gas. *Langmuir* 2012, *28* (33), 12094-12099.

71. Xu, Q.; Zhong, C., A General Approach for Estimating Framework Charges in Metal−Organic Frameworks. *The Journal of Physical Chemistry C* 2010, *114* (11), 5035-5042.

72. Qiao, Z.; Peng, C.; Zhou, J.; Jiang, J., High-throughput computational screening of 137953 metal–organic frameworks for membrane separation of a $CO_2/N_2/CH_4$ mixture. *Journal of Materials Chemistry A* 2016, *4* (41), 15904-15912.

73. Ozturk, T. N.; Keskin, S., Computational screening of porous coordination networks for adsorption and membrane-based gas separations. *The Journal of Physical Chemistry C* 2014, *118* (25), 13988-13997.

74. Canepa, P.; Arter, C. A.; Conwill, E. M.; Johnson, D. H.; Shoemaker, B. A.; Soliman, K. Z.; Thonhauser, T., High-throughput screening of small-molecule adsorption in MOF. *Journal of Materials Chemistry A* 2013, *1* (43), 13597-13604.

75. Bader, R. F., Atoms in molecules. *Encyclopedia of computational Chemistry* 2002, *1*.

76. Li, W.; Rao, Z.; Chung, Y. G.; Li, S., The Role of Partial Atomic Charge Assignment Methods on the Computational Screening of Metal-Organic Frameworks for CO_2 Capture under Humid Conditions. *ChemistrySelect* 2017, *2* (29), 9458-9465.

77. Li, S.; Chung, Y. G.; Snurr, R. Q., High-Throughput Screening of Metal–Organic Frameworks for CO_2 Capture in the Presence of Water. *Langmuir* 2016, *32* (40), 10368-10376.

78. Chung, Y. G.; Camp, J.; Haranczyk, M.; Sikora, B. J.; Bury, W.; Krungleviciute, V.; Yildirim, T.; Farha, O. K.; Sholl, D. S.; Snurr, R. Q., Computation-Ready, Experimental Metal–Organic Frameworks: A Tool To Enable High-Throughput Screening of Nanoporous Crystals. *Chemistry of Materials* 2014, *26* (21), 6185-6192.

79. Sezginel, K. B.; Uzun, A.; Keskin, S., Multivariable linear models of structural parameters to predict methane uptake in metal-organic frameworks. *Chemical Engineering Science* 2015, *124*, 125-134.

80. Willems, T. F.; Rycroft, C. H.; Kazi, M.; Meza, J. C.; Haranczyk, M., Algorithms and tools for high-throughput geometry-based analysis of crystalline porous materials. *Microporous and Mesoporous Materials* 2012, *149* (1), 134-141.

81. Sumer, Z.; Keskin, S., Ranking of MOF Adsorbents for CO_2 Separations: A Molecular Simulation Study. *Industrial & Engineering Chemistry Research* 2016, *55* (39), 10404-10419.

82. Moghadam, P. Z.; Li, A.; Wiggin, S. B.; Tao, A.; Maloney, A. G.; Wood, P. A.; Ward, S. C.; Fairen-Jimenez, D., Development of a Cambridge Structural Database subset: a collection

of metal–organic frameworks for past, present, and future. *Chemistry of Materials* 2017, *29* (7), 2618-2625.

83. KITAO, O.; OGAWA, T., I: METHODOLOGY: Consistent charge equilibration (CQEq). *Molecular Physics* 2003, *101* (1-2), 3-17.

84. Dubbeldam, D.; Calero, S.; Ellis, D. E.; Snurr, R. Q., RASPA: molecular simulation software for adsorption and diffusion in flexible nanoporous materials. *Molecular Simulation* 2016, *42* (2), 81-101.

85. DasGupta, A.; Huzinaga, S., New developments in CNDO molecular orbital theory. *Theoretica chimica acta* 1974, *35* (4), 329-340.

86. Chen, J.; Hundertmark, D.; Martínez, T. J., A unified theoretical framework for fluctuating-charge models in atom-space and in bond-space. *The Journal of chemical physics* 2008, *129* (21), 214113.

87. Frenkel, D., Introduction to monte carlo methods. *NIC series* 2004, *23*, 29-60.

88. Smith, W., The minimum image convention in non-cubic MD cells. *CCP5 Information Quarterly for Computer Simulation of Condensed Phases* 1989, *30*, 35.

89. Allen, M. P., Introduction to molecular dynamics simulation. *Computational soft matter: from synthetic polymers to proteins* 2004, *23*, 1-28.

90. Allen, M. P.; Tildesley, D. J., *Computer simulation of liquids*. Oxford university press: 1987.

91. Nosé, S., A molecular dynamics method for simulations in the canonical ensemble. *Molecular physics* 1984, *52* (2), 255-268.

92. Hoover, W. G., Canonical dynamics: equilibrium phase-space distributions. *Physical review A* 1985, *31* (3), 1695.

93. Berendsen, H. J.; Postma, J. v.; van Gunsteren, W. F.; DiNola, A.; Haak, J., Molecular dynamics with coupling to an external bath. *The Journal of chemical physics* 1984, *81* (8), 3684-3690.

94. Sholl, D. S., Understanding Macroscopic Diffusion of Adsorbed Molecules in Crystalline Nanoporous Materials via Atomistic Simulations. *Accounts of Chemical Research* 2006, *39* (6), 403-411.

95. Einstein, A., *Investigations on the Theory of the Brownian Movement*. Courier Corporation: 1956.

96. Frenkel, D.; Smit, B., *Understanding Molecular Simulation: From Algorithms to Applications*. Second ed.; Academic Press: London, 2002.

97. Keskin, S.; Sholl, D. S., Efficient methods for screening of metal organic framework membranes for gas separations using atomically detailed models. *Langmuir* 2009, *25* (19), 11786-11795.

98. Erucar, I.; Keskin, S., High CO_2 Selectivity of an Amine-Functionalized Metal Organic Framework in Adsorption-Based and Membrane-Based Gas Separations. *Industrial & Engineering Chemistry Research* 2013, *52* (9), 3462-3472.

99. J., P. J.; Ilja, S. J., Vapor–liquid equilibria of mixtures containing alkanes, carbon dioxide, and nitrogen. *AIChE Journal* 2001, *47* (7), 1676-1682.

100. Potoff, J. J.; Siepmann, J. I., Vapor–liquid equilibria of mixtures containing alkanes, carbon dioxide, and nitrogen. *AIChE Journal* 2001, *47* (7), 1676-1682.

101. Garcia-Sanchez, A.; Dubbeldam, D.; Calero, S., Modeling adsorption and self-diffusion of methane in LTA zeolites: the influence of framework flexibility. *The Journal of Physical Chemistry C* 2010, *114* (35), 15068-15074.

102. Krishna, R.; van Baten, J. M., In silica screening of zeolite membranes for CO_2 Capture. *J. Memb. Sci.* 2010, *360*, 323-333.

103. Krishna, R.; van Baten, J. M., Using molecular simulations for screening of zeolites for separation of CO_2/CH_4 mixtures *Chem. Eng. J.* 2007, *133* (1-3), 121-131.

104. Bae, Y. S.; Snurr, R. Q., Development and evaluation of porous materials for carbon dioxide separation and capture. *Angewandte Chemie International Edition* 2011, *50* (49), 11586-11596.

105. Chung, Y. G.; Gómez-Gualdrón, D. A.; Li, P.; Leperi, K. T.; Deria, P.; Zhang, H.; Vermeulen, N. A.; Stoddart, J. F.; You, F.; Hupp, J. T., In silico discovery of metal-organic frameworks for precombustion CO_2 capture using a genetic algorithm. *Science advances* 2016, *2* (10), e1600909.

106. Palomino, M.; Corma, A.; Rey, F.; Valencia, S., New Insights on CO_2−Methane Separation Using LTA Zeolites with Different Si/Al Ratios and a First Comparison with MOFs. *Langmuir* 2010, *26* (3), 1910-1917.

107. Basdogan, Y.; Sezginel, K. B.; Keskin, S., Identifying highly selective metal organic frameworks for CH_4/H_2 separations using computational tools. *Ind. Eng. Chem. Res.* 2015, *54* (34), 8479-8491.

108. Adatoz, E.; Keskin, S., Application of MD simulations to predict membrane properties of MOFs. *J. Nanomater.* 2015, *2015*, 1-9.

109. Robeson, L. M., The upper bound revisited. *Journal of Membrane Science* 2008, *320* (1), 390-400.

110. Robeson, L. M., Correlation of separation factor versus permeability for polymeric membranes. *Journal of membrane science* 1991, *62* (2), 165-185.

111. Himeno, S.; Tomita, T.; Suzuki, K.; Nakayama, K.; Yajima, K.; Yoshida, S., Synthesis and permeation properties of a DDR-type zeolite membrane for separation of CO_2/CH_4 gaseous mixtures. *Industrial & Engineering Chemistry Research* 2007, *46* (21), 6989-6997.

112. Zhu, X.; Wang, H.; Lin, Y., Effect of the membrane quality on gas permeation and chemical vapor deposition modification of MFI-type zeolite membranes. *Industrial & Engineering Chemistry Research* 2010, *49* (20), 10026-10033.

113. van den Bergh, J.; Tihaya, A.; Kapteijn, F., High temperature permeation and separation characteristics of an all-silica DDR zeolite membrane. *Microporous and Mesoporous Materials* 2010, *132* (1), 137-147.

114. Sorenson, S. G.; Payzant, E. A.; Gibbons, W. T.; Soydas, B.; Kita, H.; Noble, R. D.; Falconer, J. L., Influence of zeolite crystal expansion/contraction on NaA zeolite membrane separations. *Journal of membrane science* 2011, *366* (1), 413-420.

115. Lassinantti, M.; Jareman, F.; Hedlund, J.; Creaser, D.; Sterte, J., Preparation and evaluation of thin ZSM-5 membranes synthesized in the absence of organic template molecules. *Catalysis today* 2001, *67* (1), 109-119.

116. Keskin, S.; Sholl, D. S., Screening metal-organic framework materials for membrane-based methane/carbon dioxide separations. *J. Phys. Chem. C* 2007, *111* (38), 14055-14059.

117. Tian, Y. Q.; Yao, S. Y.; Gu, D.; Cui, K. H.; Guo, D. W.; Zhang, G.; Chen, Z. X.; Zhao, D. Y., Cadmium imidazolate frameworks with polymorphism, high thermal stability, and a large surface area. *Chemistry–A European Journal* 2010, *16* (4), 1137-1141.

118. Ma, Y.; Han, Z.; He, Y.; Yang, L., A 3D chiral Zn (II) coordination polymer with triple Zn–oba–Zn helical chains (oba= 4, 4′-oxybis (benzoate)). *Chemical Communications* 2007, (40), 4107-4109.

119. Soler, J. M.; Artacho, E.; Gale, J. D.; García, A.; Junquera, J.; Ordejón, P.; Sánchez-Portal, D., The SIESTA method for ab initio order-N materials simulation. *Journal of Physics: Condensed Matter* 2002, *14* (11), 2745.

120. Haldoupis, E.; Borycz, J.; Shi, H.; Vogiatzis, K. D.; Bai, P.; Queen, W. L.; Gagliardi, L.; Siepmann, J. I., Ab Initio Derived Force Fields for Predicting CO_2 Adsorption and Accessibility of Metal Sites in the Metal–Organic Frameworks M-MOF-74 (M = Mn, Co, Ni, Cu). *The Journal of Physical Chemistry C* 2015, *119* (28), 16058-16071.

121. Jürg, H.; Marcella, I.; Florian, S.; Joost, V., cp2k: atomistic simulations of condensed matter systems. *Wiley Interdisciplinary Reviews: Computational Molecular Science* 2014, *4* (1), 15-25.

APPENDICES

APPENDIX A: Supplementary Information for Chapter 4[†]

Table A.1. List of 139 MOFs studied in this work and their structural properties.

MOFs	Common Name	LPD (Å)	LCD (Å)	Porosity	Density (g/cm^3)	Surface Area (m^2/g)	Pore Volume (cm^3/g)
ACENIF		4.18	5.48	0.53	1.31	1123.09	0.41
AFUJUI		3.91	6.22	0.52	1.15	1145.39	0.45
ALICEE		8.88	8.89	0.58	1.70	855.53	0.34
ALICII		9.45	9.46	0.62	1.51	988.73	0.41
ALOLOD	CPM-3	6.40	9.92	0.69	0.79	2417.07	0.87
AMAFUQ		5.81	6.74	0.45	1.55	649.25	0.29
AVEROJ		6.81	7.01	0.60	1.70	1029.36	0.35
BIYTEJ		6.39	6.54	0.54	1.39	865.25	0.39
BONMAT		5.03	6.20	0.64	0.86	2603.79	0.75
BUSMUY		5.90	7.34	0.50	1.26	785.33	0.40
BUSNAF		5.43	7.08	0.45	1.32	625.93	0.34
BUVWOF02		5.39	7.03	0.47	1.26	707.80	0.37
BUVXOG01		5.43	7.08	0.47	1.33	658.04	0.36
BUVYIB01		8.63	10.82	0.71	0.70	3596.36	1.01
CAYBAH		4.07	5.33	0.50	1.49	839.46	0.34
CAYDOX		4.99	5.15	0.47	1.49	561.34	0.31
CAYGIU		5.00	5.15	0.47	1.49	577.41	0.31
CUGVUW		4.58	6.47	0.45	1.36	558.92	0.33
DIDBID		5.88	9.15	0.59	0.93	1785.42	0.64
DIDBOJ		5.75	9.16	0.60	0.92	1764.74	0.65

[†] The results given in this chapter were published in Separation and Purification Technology with following reference: Kadioglu, O., & Keskin, S. (2018). Efficient separation of helium from methane using MOF membranes. *Separation and Purification Technology, 191*, 192-199.This chapter is the reformatted version of the mentioned research paper.

DOTSOV		6.69	13.29	0.72	0.89	2507.25	0.81
EBAMOL		4.27	7.96	0.60	1.05	1784.88	0.57
ECAHIB		4.45	6.63	0.47	1.41	631.09	0.33
EJOGOZ		7.64	8.53	0.55	1.10	1290.57	0.50
EMIHAK		5.00	6.83	0.65	1.48	1605.42	0.44
EMIHIS	SCIF-9	5.92	9.63	0.69	1.48	1514.63	0.46
EXOTUH		4.41	6.06	0.62	1.09	2080.45	0.57
EYOPOY		5.28	6.13	0.57	1.13	1353.23	0.50
EYOPUE		5.70	6.46	0.53	1.20	695.58	0.44
EYOQEP		4.17	6.74	0.55	1.15	1254.70	0.48
EZILUV		3.93	9.54	0.63	0.94	2234.09	0.67
FANWIC		8.17	9.50	0.58	1.01	1362.43	0.58
FANWOI		8.59	9.82	0.58	1.00	1388.94	0.59
FAYPUS	DMOF-5	4.26	13.62	0.66	0.84	1895.97	0.78
FAYRAA	MOF-01	6.64	11.92	0.72	0.72	2713.58	0.99
FEHCOM		6.75	7.42	0.63	0.95	1940.01	0.66
FEVFUJ		10.18	11.00	0.67	0.81	1904.78	0.83
GALBUS		6.25	9.07	0.59	0.96	1703.85	0.62
GIQHAQ		14.41	14.51	0.63	1.17	1234.98	0.54
GITVIP01		5.47	17.01	0.63	1.15	1251.92	0.55
GIVDUL		4.76	6.31	0.58	1.82	949.84	0.32
GUPBEZ		4.38	7.29	0.44	2.54	235.53	0.18
GUPCOK		4.70	7.33	0.61	1.10	1450.13	0.56
GUPCUQ01		3.83	12.59	0.65	1.14	1533.97	0.58
GUSPUG	MFU-5	11.38	13.36	0.55	1.45	708.37	0.38
HASSUR		5.33	7.03	0.63	1.00	2398.88	0.63
HECQUB		5.10	8.60	0.69	0.79	2942.74	0.88
HIFVUO		5.98	7.50	0.71	0.82	2764.53	0.87
HOHMIB		11.42	13.19	0.78	0.54	4221.83	1.45
HUTZAX01		3.93	5.14	0.46	1.42	461.43	0.32
IDIWOH		7.19	7.68	0.63	1.00	1961.16	0.63
IMIXEI		5.53	7.09	0.72	0.81	3502.79	0.89
ISOJOQ		4.18	5.96	0.61	0.99	2385.50	0.62
JENKIX		7.49	9.92	0.57	1.01	1298.57	0.56

KARLAS	MCF-19-Ia	4.30	7.97	0.60	1.06	1742.22	0.57
KEYFIF		4.90	5.40	0.40	1.63	339.42	0.25
KIPKIF		10.33	10.42	0.55	1.11	724.82	0.50
KIYMIQ		5.36	5.47	0.34	1.33	284.13	0.25
KOJCUI		4.82	5.42	0.40	1.52	448.83	0.26
LARVIL		6.98	7.06	0.52	2.24	390.22	0.23
LETFEW		4.46	5.62	0.47	2.12	475.09	0.22
LUMDIG		4.95	7.91	0.55	1.29	1077.33	0.42
MAFDII		4.68	6.18	0.60	1.14	1401.33	0.53
MIBQAR		7.96	15.10	0.81	0.59	3774.44	1.38
MIYGOR		4.13	6.66	0.54	1.61	853.81	0.33
MIYGUX		3.90	6.46	0.54	1.36	772.96	0.40
NAZBAT		4.61	6.91	0.61	1.03	1972.64	0.59
NEVPUA		5.21	6.36	0.46	1.66	579.57	0.28
NEVQAH		5.17	6.31	0.45	1.82	524.88	0.25
NEXXIZ		8.71	9.67	0.54	0.90	1001.04	0.60
NEYYOG		10.67	12.40	0.50	2.30	299.21	0.22
NICJOA		4.20	5.24	0.35	2.06	233.38	0.17
OHUKIM		8.30	14.71	0.80	0.42	4895.93	1.88
OMORUE		5.34	6.44	0.71	0.80	3863.48	0.89
OTARIL		3.91	5.67	0.49	1.17	873.58	0.42
OWITAQ		5.36	7.59	0.77	0.66	4599.88	1.18
OWITEU		5.32	7.56	0.77	0.64	4682.63	1.19
OWITIY		5.80	7.66	0.77	0.59	4912.40	1.30
OWITOE		5.28	7.52	0.77	0.65	4648.37	1.17
OWITUK		5.32	7.56	0.77	0.64	4719.95	1.19
OWIVAS		5.34	7.56	0.77	0.66	4559.27	1.17
OWIVEW		4.45	6.91	0.71	0.83	3861.57	0.86
OYODEM		5.23	8.96	0.56	1.02	1207.29	0.54
PAQFIY		4.13	5.05	0.43	1.63	393.66	0.27
PEHBIO		3.83	5.33	0.63	1.14	2038.46	0.55
PEJNOJ		5.54	6.21	0.71	0.80	3506.54	0.89
PURQOJ		6.85	11.31	0.69	0.85	2543.73	0.82
PURQUP		8.13	10.70	0.69	0.87	2329.40	0.79

QEDZEG		4.33	4.65	0.50	1.27	894.89	0.39
QOCBEQ		4.26	7.46	0.55	0.97	1579.42	0.57
RAYKEJ		7.36	9.59	0.56	1.04	1174.68	0.54
RAYKIN		7.12	9.48	0.55	1.07	1092.31	0.52
RAYKUZ		5.81	8.52	0.54	1.10	1096.83	0.50
RAYLAG		5.70	8.06	0.54	1.10	1116.17	0.49
RAYLEK		5.63	8.03	0.54	1.10	1076.42	0.49
RAYLIO		5.06	7.61	0.53	1.12	1124.99	0.47
RAYLOU		5.20	6.82	0.53	1.12	1209.43	0.47
RAYMAH		4.78	6.61	0.52	1.13	1113.38	0.46
REGXOS		7.12	19.51	0.66	0.92	1705.89	0.72
REGYOT		10.17	17.69	0.74	0.70	1746.87	1.07
REPCIZ		8.08	8.97	0.68	1.03	1955.31	0.66
ROGMEG		9.88	12.37	0.78	0.54	4266.01	1.45
RUHCED		6.00	6.21	0.58	1.22	1327.75	0.48
SAHYIK	MOF-5	7.84	14.95	0.81	0.60	3704.93	1.34
SAHYOQ		7.97	15.10	0.81	0.59	3776.46	1.38
SARBOE		3.84	5.05	0.54	1.20	1137.32	0.45
SEGBIR		9.57	10.06	0.52	1.27	744.79	0.41
SEGBOX		9.54	10.03	0.52	1.38	685.19	0.38
SUGWEX03		4.20	5.95	0.54	1.09	1421.94	0.50
SUTBIT		7.96	8.39	0.66	0.86	2291.03	0.77
TEQTAM		5.82	6.97	0.52	1.26	1017.25	0.42
TIGDOD		4.62	6.09	0.60	0.94	2062.40	0.64
TUDJOS	ZIF-8	3.95	11.49	0.65	0.91	1894.28	0.71
TUDMAH		4.44	6.63	0.65	0.81	3402.22	0.80
UMUXAC		4.07	6.23	0.43	2.82	160.25	0.15
UNIGEE		7.84	14.93	0.81	0.61	3674.40	1.33
UWAGAB03		8.54	11.63	0.76	0.58	3426.70	1.32
UXEHIP		4.82	6.07	0.58	0.94	1825.43	0.62
UYAQAN		5.37	7.19	0.46	1.14	742.08	0.40
UYAQER		5.65	7.13	0.46	1.26	698.63	0.37
VAGMIB		10.14	11.07	0.81	0.46	4814.66	1.76
VAGMOH		7.67	9.56	0.79	0.49	4804.57	1.60

VEHKEA		8.62	9.90	0.71	0.88	1696.08	0.81
VEVJUD		9.22	11.96	0.76	0.94	2406.06	0.82
VURMOL		6.45	13.72	0.78	0.69	3399.24	1.14
WAJHUM		7.27	7.48	0.56	1.23	1269.67	0.45
WAJJAU		7.27	7.49	0.56	1.23	1271.57	0.45
WAJJEY		7.27	7.48	0.56	1.23	1283.94	0.45
WAJJOI		7.26	7.49	0.56	1.23	1237.53	0.45
WEMGAY		4.35	5.51	0.54	1.10	1401.13	0.49
WEMXIX		5.68	6.24	0.44	1.51	549.39	0.29
XALROT		4.29	7.85	0.65	0.97	2665.39	0.67
XIRWEB		4.29	7.22	0.49	1.42	582.20	0.35
XUNJEW		4.19	7.71	0.54	1.37	1113.58	0.40
YOZBUL01		10.11	11.96	0.52	1.11	986.83	0.47
YUKBIP		5.14	7.46	0.46	1.51	582.43	0.31
YUVSUE	BIOMOF-11	4.59	5.76	0.54	1.23	1276.92	0.44
ZESTIC		3.90	5.12	0.53	1.10	1118.81	0.48
ZIGFEC		6.85	12.83	0.72	0.80	2835.79	0.90

Table A.2. Operation conditions of the experiments for MOF membranes.

	Common Name	T (K)	P_{feed} (bar)	$P_{permeate}$ (bar)	Ref.
EDUSIF	MOF-5	298	2.7	1.01	[58]
EDUSUR	IRMOF-3	298	1	10^{-6}	[57]
FIQCEN	CuBTC	298	2	1	[59]
FIQCEN		325	2	1	[59]
FIQCEN		355	2	1	[59]
GITTUZ	ZIF-68	298	2	1	[61]
HAGSOY		293	1.5	1	[56]
MMOF		298	1	10^{-6}	[55]
OFERUN	ZIF-8	298	2	1	[60]

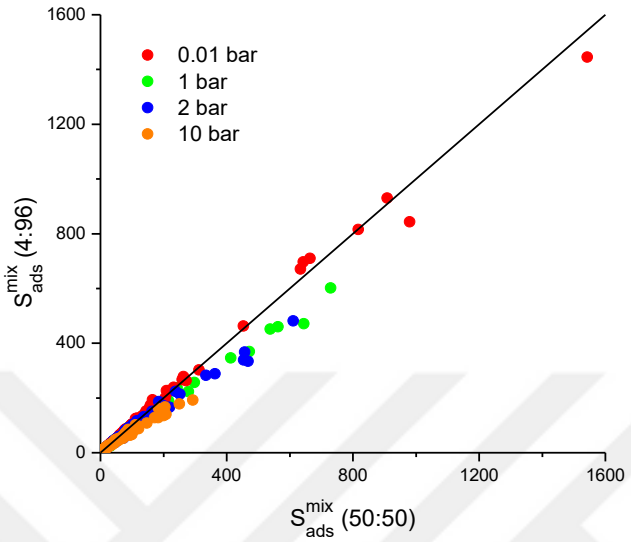

Figure A.1. Comparison of adsorption selectivities of mixtures with bulk compositions of He/CH_4:4/96 and He/CH_4:50/50. Data was produced for 0.01, 1, 2, and 10 bar at 298 K. The x=y line is given to guide the eye.

APPENDIX B: Python Script for the Unit Cell Calculation and Simulation Input Generation for RASPA

```
#!/usr/bin/python3

import numpy as np
import math
import argparse
import os

parser = argparse.ArgumentParser(description='Program to read,
extract info from cif to create simulation.input (by Ozgecim,
last update=24April2018)')

parser.add_argument("inputfile",
                    type = str,
                    help = "path to the input file to read")
parser.add_argument("framework",
                    type = str,
                    help = "name of the framework")

parser.add_argument("-raspa1",
                    action= "store_true",
                    default = None,
                    help = "If the cif file is a P1 structure
written at the end of a raspa run")

parser.add_argument("-ddec",
                    action= "store_true",
                    default = None,
                    help = "If the cif file is from CoRE-MOF
DDEC database")

parser.add_argument("-cutoff",
                    action="store",
                    type=float,
                    dest="cutoff",
                    default=None,
                    help="Auto")

args = parser.parse_args()
path = "/home/user/Documents/example_inputs/simulation.input"
inputfilename = os.path.splitext(args.inputfile)[0]
inputformat =   os.path.splitext(args.inputfile)[1][1:]
file = open(inputfilename+"."+inputformat,'r')
```

```
if inputformat=='cif' and args.raspl:
    i = 0
    k = 0
    print(args.inputfile)

    with open(args.inputfile) as f:
        data = f.read().splitlines()

    beg = data.index('_atom_site_charge')
    count = -1
    for dat in data:
        count = count + 1
        if '_cell_length_a' in dat:
            cell_a = count

    a = float(data[cell_a].split()[1])
    b = float(data[cell_a+1].split()[1])
    c = float(data[cell_a+2].split()[1])
    alpha = float(data[cell_a+3].split()[1])
    beta = float(data[cell_a+4].split()[1])
    gamma = float(data[cell_a+5].split()[1])

if inputformat=='xyz':
     with open(args.inputfile) as f:
        data = f.read().splitlines()

     a = float(data[1].split()[1])
     b = float(data[1].split()[2])
     c = float(data[1].split()[3])
     alpha = float(data[1].split()[4])
     beta = float(data[1].split()[5])
     gamma = float(data[1].split()[6])

if inputformat=='cif' and args.ddec:
    print(args.inputfile)

    with open(args.inputfile) as f:
        data = f.read().splitlines()

    count = -1
    for dat in data:
        count = count + 1
        if '_cell_length_a' in dat:
            cell_a = count

    a = float(data[cell_a].split()[1])
    b = float(data[cell_a+1].split()[1])
    c = float(data[cell_a+2].split()[1])
```

```
    alpha = float(data[cell_a+3].split()[1])
    beta = float(data[cell_a+4].split()[1])
    gamma = float(data[cell_a+5].split()[1])

alpha = alpha * math.pi/180
beta  = beta * math.pi/180
gamma = gamma * math.pi/180

A = [a, 0, 0]
B = [b*np.cos(gamma), b*np.sin(gamma), 0]
C = [c*np.cos(beta), c*(np.cos(alpha)-
np.cos(beta)*np.cos(gamma))/np.sin(gamma), a*b*c*np.sqrt(1-
np.cos(alpha)**2.-np.cos(beta)**2.-
np.cos(gamma)**2.+2.*np.cos(alpha)*np.cos(beta)*np.cos(gamma))/(
a*b*np.sin(gamma))]

W_A = np.dot(A,np.cross(B,C)) / np.linalg.norm(np.cross(B,C))
W_B = np.dot(B,np.cross(C,A)) / np.linalg.norm(np.cross(C,A))
W_C = np.dot(C,np.cross(A,B)) / np.linalg.norm(np.cross(A,B))
print(W_A, W_B, W_C)

x=1
y=1
z=1

while W_A*x < 2*args.cutoff:
    x=x+1
while W_B*y < 2*args.cutoff:
    y=y+1
while W_C*z < 2*args.cutoff:
    z=z+1

print(x, y, z)

with open(path, 'r') as file :
    filedata = file.read()
filedata = filedata.replace('FrameworkName', 'FrameworkName
%s'%args.framework)
filedata = filedata.replace('CutOff',        'CutOff
%s'%args.cutoff)
filedata = filedata.replace('UnitCells',     'UnitCells
%s %s %s'%(x,y,z))

with open("simulation.input", 'w+') as file:
    file.write(filedata)
```

VITA

Özge Kadıoğlu was born in Rize, Turkey on January 28, 1992. In 2016, she graduated from the Department of Chemical Engineering at Boğaziçi University. She successfully got her M.Sc. degree from the Department of Chemical and Biological Engineering at Koç University. Her research interests are molecular dynamics, advanced sampling methods, molecular simulations of nanomaterials, molecular thermodynamics, and adsorption and diffusion behaviors of gas molecules inside membranes. She will continue her career at the Department of Chemistry and Chemical Engineering at École Polytechnique Fédérale de Lausanne as a Ph.D. student.

Pubslications:

Kadioglu, O., & Keskin, S. (2018). Efficient separation of helium from methane using MOF membranes. Separation and Purification Technology, 191, 192-199.